STUDIES INTO ELECTRON SPIN EXCHANGE PHENOMENA.

D.M. CAMPBELL.

Ph.D.

University of Edinburgh

1971.

SUMMARY.

The method proposed by Byrne and Farago (1965) for the production of a polarised electron beam, by means of a spin exchange interaction between trapped electrons and a polarised potassium atomic beam, has been investigated. A pulsed beam of polarised electrons has been generated by this method, with 10^5 electrons per pulse, a pulse length of the order of one microsecond, and a polarisation of 0.5 at a repetition rate of 55 Hz. The repetition rate could be increased at the expense of the polarisation; at a repetition rate of 120 Hz the polarisation was reduced to 0.4. The polarisation and average intensity of the electron beam was limited principally by the properties of the trap in which the electrons were confined during the interaction; as a result of various suggested improvements, it should be possible to increase the polarisation to 0.8, and the average intensity by several orders of magnitude.

From a study of the behaviour of this polarised electron source, it has been possible to derive estimates of the cross-section for spin exchange collisions between potassium atoms and electrons, at three different average kinetic energies in the range 0-4eV. These values of the spin exchange cross-section are in reasonable agreement with previous experimental results, and confirm the theoretical prediction of a rapid decrease in cross-section with increasing energy over this energy range.

C O N T E N T S

CHAPTER I. INTRODUCTION

1.1. Purposes of the Investigation

The discovery of the electron by Thomson in 1897 may be taken as the starting point of atomic physics in the modern sense. Ever since, free electrons have provided physicists with an indispensible tool in the investigation of atomic structure. The classic experiments of Franck and Hertz (1914) in which the excitation potentials of mercury were investigated by electron bombardment, are only one example of an important class of experiments in which the study of electron atom collision processes has yielded information about the target atom. As the sophistication of theoretical methods has increased, it has become possible to predict with increasing accuracy the nature of the interaction between electrons and atoms; the experimental verification of these predictions has provided evidence of the basic soundness of the quantum mechanical postulates on which they are based. In all but the simplest cases, it has been necessary to employ approximation methods in the predictions; such approximations are normally valid only over a limited range of electron energies and types of atom, and experimental study of the range of validity of a given approximation may provide valuable guidance in its improvement. For such reasons, the investigation of electron-atom scattering processes is still an important field of research in modern physics.

In any experiment in which a projectile interacts with a target, the information which may be obtained (either about the target or about the interaction) will depend on the degree of knowledge of the initial properties of the projectile. For example, the fine structure of an electron excitation function can only be resolved by the use of a sufficiently monochromatic incident electron beam. The practical problems involved in the production and use of electron beams with very small energy spread have until recently been prohibitive, and optical excitation has normally been used in investigations of atomic structure which require excitation of a particular atomic state. Apart from the increased ease of collimation and monochromation, excitation by a light beam possesses an additional advantage, in that another property of the beam may be predetermined: its polarisation. By selection of a particular polarisation state of the incident beam, it is possible to discriminate between magnetic sublevels of the excited atom; the whole field of optical pumping, one of the most fruitful in present day atomic physics, depends on this possibility.

The realisation by Uhlenbeck and Goudsmit (1925) that the electron possessed an internal degree of freedom, corresponding to an inherent "spin" angular momentum, made it possible to conceive of a similar preselection of the spin state of an electron beam. If an external magnetic field defines an axis of quantisation, the component of electron spin in the

quantisation direction has a value $\pm\frac{1}{2}\hbar$; if an ensemble of electrons contains n_+ electrons with spin component $+\frac{1}{2}\hbar$, and n_- electrons with spin component $-\frac{1}{2}\hbar$, the polarisation of the ensemble is defined as a vector in the quantisation direction, of magnitude

$$P = \frac{n_+ - n_-}{n_+ + n_-}$$

The polarisation of the ensemble is clearly proportional to the expectation value of the electron spin angular momentum.

In fact, within four years of the postulation of the existence of electron spin, Mott (1929) had proposed a method of producing a polarised electron beam, and of measuring its polarisation (see Section 3.3.1.). Because of the great technical difficulties of the double-scattering experiment involved, the predictions of Mott were not confirmed until 1942, by Schull et al (1942). Somewhat ironically, a further fourteen years elapsed before it was discovered that electrons emitted in beta decay were normally quite highly polarised (Lee, 1957).

The experimental analysis of the spin-dependent features of Mott scattering and beta decay provided valuable information about the interactions involved. In both these cases, the electron energies involved are high (typically > 100 keV). The possibility of investigating spin-dependent features of low-energy electron-atom scattering has only recently been followed up, largely because of the difficulty of obtaining polarised electron beams of sufficiently high current to make such experiments

feasible. In recent years much effort has been devoted to the development of a suitable polarised electron source; a wide variety of techniques has been suggested and investigated (Farago, 1965; Brash, 1969). In the work here described, a proposal by Byrne and Farago (1965) has been developed. This proposal was based on the fact that it is a relatively straightforward task to produce a beam of highly polarised atoms, by deflection in an inhomogeneous magnetic field (see Section 3.1). If an unpolarised electron beam is allowed to interact with such a polarised atomic beam, at an energy of a few electron volts, the mechanism of spin exchange collisions (see Section 1.2) should result in a partial polarisation of the electron beam, with a corresponding decrease in the atomic beam polarisation.

The present experiment was conceived as the first stage of a programme of investigation into spin dependent aspects of low energy scattering of electrons from alkali atoms. The primary consideration in the design of the apparatus was to produce a source of polarised electrons suitable for use in subsequent stages of this programme. However, very little work, either theoretical or experimental, has been done on spin exchange collisions between electrons and alkali atoms (see Section 1.2.); it was therefore anticipated that useful information on the nature of the interaction might be obtained from a study of the mode of operation of the source. In particular, it was expected that the spin exchange cross-section would depend on the energy of the electrons (Section 1.2.2); although the nature of the experimental method implied a considerable uncertainty in the electron energy, it seemed likely that any gross dependence would be observable.

1.2. SPIN EXCHANGE IN ELECTRON ALKALI ATOM COLLISIONS

1.2.1. Theoretical Background

A rigorous quantum mechanical treatment of an interaction involving electron spin should start from Dirac's equations (see, e.g. Mott and Massey, 1965, p.219). However, in the case of the very low electron energies used in the present experiment, for which spin-orbit effects may be neglected, the non-relativistic treatment in terms of the Schrödinger equation may be used, modified by the additional postulate of the Pauli principle. If the valence electron of the alkali atom is assumed to move in a Coulomb field due to the screened nucleus, the Pauli principle implies that the wave function describing the collision must be antisymmetric with respect to the interchange of the spatial and spin co-ordinates of the bound and free electrons.

Thus if the total wave function is symmetric with respect to interchange of spatial co-ordinates, it must be antisymmetric with respect to exchange of spin co-ordinates, and vice versa. Denoting the spin state of the bound electron by $|s\rangle_B$ and that of the free electron by $|s\rangle_F$, with $s = \pm \frac{1}{2}$, the total spin will have four stationary states, described by $|S, m_S\rangle$:

$$\left.\begin{aligned} |1,+1\rangle &= |+\tfrac{1}{2}\rangle_B |+\tfrac{1}{2}\rangle_F \\ |1,0\rangle &= \tfrac{1}{\sqrt{2}}\{|+\tfrac{1}{2}\rangle_B |-\tfrac{1}{2}\rangle_F + |-\tfrac{1}{2}\rangle_B |+\tfrac{1}{2}\rangle_F\} \\ |1,-1\rangle &= |-\tfrac{1}{2}\rangle_B |-\tfrac{1}{2}\rangle_F \\ |0,0\rangle &= \tfrac{1}{\sqrt{2}}\{|+\tfrac{1}{2}\rangle_B |-\tfrac{1}{2}\rangle_F - |-\tfrac{1}{2}\rangle_B |+\tfrac{1}{2}\rangle_F\} \end{aligned}\right\} \quad 1.1.$$

The first three total spin states (the "triplet" states) are symmetric with respect to interchange of the spin coordinates of the two electrons; the last (the "singlet" state) is antisymmetric in this respect.

Burke and Schey, (1962), in a discussion of electron-hydrogen spin exchange collisions, have pointed out that a consequence of the difference in symmetry between the singlet and triplet states of the total spin is the introduction of an effective spin dependence in the scattering forces. Since the total state function (spatial and spin parts together) must be antisymmetric, the triplet state will be antisymmetric with respect to interchange of spatial coordinates, while the singlet state will be symmetric in this respect. This implies that, on average, electrons move in different regions of the interaction potentials in the different spin states, so that the strength of the interaction can be spin dependent.

This effective spin dependence may be allowed for in the discussion of the scattering of a beam of electrons by an alkali atom by defining the singlet and triplet scattering amplitudes $f_1(\theta)$ and $f_3(\theta)$ respectively, such that the probability per unit time, per unit incident flux, of scattering into a solid angle $d\omega$ through an angle θ due to an interaction in the singlet state is $|f_1(\theta)|^2 d\omega$, while the corresponding probability for an interaction in the triplet state is $|f_3(\theta)|^2 d\omega$. These are related to the corresponding total cross-sections for singlet and triplet

scattering by the expressions

$$\left.\begin{aligned} Q_1 &= 2\pi \int_0^{\pi} |f_1(\theta)|^2 \sin^2\theta \, d\theta \\ Q_3 &= 2\pi \int_0^{\pi} |f_3(\theta)|^2 \sin^2\theta \, d\theta \end{aligned}\right\} \quad 1.2.$$

For an electron of energy 1eV, $\lambda \simeq 20\, a_0$ (where $a_0 = 0.53 \times 10^{-10}$m); since the radius of the potassium atom is $r_0 \simeq 6a_0$ (Mott and Massey, p.572), the effective range of the interaction will clearly be comparable with the electron wavelength, so that several partial waves will be necessary to describe the scattering. A calculation by Karule (1965) indicated that the triplet scattering was predominantly P - wave, while the singlet scattering was predominantly D-wave; the total cross-sections were found to be

$$\begin{aligned} Q_1 &\simeq 240\, \pi a_0^2 \\ Q_3 &\simeq 290\, \pi a_0^2 \end{aligned}$$

The spin exchange scattering cross-section Q_e is defined (Dehmelt, 1958) as the cross-section for an interaction in which the spin of the incident electron is initially oppositely oriented to that of the valence electron of the atom, and electron exchange occurs; the outgoing electron is therefore in the opposite spin state to that of the incoming electron. Thus although electron exchange can also occur between electrons whose spins are parallel, this constitutes an unobservable interchange of identical particles, and is excluded by the above definition. Burke and Schey (1962)

have used the alternative nomenclature "spin-flip cross-section" to describe Q_e; although this makes it clear that the exchange of identical spins is excluded, we have preferred to retain the term "spin-flip cross-section" for the description of the total scattering cross-section by any process which reverses the spin direction of the scattered electron, including thereby possible contributions from spin orbit interactions (see, e.g. Kessler, 1969).

The dependence of Q_e on the singlet and triplet scattering amplitudes f_1 and f_3 may be examined by expanding an initial spin state of the total wave function, in which incident and bound electrons have opposite spin orientation, in terms of the stationary states of the total spin. If the incident electron is described by $|-\tfrac{1}{2}\rangle_F$, and the bound electron by $|+\tfrac{1}{2}\rangle_B$, the initial total spin state can be written as

$$|i\rangle = |+\tfrac{1}{2}\rangle_B |-\tfrac{1}{2}\rangle_F = \frac{1}{\sqrt{2}}\left\{ |1,0\rangle + |0,0\rangle \right\}.$$

Scattering into unit solid angle at an angle θ will take place with amplitude $f_3(\theta)$ for the triplet component, and with amplitude $f_1(\theta)$ for the single component, corresponding to a final state

$$|f\rangle = \frac{1}{\sqrt{2}}\left\{ f_3 |1,0\rangle + f_1 |0,0\rangle \right\}.$$

In terms of the singlet particle states, this can be written

$$|f\rangle = \tfrac{1}{2}(f_3 + f_1)|+\tfrac{1}{2}\rangle_B |-\tfrac{1}{2}\rangle_F + \tfrac{1}{2}(f_3 - f_1)|-\tfrac{1}{2}\rangle_B |+\tfrac{1}{2}\rangle_F$$

$$= f_d |+\tfrac{1}{2}\rangle_B |-\tfrac{1}{2}\rangle_F + f_e |-\tfrac{1}{2}\rangle_B |+\tfrac{1}{2}\rangle_F$$

where $f_d(\theta) = \frac{1}{2}(f_3 + f_1)$ represents the scattering amplitude with no interchange of spin coordinates ("direct" scattering); and $f_e(\theta) = \frac{1}{2}(f_3 - f_1)$ the scattering amplitude with spin exchange. Thus the possibility of spin exchange scattering depends on a difference existing between the singlet and triplet scattering amplitudes.

The direct and exchange total cross-sections are given by

$$Q_d = 2\pi \int_0^{\pi} |f_d|^2 \sin\theta \, d\theta = \frac{1}{4}(Q_1 + Q_3 + \gamma)$$

$$Q_e = 2\pi \int_0^{\pi} |f_e|^2 \sin\theta \, d\theta = \frac{1}{4}(Q_1 + Q_3 - \gamma)$$

where $\gamma = 2\pi \int_0^{\pi} (f_1 f_3^* + f_1^* f_3) \sin\theta \, d\theta$. In section 3.2. the interaction of partially polarised ensembles of electrons and potassium atoms is discussed in terms of the cross-sections defined here. The available theoretical and experimental evidence on the magnitude of the electron-potassium spin exchange cross-section is summarised in Section 1.2.2.

1.2.2. Previous Experimental and Theoretical Estimates of Q_e for Potassium.

The total cross-section for spin exchange collision between electrons and potassium atoms has been measured in three previous experiments. In each of these experiments the spin-exchange process was investigated by allowing an ensemble of unpolarised electrons to interact with an ensemble of polarised atoms, and observing the transference of spin from one ensemble to the other. The method by which this transference was observed was, however,

quite different in the three experiments.

The earliest experiment was performed by Franken et al. (1958), using a method pioneered by Dehmelt (1958). The polarised atom ensemble was produced by optically pumping a potassium vapour cell with circularly polarised potassium resonance radiation. Since the transmission of the pumping radiation increased with the orientation of the ensemble of potassium atoms in the cell, changes in the polarisation of the atoms could be monitored by observing the corresponding changes in transmission. When an ensemble of unpolarised electrons was introduced into the cell (by an R.F. discharge), a transference of spin took place, the atoms becoming partially depolarised, and the electron polarisation increasing to an equilibrium value determined by the relative magnitudes of the optical pumping rate, the spin transference rate, and the rate of depolarisation of the electrons due to spin relaxation effects. The diffusion of electrons to the walls was inhibited by the introduction of an inert buffer gas.

A uniform magnetic field B_o was applied to the vapour cell. When a radio frequency magnetic field was applied perpendicular to B_o, its frequency satisfying the relationship

$$\omega_o = \frac{g e B_o}{2m} ,$$

the electrons were disoriented by electron spin resonance. This disorientation was in turn communicated to the ensemble of atoms by spin exchange collisions, and was detected by a further decrease in the transmission of the pumping radiation. Detailed analysis of the processes involved showed that the spin exchange cross-section could be derived from a measurement of the width of the resonance signal in the transmitted radiation intensity, when ω_o was held constant and the steady field was swept through the value B_o. In this way Franken et al. obtained an upper limit

$$Q_e \leq 3 \cdot 0 \times 10^{-18} \text{ m}^2$$

for the potassium-electron spin exchange cross-section. Because of the high collision frequency with buffer gas atoms, the energies of the electrons created by the R.F. discharge were rapidly reduced to a distribution in thermal equilibrium with the buffer gas ($T = 573$ K); the above measurement of the spin exchange cross-section therefore corresponded to an average electron energy of about 0.07 eV.

In the experiment of Rubin et al. (1960), the oriented atomic ensemble was produced by polarising a potassium atomic beam. This was done by passing the beam through a strongly inhomogeneous magnetic field (cf. Section 3.3.4.); by suitably rigorous collimation, a highly polarised beam with a reasonable degree of velocity selection was obtained. This beam was cross-fired by an electron beam with an energy spread of about 0.5 eV, the electron

energy being varied between 0.5 eV and 4.0 eV. No attempt was made to analyse the scattered electron distribution or polarisation; instead, the polarisation of atoms scattered through a given angle was examined by passing them through a second inhomogeneous magnetic field. By observing the depolarisation of the atoms as a function of the atomic scattering angle, and relating this to the corresponding electron scattering angle (uniquely determined if both atomic and electron velocities were known), the ratio of the differential spin exchange scattering cross-section to the total differential cross-section was determined.

Because of mechanical limitations, it was not possible to carry these measurements to very high scattering angles. It was therefore necessary to make some assumptions about the behaviour of the differential cross-sections at high scattering angles in order to obtain the ratio of the total spin exchange cross-section Q_e to the total elastic scattering cross-section Q. Depending on the nature of these assumptions, upper and lower bounds were placed on the absolute value of Q_e by comparison with measurements of Q made by Brode (1929). Recent measurements (Collins et al., 1968) have suggested that Brode's values for the total elastic scattering cross-section Q were a factor 2 too large; the limits given by Rubin et al. should therefore be divided by two. The corrected values for these limits, with the average electron energy at which they were determined, are given in Table 1.1.

The experiment of Farago and Siegmann, (1966), the development of which constituted the present work, also used a polarised

Electron energy (eV)	Q_e (10^{-18} m^2) Lower bound	Upper bound
0.5	0.43	0.8
1.0	0.27	0.8
2.0	0.28	1.0
3.0	0.22	1.0
4.0	0.16	0.9

Table 1.1: Experimental results of Rubin et al. (With subsequent corrections).

atomic beam. Apart from this, it had more in common with the method of Dehmelt. An ensemble of electrons was trapped by a combination of electric and magnetic fields (see Chapter 2) in a region through which the polarised atomic beam was flowing. Since a given atom only spent a short time ($\sim 20\mu s$) in the interaction region, the polarisation of the atomic ensemble was effectively undiminished by the interaction; the electrons, on the other hand, were retained in the interaction region until the probability of a given electron suffering a collision with a potassium atom approached unity. The electrons were then extracted from the interaction region, and their polarisation was analysed by Mott scattering (see Section 3.3.).

By varying the time for which the electrons were trapped in the interaction region, and measuring the electron polarisation as a function of this trapping time, the rate of transfer of spin could be observed directly. One disadvantage that this method suffers from is the necessity for an absolute measurement of the atomic beam density in the interaction region, the estimation of which results in a large uncertainty in the value of Q_e. However, it is undoubtedly the most direct method of observing the total spin exchange cross-section. The value obtained by Farago and Siegmann with an average electron energy of about 1eV, was

$$Q_e = (1{\cdot}6 \pm 0{\cdot}8) \times 10^{-18} m^2.$$

The only currently available theoretical results for the total elastic spin exchange cross-section for potassium are those of Karule (1965), and Karule and Peterkop (1965). The latter give values for Q_e over a range of energies from 1.8eV to 5.0eV. The calculation by Karule relates to energies below the excitation threshold; she derives the zero energy limit of Q_e, and also gives singlet and triplet phase shifts, from which values of Q_e may be derived in the energy range 0eV to 1.6eV. In both cases, the calculations employed a two-state close-coupling approximation.

These theoretical values are presented in Table 1.2. A comparison with the previously quoted experimental results shows that the zero energy limit for Q_e given by Karule is consistent with the upper bound derived by Franken et al. from measurements on thermal energy electrons. The theoretical treatment predicts a rapid fall in the spin exchange cross-section with increasing electron energy, up to 3eV; some evidence of a similar trend may be discerned in the general behaviour of the lower bound derived by Rubin et al. (cf. Tables 1 and 2). However, there are considerable quantitative discrepancies; for example, at an electron energy of 3eV, the theoretical value of Q_e is a factor 3 smaller than the experimental lower bound.

Electron energy (eV)	$Q_e(10^{-20}m^2)$	Source
0.0	212	1
0.4	104	1
0.6	68	1
1.0	39	1
1.6	27	1
1.8	21.0	2
2.0	16.6	2
3.0	6.8	2
4.0	7.1	2
5.0	5.8	2

Table 1.2: Theoretical results from (1) Karule, (2) Karule and Peterkop.

1.3. Outline of the Present Experiment

A schematic diagram of the experimental arrangement used in the present work is shown in Fig. 1.1. A potassium atomic beam issued from a circular aperture in an oven at 583K, and after collimation was polarised by passage through a six-pole magnetic field (Section 3.1.). The polarised beam then flowed through the centre of the electron trap, in which electrons with an energy of a few electron volts were confined by an electrostatic potential well and a uniform magnetic field in such a way that they oscillated backwards and forwards across the atomic beam (Section 2.1.). The electrons were supplied by a conventional electron gun, outside the trapping region, and were injected into the trap by the application of a pulse to one of the electrodes determining the form of the trapping potential. After a defined trapping time, in which many traverses of the atomic beam occurred, the electrons were released from the trap in a similar way. Since the uniform magnetic field was directed along the electron beam axis, the electrons were longitudinally polarised by spin-exchange collisions with the potassium atoms during the interaction time; because of the rapidity of the transition to a region of zero magnetic field when the electrons were extracted from the trapping region, the direction in space of the polarisation vector remained unchanged.

The degree of polarisation of the electrons was measured by Mott scattering analysis (Section 3.3.). The longitudinal polarisation was converted to transverse polarisation by rotating

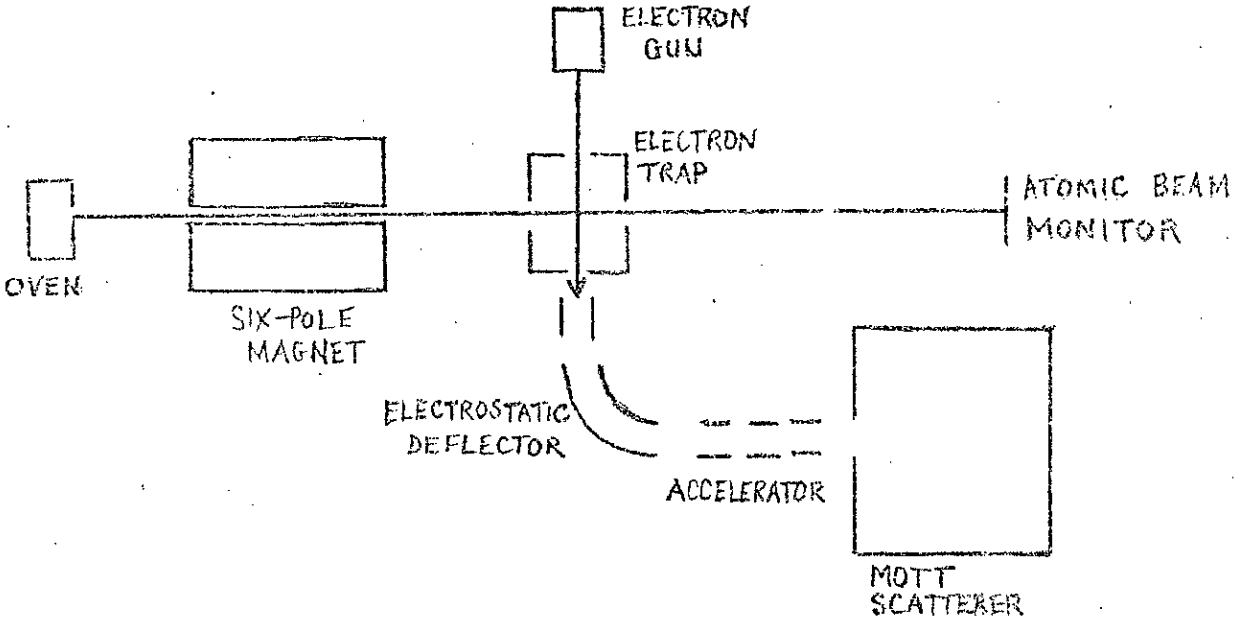

Fig. 1.1: Schematic diagram of the present experiment.

the momentum vectors through 90° in an electrostatic deflector; after acceleration through 50kV, the electrons were scattered from a thin gold film target, and the asymmetry in scattering at an angle of 120° was measured by allowing the scattered electrons to fall on two scintillation counters. The intensity of the atomic beam was measured by a Langmuir Taylor surface ionisation detector.

The experiment was partially automated to allow the repetition of a series of polarisation measurements at different trapping times (Section 3.3.7.). In this way, it was possible to establish the time constant governing the approach of the electron polarisation to the equilibrium value, determined by the competition of spin exchange and relaxation processes. Since the relative magnitudes of these processes could be estimated by comparing the equilibrium electron polarisation with the polarisation of the atomic beam, a subsidiary measurement of the number density of the atomic beam in the interaction region enabled a value for the spin exchange cross-section to be derived.

The arrangement outlined above was basically similar to that proposed by Byrne and Farago (1965), and used by Farago and Siegmann (1966). The most significant improvement made was the use of a six-pole magnet to polarise the atomic beam, instead of the dipole magnet used by Farago and Siegmann. The principal advantage of the six-pole magnet was its property of focussing one spin state in the atomic beam and defocussing the other; by a proper adjustment of the "optics" of the system (Brash et al., 1969), it was possible to achieve a polarisation close to unity

in the interaction region, with an atomic number density more than an order of magnitude higher than that obtained with the dipole magnet.

The importance of the increase in atomic beam number density lay in the fact that the rate at which the electron polarisation approached its equilibrium value was correspondingly increased (see Sections 3.2; 4.1). In the experiment of Farago and Siegmann, it was not possible to extend the trapping time sufficiently to determine this equilibrium value; it was therefore not possible to establish the importance of relaxation effects. In the present experiment, it has been possible to observe convincingly the approach to saturation of the electron polarisation (see, for example, Fig. 4.1); in this way it has been shown that relaxation effects are probably negligible under the present circumstances. Values for the spin exchange cross-section at three different electron energies have been derived (Table 4.7.); these are in broad agreement with the results quoted in Section 1.2.2. and confirm the decrease in Q_e with increasing electron energy suggested there.

It was pointed out in Section 1.1. that the purpose of the present work was not only to derive information on the spin exchange process directly, but also to examine experimentally the conditions under which this process could be made the basis of a usable source of polarised electrons. The polarisation and average intensity of the electron beam extracted from the electron trap were limited basically by the properties of the trap, which

are discussed in Chapter 2. Under optimum conditions (Section 4.1.4.), it was possible to obtain a pulse containing 10^5 electrons with a polarisation of 0.5, at a repetition frequency of 55Hz. This corresponded to a trapping time of 17ms; since the electron polarisation was then close to its equilibrium value (Fig.4.6.), it was possible to reduce the trapping time to 7ms, corresponding to a repetition frequency of 120 Hz, without reducing the polarisation below 0.4. These results are fully presented in Chapter 4.

CHAPTER 2

THE ELECTRON TRAP

2.1. DESCRIPTION OF THE ELECTRON TRAP

2.1.1. Theory of Penning Trap with Hyperbolic Electrodes

The general behaviour of electrons trapped by a combination of electric and magnetic fields can be illustrated by considering the theoretically simple case in which the electrostatic potential distribution, rotationally symmetric about the z axis, is described by

$$\phi = A \left(\frac{r^2}{2} - z^2\right).$$

Such a potential distribution can be created by using as electrodes the surfaces formed by rotating Fig. 2.1 about the z axis (Graff et al. 1968).

Since the potential distribution on the z axis has the form of a parabolic well, an electron of energy eV will be trapped between the limits $z = \pm \left(\left|\frac{V}{A}\right|\right)^{\frac{1}{2}}$, and will perform simple harmonic motion in the z direction with angular frequency

$$\omega_z = \left(\left|\frac{2eA}{m}\right|\right)^{\frac{1}{2}}.$$

The term in ϕ involving r^2, necessary to satisfy Laplace's theorem, means that an electron on the axis is in a state of unstable equilibrium with respect to its radial motion. In order to ensure radial trapping, an axial magnetic field can be applied; if this is a uniform field it will have no effect on the axial motion of the electrons. The radial motion is described by the equation (Byrne and Farago, 1965)

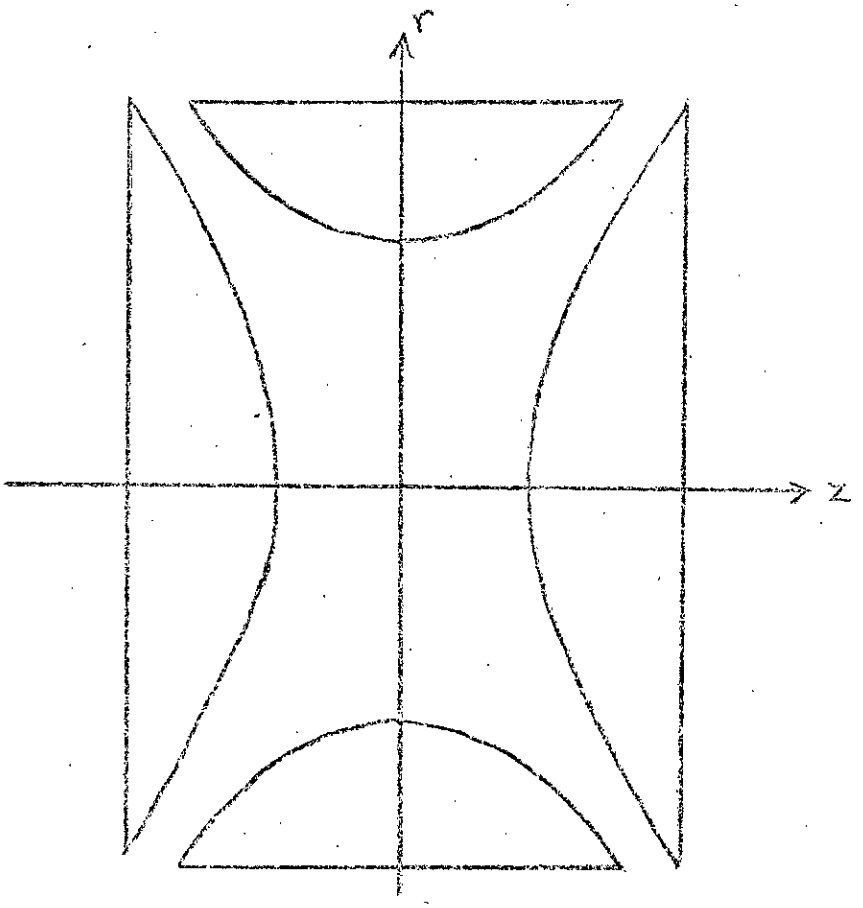

Fig. 2.1: Cross-section of trap with hyperboloid electrodes.

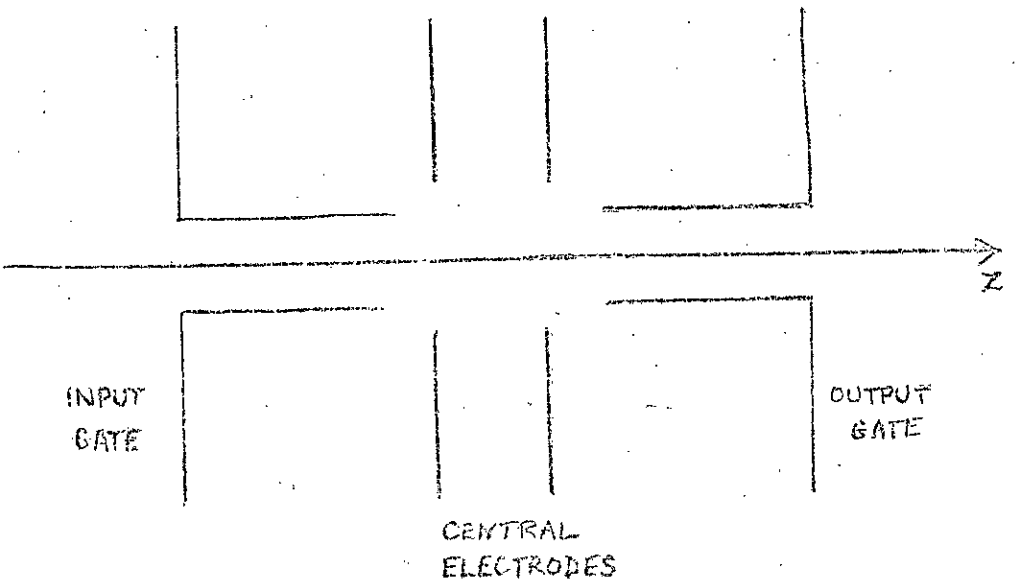

Fig. 2.2: Cross-section of the trap electrodes used here.

$$r = e^{\frac{1}{2}i\omega_c t}\left[ae^{\omega t} + be^{-\omega t}\right], \qquad 2.1.$$

where ω_c is the cyclotron frequency of the electrons in the field B:

$$\omega_c = \frac{eB}{m},$$

and

$$\omega^2 = \frac{1}{2}\omega_z^2 - \frac{1}{4}\omega_c^2 .$$

Radial trapping can be achieved only if the argument of the first exponential inside the square brackets is imaginary: that is, if

$$\omega_c^2 - 2\omega_z^2 > 0. \qquad (2.2)$$

When this condition is satisfied by the more stringent condition

$$\frac{\omega_z}{\omega_c} \ll 1, \qquad (2.3)$$

Equation 2.1 can be written as

$$r = a e^{i(\omega_c - \omega_p)t} + b e^{i\omega_p t}$$

where

$$\omega_p = \frac{1}{2}\frac{\omega_z^2}{\omega_c} = \frac{A}{B} .$$

Three periodicities can then be identified in the motion of electrons in the trap: axial oscillation with angular frequency ω_z, rotation in a plane perpendicular to the z axis with angular frequency $\omega_c - \omega_p$, and a precession of the orbital centre of this rotation about the z axis with angular frequency ω_p.

2.1.2. The Trap used in the Present Experiment

The system of electrodes used in the present trap is shown in Fig.2.2. It consisted of a series of discs and cylinders, which were used to define an approximately parabolic potential well along the axis. This arrangement was chosen in preference to the hyperbolic electrode structure partly because of simplicity of manufacture, but also because in the present case it was desired to inject electrons into the trap from outside, and to extract them after trapping, so that a structure open along the axis was in any case required.

The two outer electrodes were turned from copper, and the central discs were of stainless steel. The electrodes were supported on four ceramic rods, their relative spacing and orientation being determined by quartz tube spacers. A plot of the axial potential, made using a scale model in an electrolytic tank (Fig. 2.3), showed that, with appropriate voltages applied to the electrodes, a close approximation to a parabolic variation could be obtained over the central region of the trap.

The trap was mounted between the polefaces of an electromagnet, as shown in Fig.2.4. The magnet was capable of supplying a field of up to 400 gauss, more than adequate for radial confinement of the electrons. A simple electron gun was mounted on the outside of one of the polefaces, the filament being in a region of very low magnetic field. A potential difference of 80 volts between filament and polepiece accelerated the electrons, and they passed at this energy through a cylindrical channel in the polepiece into the trapping region. The normal axial

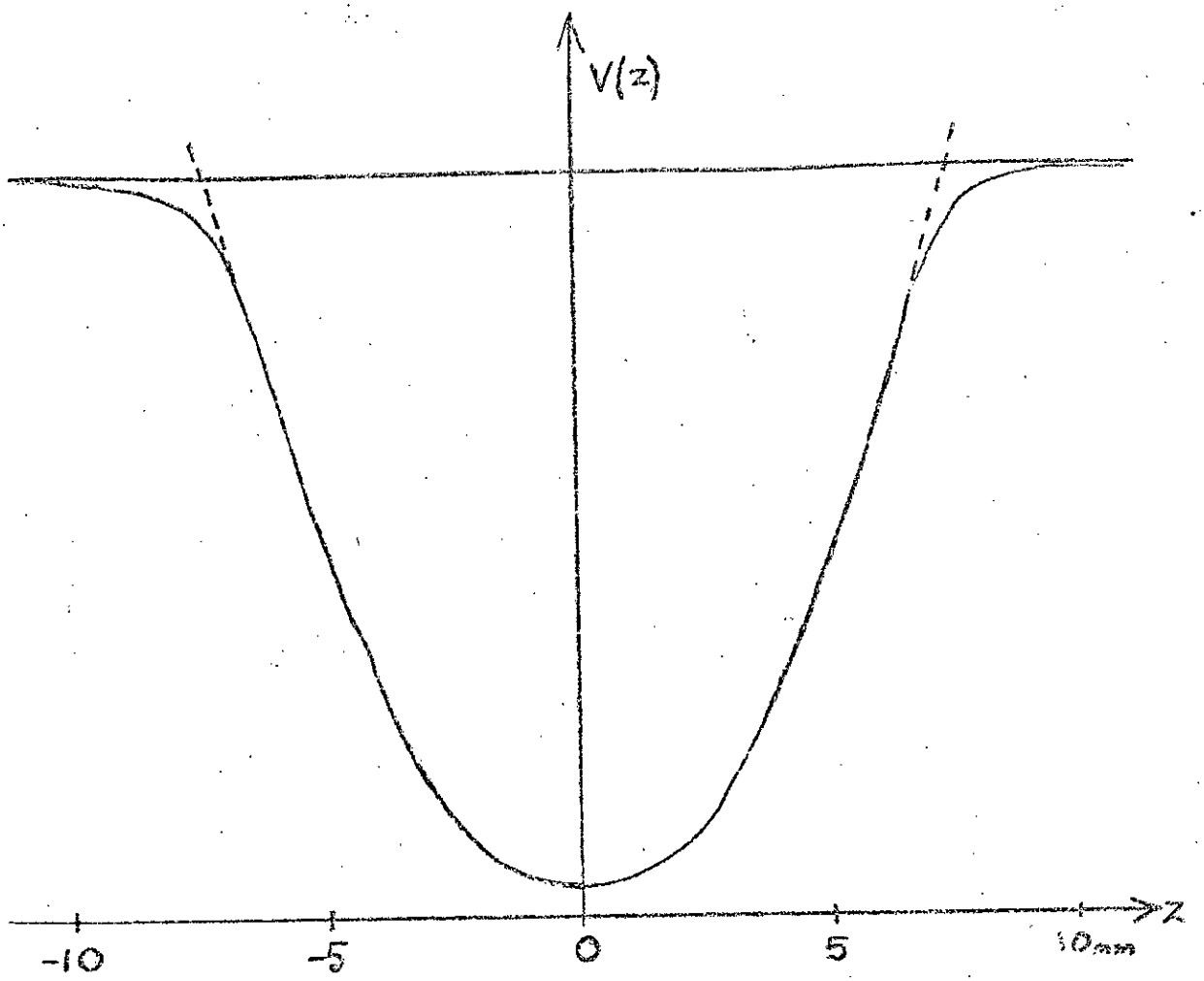

Fig. 2.3: Electrolytic tank plot of potential distribution on trap axis.

potential distribution is shown in Fig.2.5, from which it will be seen that the first trap electrode (the "input gate") was normally held about 1 volt negative relative to the filament; electrons were therefore reflected at this barrier. Injection of electrons into the trap was accomplished by applying a positive pulse to the input gate. This pulse was of sufficient magnitude to open the gate to electrons, which were then reflected by the third electrode (the "output gate"). On closure of the input gate, electrons between the two gates were trapped; they were released after a predetermined trapping time (ranging from 0,25 ms to 18 ms.) by the application of a positive pulse to the output gate. The ejected electrons were accelerated towards the other poleface of the magnet, again at +90 volts relative to the filament; passing through an aperture in this polepiece, they were further accelerated in two stages to 3 kilovolts, and injected into the electrostatic deflector which preceded the Mott scatterer. The sequence of pulses applied to the trap electrodes is shown in Fig. 2.6.

2.1.3. Normal operating Conditions of Trap

To simplify the analysis of the interaction between the trapped electrons and the potassium atomic beam, it was desirable that the electrons should have insufficient energy to undergo inelastic collisions. Since the threshold for the first excited state of potassium is 1.6eV, the nominal trap depth (the difference in potential between the gates and the centre electrode) was chosen to be 1,5 volts. The axial potential in the central

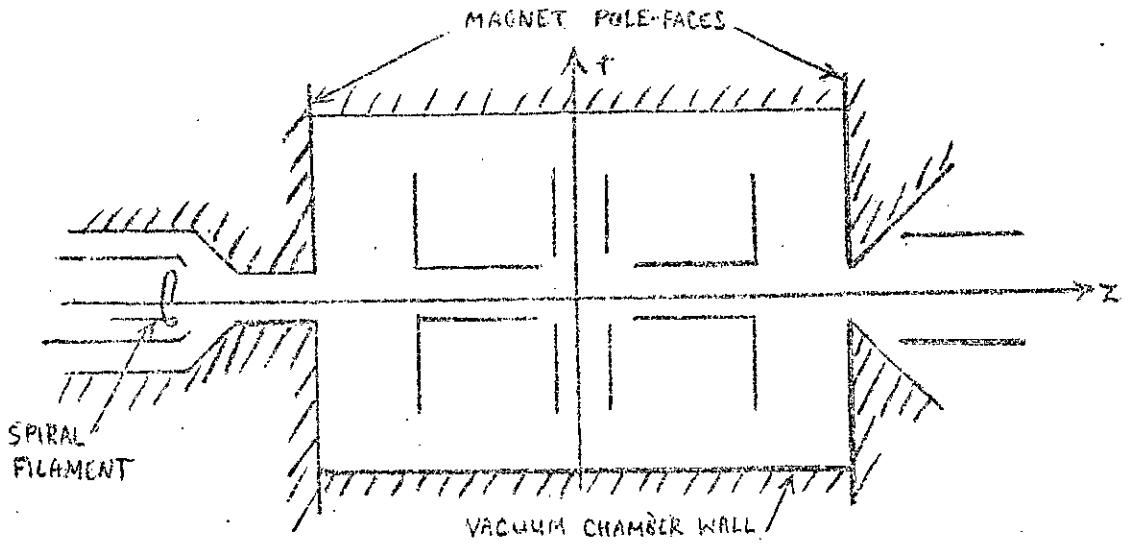

Fig. 2.4: Trapping region (scale 1:1)

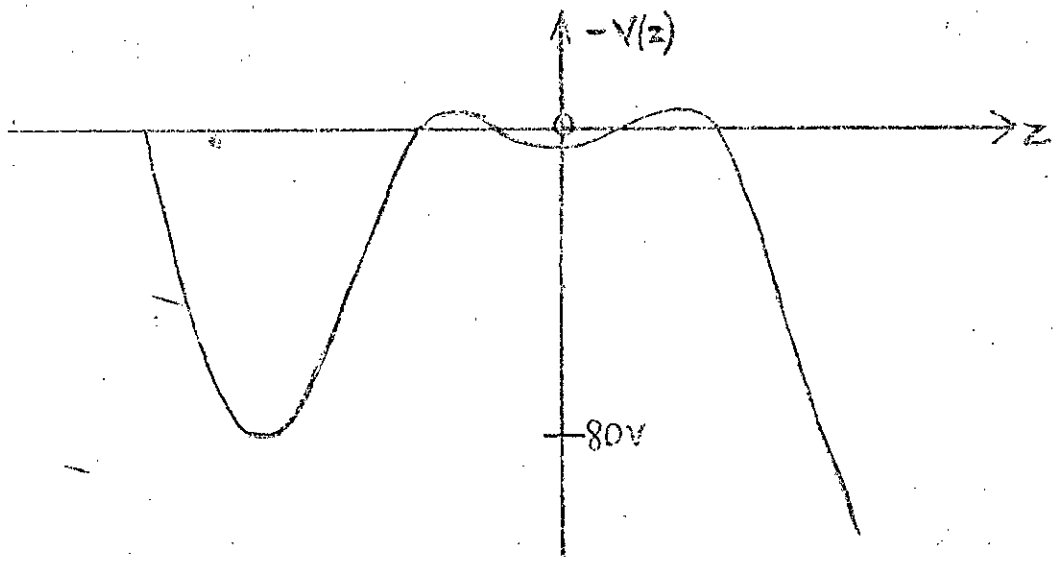

Fig. 2.5: Axial potential distribution in trapping region (trap closed).

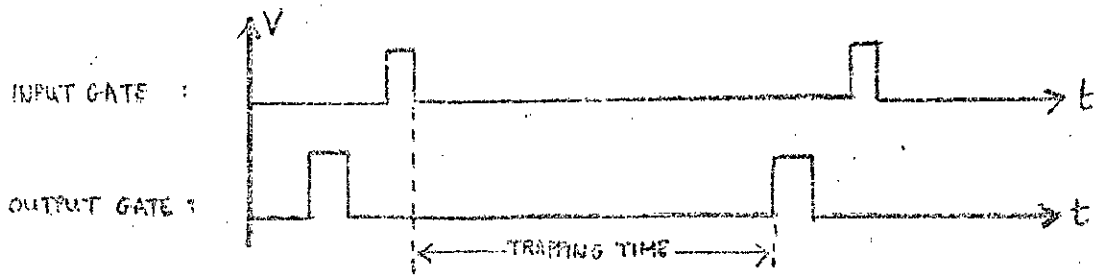

Fig. 2.6: Sequence of pulses applied to the trap.

region of the trap was thus approximately described by

$$\phi = -Az^2$$

with $A = 3 \times 10^4$ Vm^{-2} (see Fig. 2.3).

The angular frequency of axial oscillation of electrons in the trap was then

$$\omega_z = 1.0 \times 10^8 \ s^{-1}$$

The minimum magnetic field necessary for radial confinement was (from Equation 2.2)

$$B_{min.} = 10^{-3} \ T.$$

For reasons given in Sect. 2.2.1, the magnetic field in the trap was normally restricted to 6×10^{-3} T; for this field

$$\omega_c = 1.1 \times 10^9 \ s^{-1}$$

Since $\frac{\omega_z}{\omega_c} \simeq 0.1$, Equation 2.3 was also satisfied.

The precession frequency was given by

$$\omega_p = \frac{A}{B} \simeq 5 \times 10^6 \ s^{-1}.$$

An electron trapped for 10 milliseconds would therefore undergo 3.4×10^5 traverses of the interaction region; during each traverse it would perform approximately five cyclotron orbits in the radial plane, and the centre of these orbits would precess around the axis through about 9^o.

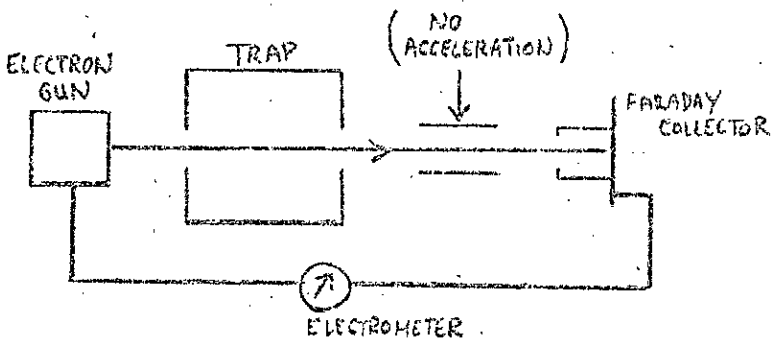

(a) Measurement of beam current.

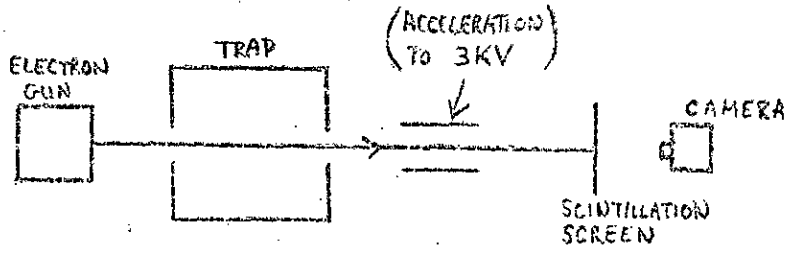

(b) Observations with scintillation screen.

Fig. 2.7: Study of electron beam emerging from trap.

2.2. Measurements of Trapped Current

2.2.1 Dependence on magnetic field

Initially, the behaviour of the electron trap was examined by collecting in a Faraday cup the emergent electron beam (Fig.2.7). In order to ascertain that the electrons had not come straight through the system but had in fact been trapped, it was verified that the current disappeared unless both input and output pulses were applied to the appropriate electrodes. This trapped current was measured as a function of several of the experimental parameters, and some curious features emerged. The most important of these is illustrated by the experimental plot of trapped current versus magnetic field strength, shown in Fig.2.8: the current was found to depend strongly on both the magnitude and the direction of the magnetic field, rising to a sharp maximum at around 6×10^{-3} T , and falling off rapidly for higher fields.

It had been expected that the trap would function more efficiently at high fields, since radial confinement would be more stringent, and losses due to radial diffusion reduced (see Sect.2.4). An earlier trap, of basically similar design (Farago and Siegmann, 1966) had behaved satisfactorily with a field of 3×10^{-1} T . The suspicion therefore arose that the decrease in current at high fields was not directly related to the trapping, but might be due to losses in the electron injection or extraction processes. This suspicion was confirmed by the measurements shown in Fig.2.9. The three trap electrodes were raised to +8 volts, and the current

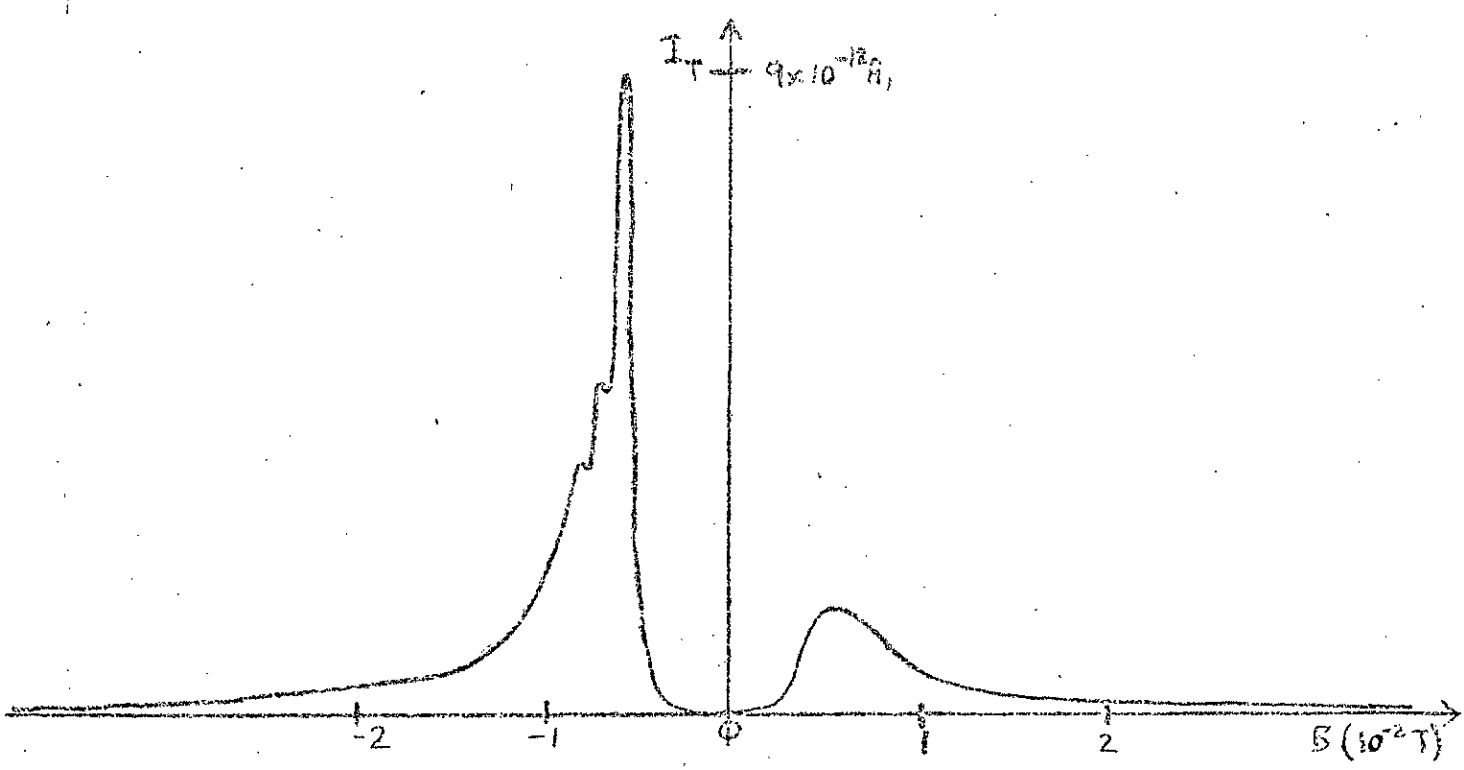

Fig. 2.8: Trapped current I_T versus maghetic field B.

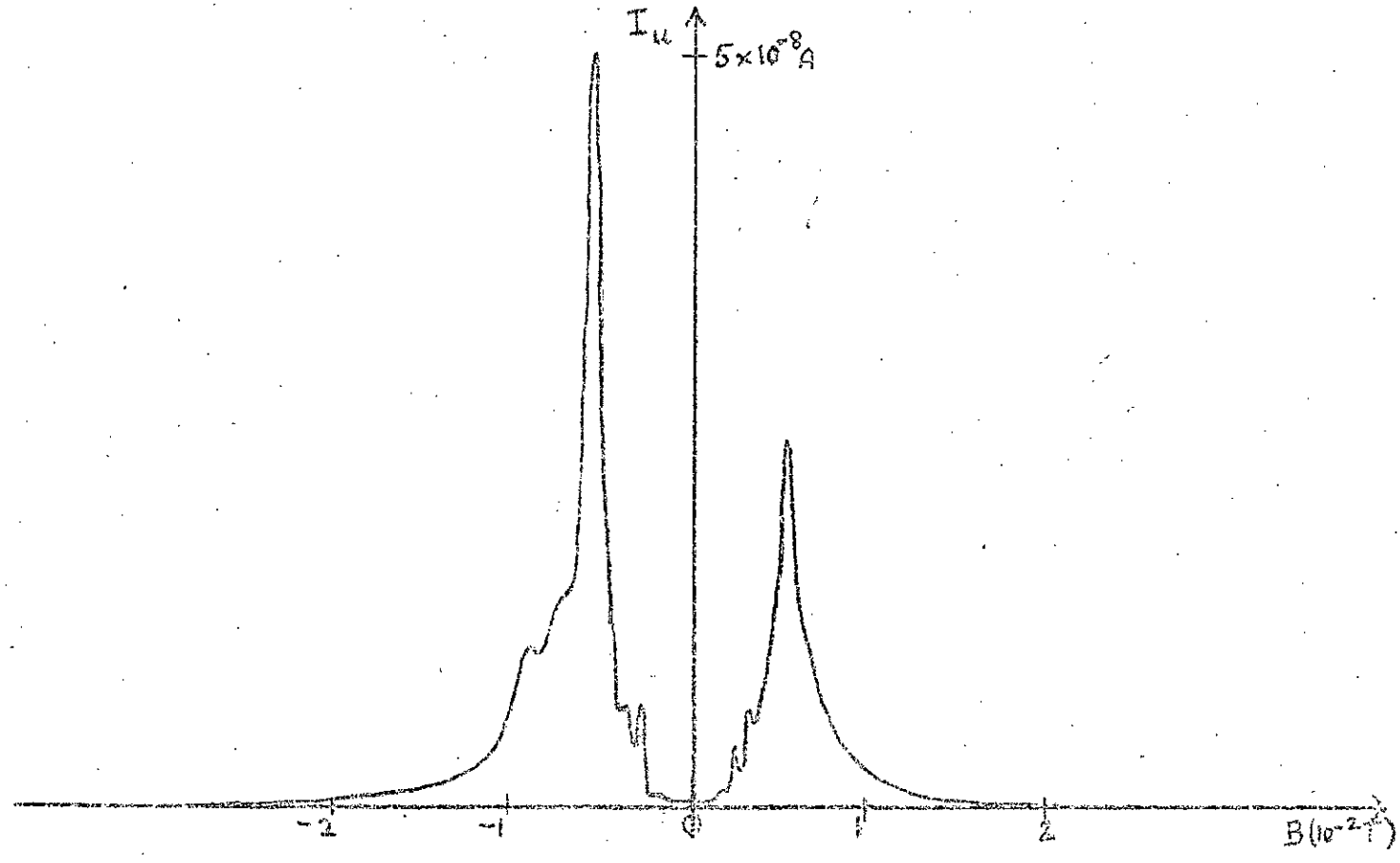

Fig. 2.9: Untrapped current I_U versus magnetic field B.

passing straight through the trap plotted as a function of magnetic field. The similarity of form between the curves in Figs.2.8 and 2.9 left no doubt that the dependence on magnetic field was not a consequance of the trapping of the electrons.

Quite apart from improvements in trapping efficiency, it was desirable to have a relatively high magnetic field in the interaction region in order to decouple the nuclear and electronic spins in the potassium atoms (see Sect.3.1.4). It had been hoped that a field of 2×10^{-2} T could be applied; in this the effective atomic beam polarisation would be $> 75\%$. In such a field, however, the trapped current was reduced to $\sim 6\%$ of its maximum value, and was so low that polarisation measurements would be complicated by the difficulty of distinguishing signal from background. Furthermore, if the losses were occurring after the trap, the polarisation measurement would effectively be performed on a very small and not necessarily representative sample of the trap output.

Some further investigation of the cause of this effect was therefore necessary. This was accomplished by replacing the Faraday cup which had been used to collect and measure the emergent electron beam, by a scintillating screen, made by depositing silver-activated zinc sulphide on a mica backing. The electrons bombarded this screen with an energy of 3 KeV, yielding a visible fluorescent image of the beam cross-section which could be viewed from behind. Only the direct (untrapped) beam was examined in this way; the trapped currents were too low to provide visible images, and the background of light from the electron gun filament prevented the

use of long exposure photography. However, it seemed almost certain that the same mechanism was responsible for the forms of the curves in Figs. 2.8 and 2.9, and that any conclusions as to the reasons for losses in the untrapped beam would apply with equal validity to the trapped electrons.

The series of photographs comprising Fig. 2.10 show the images produced on the scintillating screen by the electron beam at various values of the magnetic field. On examing these images, it became clear that the primary reason for the decrease of current with increasing field was the increasing divergence of the electron beam. For fields of up to 6×10^{-3} T, the beam was confined to a diameter of about 5mm., and increased steadily in intensity. As the field increased further the beam "blew up"; the highly diffuse image became increasingly eccentric and distorted; and at a field of 4×10^{-2} T it was no longer visible.

When the loss of current at high fields was first observed, the injection of the electron beam through the polepiece into the magnetic field had been considered a likely source of such a field dependence. The maximum current which can be passed through the cylindrical aperture of radius a (Fig.2.4), for a given accelerating voltage V, is obtained in the special case of Brillouin flow (see, e.g. Pierce, 1954, p.152); in this case the beam is parallel, and the necessary magnetic field is given by

$$B = \left(\frac{16mV}{3ea^2}\right)^{\frac{1}{2}}$$

where e and m are the electron charge and mass respectively. If

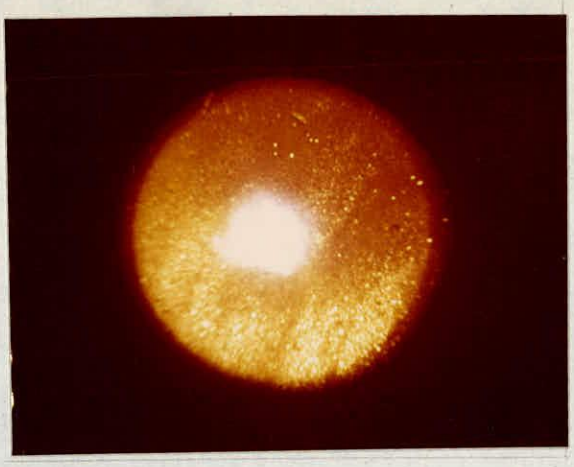

(a): B = 0·0 T.

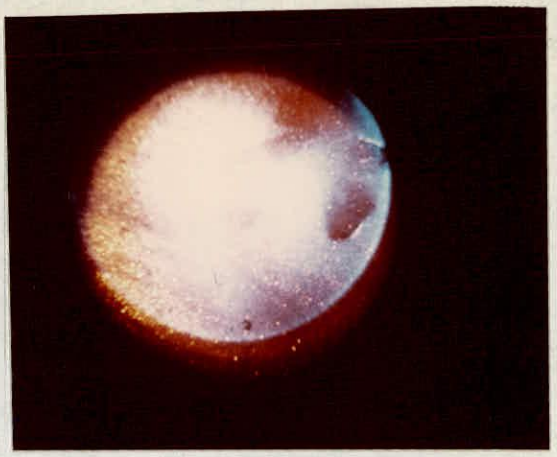

(d): B = 1.3×10^{-2} T.

(b): B = 6×10^{-3} T.

(e): B = 2.6×10^{-2} T.

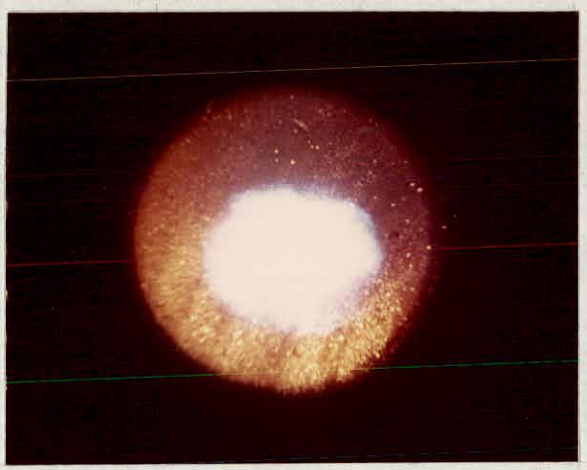

(c) B = 10^{-2} T.

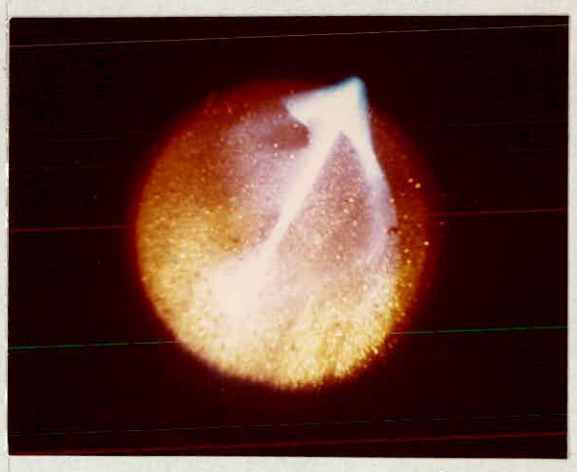

(f): B = 3.8×10^{-2} T.

Fig. 2.10: Beam cross-section at spin-twister entrance.

the magnetic field is increased beyond this value, the beam which emerges from the aperture in the polepiece is no longer parallel, but periodically converging and diverging along the axis; the current is also reduced. Thus a dependence of current on magnetic field similar in form to that found experimentally is predicted.

In order to obtain pure Brillouin flow, the electric field in the region between cathode and polepiece must be carefully shaped so that the electron beam is parallel when it enters the magnetic field. In the present case, electrons entered the transition region of the magnetic field with a considerable angular spread, so that the theory of Brillouin flow could not be exactly applied. Nevertheless, it seemed likely that the dependence of the current on the magnetic field would exhibit the same general features: in particular, that for a given accelerating voltage there would be an optimum magnetic field corresponding to a maximum transmission of current through the aperture. In fact, for an accelerating voltage V = 80 volts, the maximum current was obtained at a field of 6×10^{-3} T compared with the optimum field of 1.6×10^{-2} T, for Brillouin flow through the aperture (a = 3mm).

However, the steadily increasing divergence of the beam with increasing magnetic field, revealed by the scintillation screen observations, seemed more likely to have arisen at the second polepiece. After leaving the trap, the beam entered this polepiece through another aperture. The axial component of the magnetic field dropped rapidly to zero (Fig. 2.11), implying the existence of a significant radial field component. An estimate of the beam

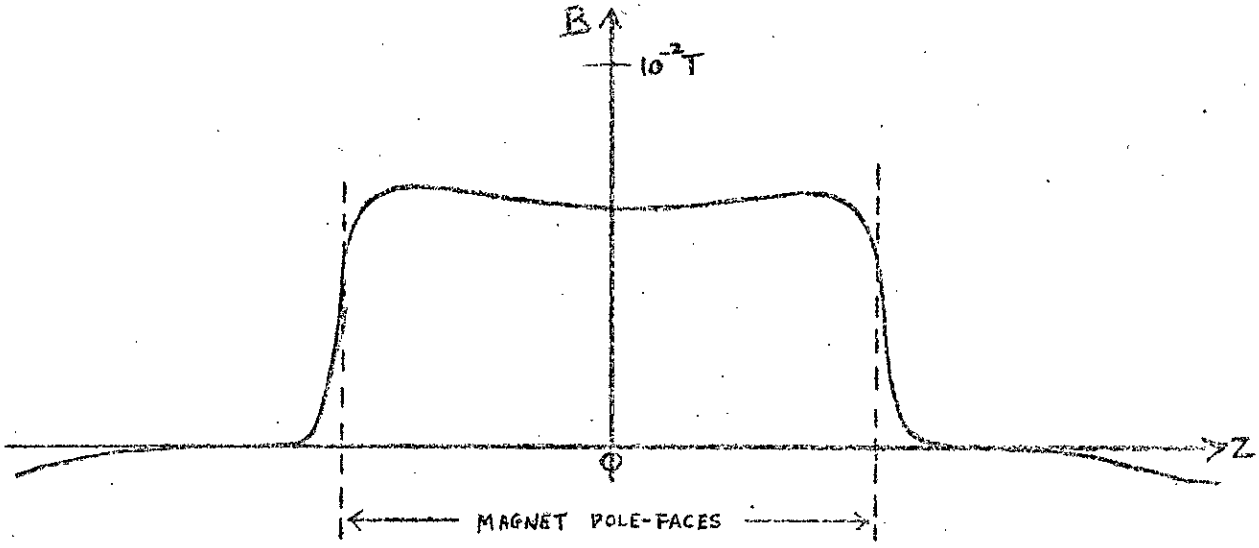

Fig. 2.11: Axial magnetic field in region of trap (electromagnet current 0·5A).

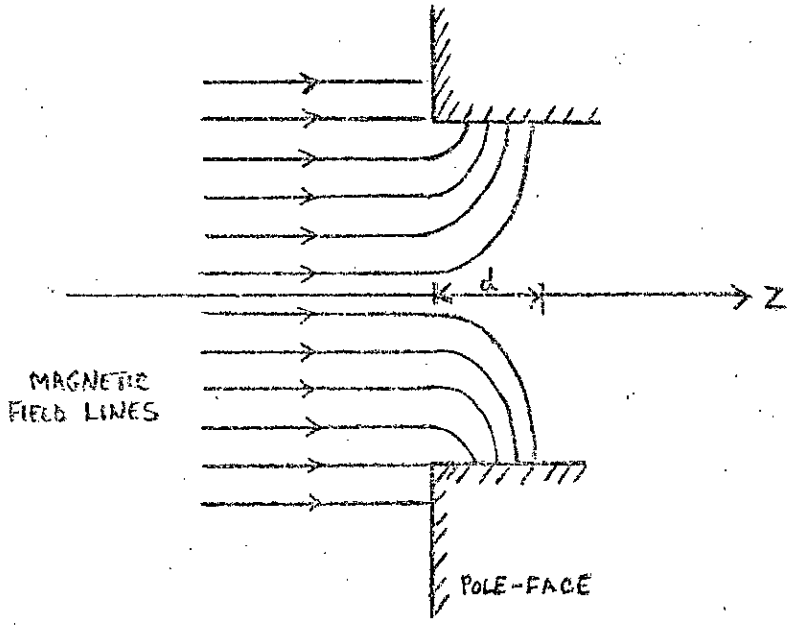

Fig. 2.12: Simplification of magnetic field in region of poleface.

divergence caused by this transition field may be obtained by considering the somewhat simplified case illustrated in Fig.2.12. It is assumed that the magnetic field has uniform magnitude B_z at every point in the plane of the poleface, and has decreased to zero at every point in a parallel plane a distance d from the poleface. Applying Gauss's theorem to the volume bounded by these two planes and a cylindrical surface of radius r coaxial with the beam:

$$\int_{\text{CLOSED SURFACE}} \underline{B} . \underline{dS} = 0 \quad ;$$

$$\therefore \pi r^2 B_z = 2\pi r d \bar{B}_r , \qquad (2.4)$$

where $\bar{B}_r$ is the average value of the radial field component over the cylindrical surface.

Consider now an electron which enters the aperture at a radial distance r from the axis, with a velocity v_z parallel to the axis. It will experience a deflecting force due to the radial component of the magnetic field: the average force, over the distance d within which the radial field exists, is given by

$$\bar{F}_\theta = e v_z \bar{B}_r$$

(assuming that the deflection θ is small). The electron will therefore acquire a transverse velocity v_θ, given by

$$v_\theta = \frac{e}{m} v_z \bar{B}_r \left(\frac{d}{v_z}\right) = \frac{e d \bar{B}_r}{m} .$$

This corresponds to an angular deviation

$$\theta \simeq \tan\theta = \frac{v_\theta}{v_z} = \frac{ed\overline{B}_r}{mv_z} .$$

The axial velocity v_z can be expressed in terms of the accelerating voltage between cathode and polepiece:

$$v_z = \left(\left|\frac{2eV}{m}\right|\right)^{\frac{1}{2}} ;$$

using the relationship (Eqn.2.4) between $\overline{B}_v$ and B_z, we obtain finally an expression giving the deflection in terms of the known fields:

$$\theta \simeq \left(\frac{e}{8mV}\right)^{\frac{1}{2}} r B_z . \qquad (2.5)$$

If we consider an initially parallel beam of 2mm. radius entering the aperture, and take V = 80 volts, $B = 6 \times 10^{-3}$ T, we find that

$$\theta \simeq 0.2 \text{ radians} \simeq 12^\circ$$

for an electron at the surface of the beam. Since the deflection is proportional to r, the central region of the beam will remain relatively parallel, but as the magnetic field increases, the whole beam will spread out. The effect is clearly strong enough to explain the observed divergence of the beam.

For a given magnetic field B_z, Equation 2.5 states that

$$\theta \simeq r V^{-\frac{1}{2}} .$$

The divergence may therefore be reduced either by reducing the diameter of the beam at the aperture, or by increasing its velocity. In the present case, it did not seem possible to reduce the beam diameter without incurring further loss of current. The possibility of increasing the beam velocity, by increasing the potential difference between the filament and the second polepiece, was considered; unfortunately, since the two polepieces were electrically connected by the trap vacuum chamber, this also implied an increase in the acceleration voltage between filament and first polepiece. As this latter voltage was increased beyond the optimum value for the given magnetic field, an increasing fraction of the electrons emitted by the filament would be collected on the first polepiece, instead of being channelled through the aperture by the magnetic field.

A compromise was obviously required between the conditions for optimum injection through the first polepiece, and those for optimum extraction through the second. To establish the best compromise, the beam current I_B was measured as a function of magnetic field B for several values of accelerating voltage V. Fig.2.13 shows the maximum beam current obtained in each case, plotted against the accelerating voltage. Simultaneous

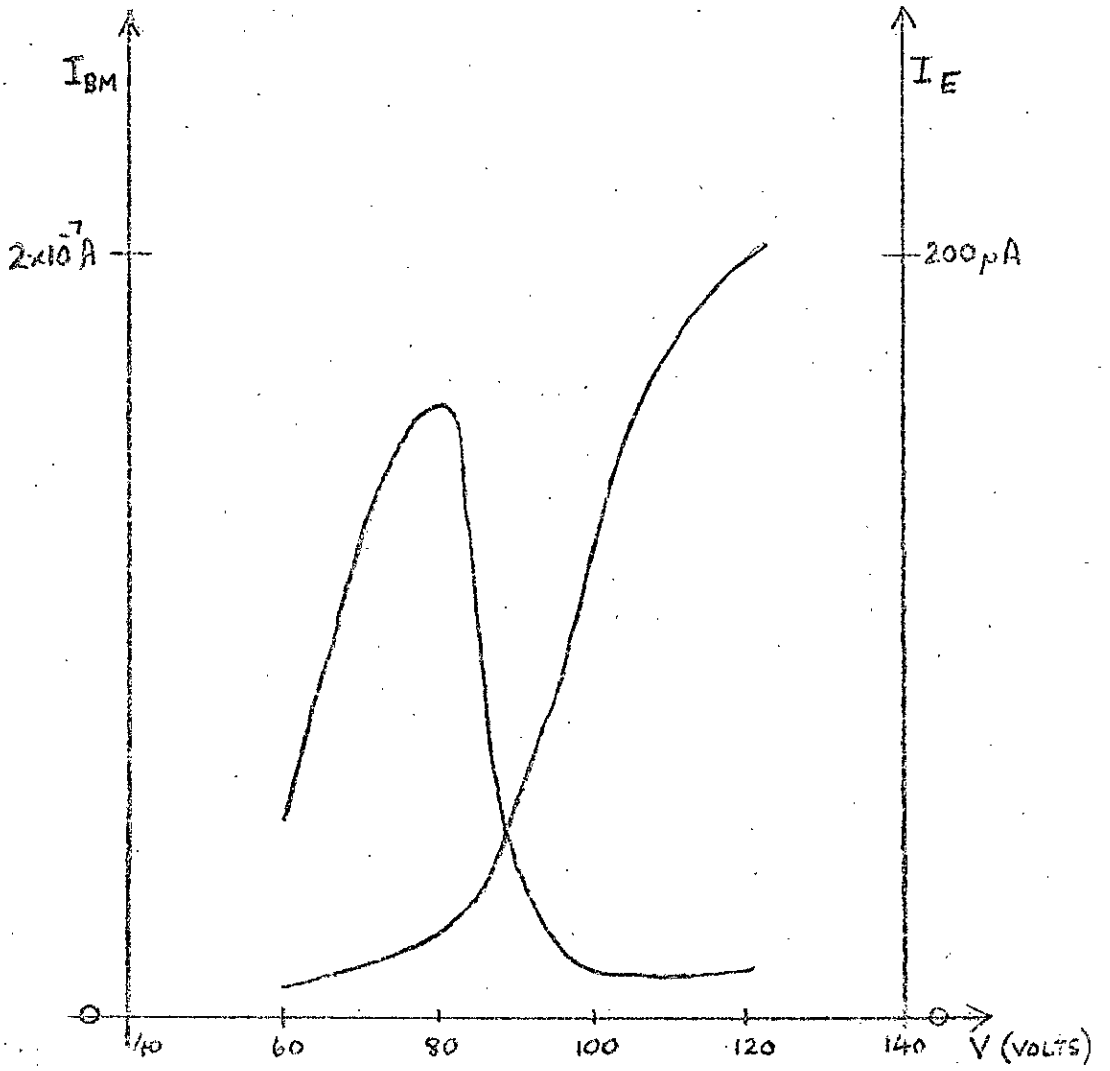

Fig. 2.13: Maximum trapped beam current I_{BM}, and emission current I_E. versus accelerating voltage V.

measurements were made of the current collected on the pole-piece (I_A), and these are shown on the same graph. Since only a small fraction of the current emitted by the filament did in fact pass through the aperture in the polepiece, I_A may also be taken as the emission current of the gun; it increased continuously with V, showing that, at the filament temperature used, the electron gun emission was space-charge limited. The beam current, collected as usual in a Faraday cup beyond the second polepiece, increased with increasing V up to 80 volts, and then dropped sharply.

It was therefore decided to operate the system with an accelerating voltage of 80 volts. To achieve maximum beam current, a magnetic field of 6×10^{-3} T was then required in the trap. As previously explained, this was undesirably low from the point of view of the hyperfine coupling in the potassium atom. It was found that the field could be increased to about 1.5×10^{-2} T before the current decreased to such an extent that polarisation measurement was no longer possible; in practice, however, fields above 10^{-2} T were not used, since it seemed possible that the increasing divergence of the beam, revealed by Fig. 2.10, might result in a significant degree of depolarisation due to scattering and secondary emission in the spintwister and accelerator.

2.2.2 Space Charge Limitations in the Trap

The graph of average trap output current against magnetic field previously given (Fig. 2.8), showed a maximum current of 10^{-11} amps at a field of 6×10^{-3} T. This was a typical value of maximum average beam current. Under certain circumstances, it was found possible to obtain considerably higher currents; in particular, when the electron gun was switched on after a "rest" of several days, the current was initially high, and decreased steadily for several hours before reaching a stable value. The untrapped electron beam also displayed this behaviour, which seemed to be due to variations in the efficiency of injection through the first polepiece. The explanation might lie in the temporary increase in pressure in the gun region when the filament was newly heated, resulting in a temporary improvement in injection efficiency due to space-charge compensation by outgassed ions.

In these measurements, the trap was operated with a repetition frequency of 3KHz. An average current of 10^{-11}A was therefore equivalent to 2×10^{4} electrons from each trap output pulse. This provided an adequate counting rate for Mott scattering analysis of the polarisation (see Sect.3.3), but if the apparatus were to be usable as a source of polarised electrons for future experiments, an increase in the number of electrons contained in the trap was highly desirable. An upper limit to this number was set by space-charge considerations, the containing forces due to the applied fields being counteracted by the mutual repulsion of the electrons. To obtain a rough estimate of this upper limit under the present

circumstances, the change in axial potential in the trap due to the presence of a cylindrical space-charge cloud of uniform density was calculated. The radius of the cylinder was taken to be 2mm., and the length 10mm.; it thus nearly filled the central region of the trap.

The results of these calculations, with a diagram illustrating the simplified situa tion for which they were derived, are given in Fig. 2.14. The original potential well was taken to have a depth of 1.5 volts. With a charge density of $1.3 \times 10^{-6} Cm^{-3}$ in the defined trapping volume, corresponding to a number of trapped electrons $N = 10^6$, the well retained an approximately parabolic shape, the potential at the centre rising by 0.6 volts, and the well depth dropping to just over 1 volt. For $N = 3 \times 10^6$, the potential at the centre had risen to 1.8 volts, and was almost uniform throughout the trapping volume. Further increase in the density of trapped electrons was not possible, as can be seen from the curve for $N = 4 \times 10^6$: the net electrostatic forces at the edge of the space-charge cloud were now directed away from the centre, so that the electrons were no longer trapped.

The assumption of uniform charge density in the trapping volume implied a particular distribution of electron kinetic energies; the limiting case, for which the axial potential throughout the trap was uniform, could be achieved only if all the electrons were stationary. In practice, of course, the situation would be much more complicated. The charge density of the electron cloud would vary continuously throughout the trapping

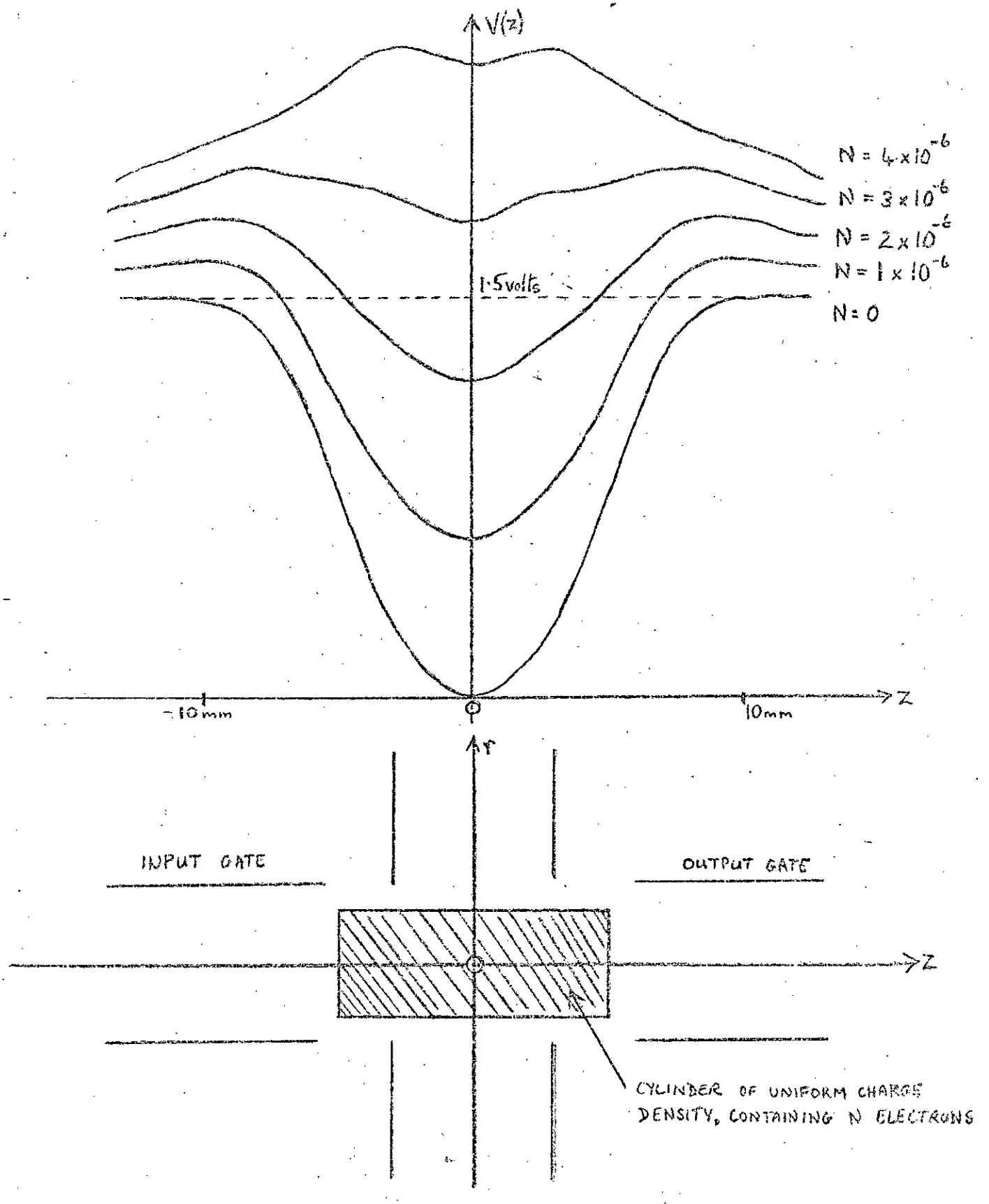

Fig. 2.14: Illustration of the effect of space charge on the axial potential distribution in the trap.

volume; the precise nature of this variation would depend on the energy distribution of electrons in the trap, which would in turn depend on the method by which the electrons were injected into the trap. In the present case, the electrons were of such an energy that they were normally completely reflected by the closed input gate, which was at a potential of 1.5 volts relative to the centre of the trap. It was therefore energetically impossible for electrons to exist in the trap in a region where the potential exceeded 1.5 volts; from Fig.2.14, it may be seen that values of $N > 2 \times 10^6$ were thus excluded.

The conclusion drawn from these considerations was that the limit set by space charge effects on the number of electrons which could be contained in the trap was of the order of 10^6. The typical experimental value of 2×10^4 electrons per output pulse was therefore well below this limit. Even allowing for the loss of a considerable fraction of the electrons during extraction, it seemed unlikely that sufficient electrons had been trapped to appreciably modify the potential distribution in the trap.

Improvements in the electron gun, and in the method of filling the trap, might therefore be expected to increase the trapped current by an order of magnitude. Further improvement would depend on modification of the trap itself. The space-charge limit could be raised by increasing the trapping volume; to achieve a significant increase, a "merged beam" type of arrangement would be desirable, in which the atomic beam could be fired along the axis of the trap rather than across it (Fig.2.15). Such a system is

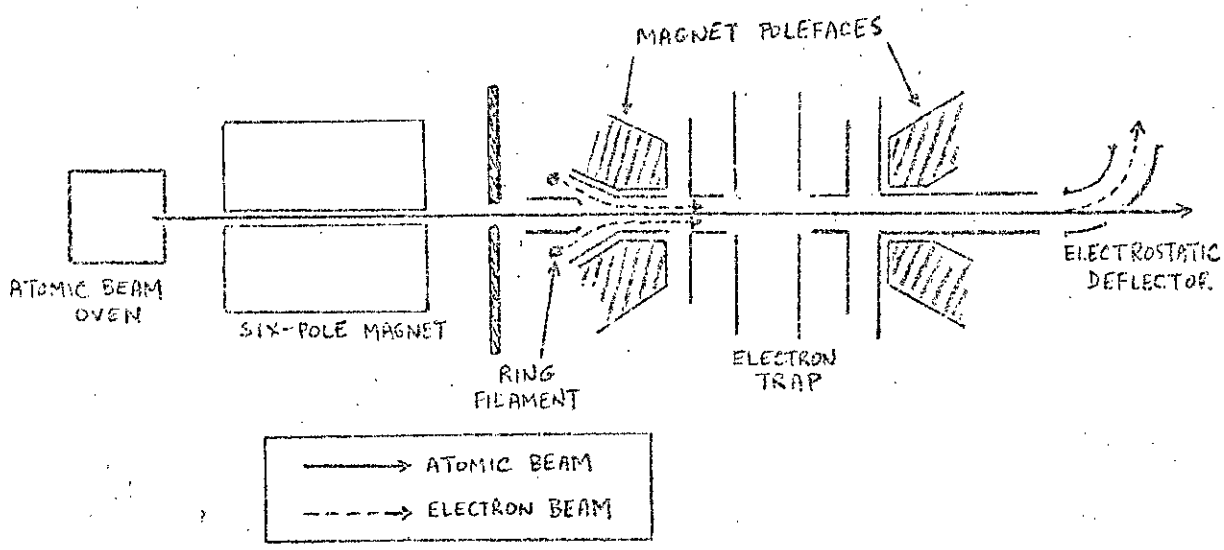

Fig. 2.15: "Merged beam" apparatus (Vass, 1971).

at present under construction in this laboratory. The length of the trapping volume, and therefore of the interaction region, could then in principle be increased up to the limit set by depolarisation of the atomic beam. This limit may be estimated by noting that the total spin angular momentum carried out of the interaction region by the electron beam in unit time cannot exceed that carried into the interaction region by the atomic beam. In order to achieve high electron polarisation, the atomic beam polarisation must remain close to unity throughout the interaction region; this implies that only a small fraction of the total flux of spin angular momentum carried by the atomic beam may be transferred to the electron beam. If the number of atoms entering the interaction region per unit time is I_A, and the average number of electrons leaving the trap per unit time is I_E, high electron polarisation can be achieved only if $I_E \ll I_A$. In the present case, $I_A \simeq 10^{12}$ atoms s^{-1}, so that the highest average current of fully polarised electrons which could be achieved with such a beam is $\sim 10^{-9}$A. With a repetition rate of 50Hz, this would correspond to 5×10^8 electrons per output pulse. It therefore appears that the number of trapped electrons could be increased by several orders of magnitude before depolarisation of the atomic beam became serious.

The number of electrons which can be trapped in a given volume is approximately proportional to the depth of the potential well which confines them. However, if this number is to be increased by using a deeper well, care has to be taken in the method by which the trap is filled. The space-charge limit can

only be approached if the average kinetic energy of the electrons in the trap is very low; (in the present experiment, the requirement of low kinetic energy was also necessary in order to ensure that only elastic collisions between electrons and potassium atoms occurred). The simple method of injecting electrons into the trap described in Section 2.1.2 would almost certainly lead to a considerable distribution of kinetic energies; in a deep well, a large fraction of the electrons would have energies well in excess of the excitation threshold.

Krisciokaitis and Tsai (1969) have suggested that a deep well may be filled with low velocity electrons by continuously modifying the potentials on the trap electrodes, as the filling proceeds, in such a way as to counteract the changes in potential due to the accumulating space charge. The scheme which they proposed involved a gradual increase in the potentials of both filament (V_F) and input (V_I), the potentials on the trap centre and the output gate remaining constant (see Fig.2.16). At an intermediate stage in the filling process, the potential at the centre of the trap would have become ϕ volts more negative due to the space charge by then accumulated in the trap. If the rate of change of filament potential V_F were not greater than the rate of change of ϕ, the kinetic energies of the electrons entering the trap would remain low throughout the filling process.

The same result could be achieved by a gradual change in the potential V_C on the central trap electrode, all other potentials being held constant (Fig.2.17). As the bottom of the potential

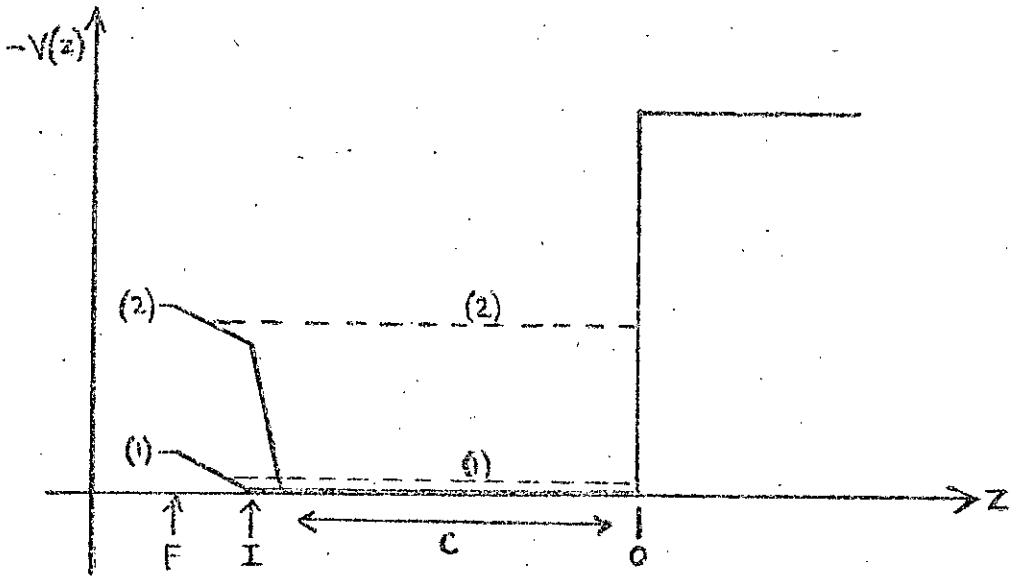

Fig. 2.16: Method of trap filling proposed by Krisciokaitis and Tsai.

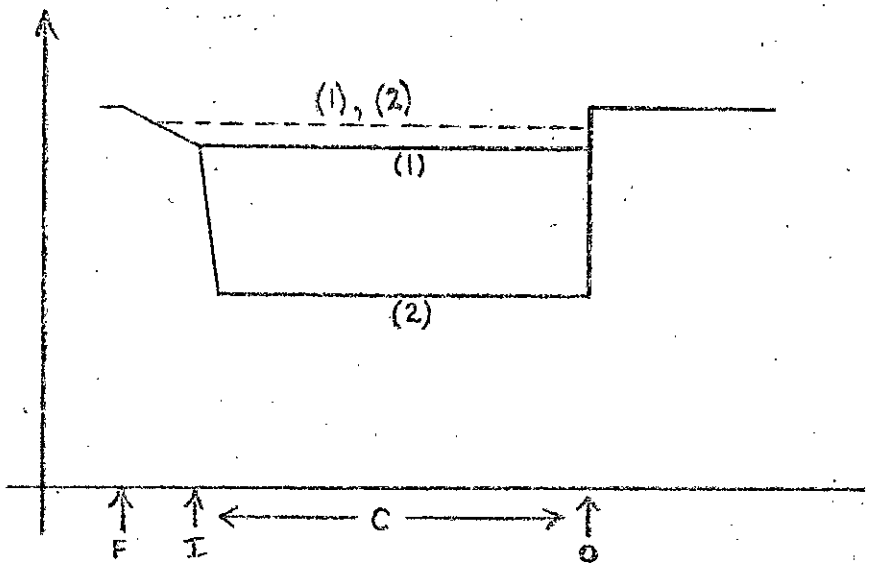

Fig. 2.17: Alternative method to that of Fig. 2.16.
F,I,C and O denote the positions of filament, input gate, central electrode and output gate respectively.
Solid lines represent potentials in absence of space charge; dashed lines show potentials including space charge.
(1) start of filling process; (2) intermediate stage in filling process.

well was lowered, electrons in the central region of the trap would lose energy, and become trapped; if the rate of change of V_e were matched to the rate of accumulation of trapped electrons, the increase in the potential difference $(V_F - V_C)$ between filament and central electrode would be compensated on the axis by the increase in space-charge potential ϕ. The well could thus be made very deep without increasing the kinetic energy of the trapped electrons.

The rate at which such a filling process could be carried out would be determined principally by the rate at which electrons could be supplied to maintain the condition of space-charge saturation in the trapping region. If the rate of change of the applied potential were too rapid, the equilibrium distribution of the space-charge would be upset, resulting in an increase in the average electron kinetic energy. In practice, the optimum filling rate would have to be determined empirically. At present, this method is being tested on the trap previously described, in an attempt to increase the final trap depth to 100 volts. If this can be done without increasing the average electron kinetic energy beyond 1eV, the trap should be capable of containing 10^8 electrons. The extension of the method much beyond this point would be useful only if the intensity of the atomic beam could also be increased.

2.3. Electron Energies in the Trap

2.3.1 General Considerations

One of the aims of the present experiment was to investigate the energy dependence of the cross-section for spin-exchange collisions between electrons and potassium atoms. This was to be done by measuring the polarisation of the electrons as a function of the depth of the potential well in which they had been trapped during their interaction with the atomic beam. In order to interpret the results of these measurements, it was necessary to know the distribution of electron kinetic energies in a potential well of a given depth.

In the following discussion, the effects of space charge in the trap are neglected. If the trap were filled to the space-charge limit, the effective depth of the well, and therefore the maximum possible kinetic energy, would be greatly reduced; however, the measurements quoted in Section 2.2.2 showed that, under normal experimental conditions, space charge effects were not significant.

Consider an electron trapped in a static potential well of depth D volts, as shown in Fig. 2.18. It is convenient to choose the potential on the axis at the centre of the trap as the zero of potential. If the electron has momentum p at the centre of the well, with components p_z and p_t parallel and transverse respectively to the z axis, the fact that it is trapped implies that

$$\frac{p_z^2}{2m} < |eD| .$$

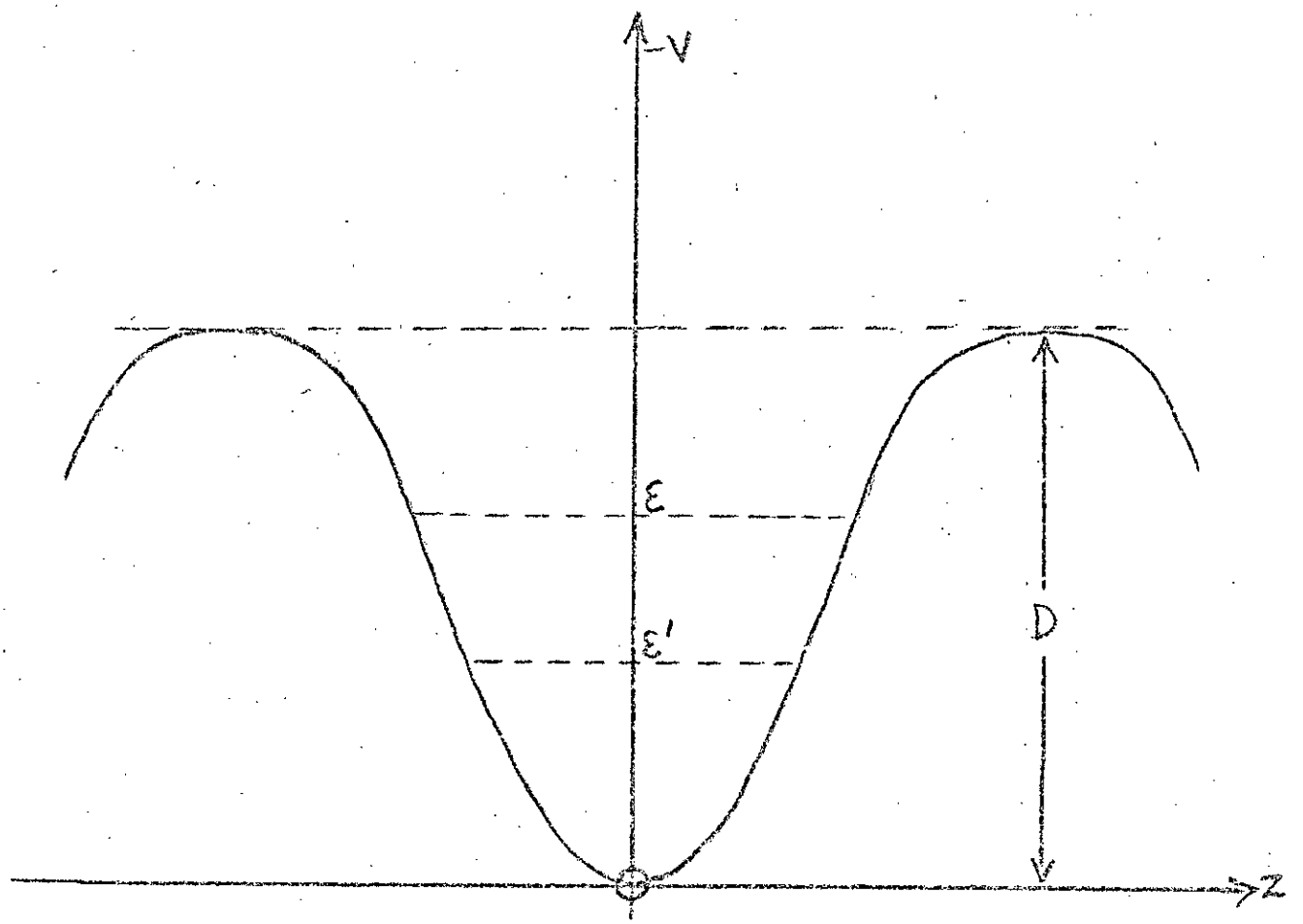

Fig. 2.18: Energy levels of an electron in a potential well of depth D.

This does not yield information directly about the total energy, since the transverse momentum p_t can have a range of values up to the limit set by the maximum permissible cyclotron orbit radius. In practice, however, the potential difference between the cathode of the electron gun, and the trap input gate was set so that, with the input gate closed (as in Fig. 2.18), all electrons were reflected. The electrons with the highest possible axial momentum would be those with maximum total energy, and no transverse momentum; since these were unable to surmount the barrier of the closed input gate, it could be deduced that the maximum kinetic energy of electrons in the trap was less than $|eD|$.

The total energy of a trapped electron with purely axial momentum can then be represented on Fig. 2.18 by a horizontal line $\mathcal{E}$ volts above the bottom of the well: this total energy is

$$\frac{p^2}{2m} = e\mathcal{E} .$$

If such an electron undergoes an elastic collision, either with a potassium atom or with a residual gas atom, the magnitude of its momentum will remain unaltered, but its direction will change. It will thus acquire a transverse momentum component, and its axial momentum will decrease. The electron's axial motion will now be characterised by a lower level in the potential well (that is, it will oscillate over a more confined region of the z axis); this level will be $\mathcal{E}'$ volts above the well bottom, where

$$e\mathcal{E}' = \frac{p_z^2}{2m} ,$$

and p_z is the new axial component of momentum at the centre of the trap. The total kinetic energy at this point is, of course, unchanged. After a large number of elastic collisions, an ensemble of such electrons, initially having purely axial momentum, will have their momentum vectors randomly distributed in momentum space; this corresponds to a continuous distribution of levels in the trap of Fig. 2.18 from $\mathcal{E}$ volts down to zero. Those at the bottom of the well will have no axial momentum, and will be performing cyclotron orbits at the centre of the trap, with orbital kinetic energy $e\mathcal{E}$ electron volts.

The experimental situation was complicated by the fact that the electron beam used to fill the trap was neither monoenergetic nor parallel. Electrons whose momentum vectors were equal in magnitude, but at different angles to the axis, would occupy different levels in the well, corresponding to differences in their axial momentum components. The thermal spread in the total energies of electrons emitted by the filament would, of course, be reflected in a range of momentum magnitudes as well as directions; changes in total electron energy would result from the time dependence of the potential distribution during the trap filling and emptying processes.

Over the interaction region, the axial potential did not vary with z by more than 10% of the well depth. The kinetic energy of the electrons at the centre of the trap was therefore taken as the approximate average kinetic energy of interaction with the atomic

beam. In estimating this average kinetic energy, and the width of the energy distribution, reliance was placed as much as possible on direct measurements on the electron beam, rather than on theoretical computations. The principal reason for this was that factors such as contact potentials, charging of insulating surfaces, and finite mechanical tolerances in electrode construction and alignment, whose magnitudes were difficult or impossible to estimate, seemed likely to play a significant role in determining the behaviour of the electrons. In addition, the thermal spread of electron energies (of the order of 0.5 eV) limited the accuracy with which the energy dependence of the spin-exchange cross-section could be measured; thus the somewhat unrefined measurements presented in the following sections provided as much information as could be meaningfully used in interpreting the results of the electron polarisation measurements.

2.3.2 Measurements on the Untrapped Beam

The energy spread of the electron beam which was injected into the trap was investigated by allowing the beam to pass freely through the trap, then stopping it by gradually applying a retarding potential to one of the trap electrodes. The graph in Fig.2.19 shows the results of such a measurement: the untrapped beam current is plotted against the difference between the potential, V_o, applied to the output gate electrode, and the nominal filament potential (taken as zero in this discussion). The curve in Fig.2.20 was obtained by differentiating that in Fig.2.19, and gives an indication of the spread of components of axial momentum in the

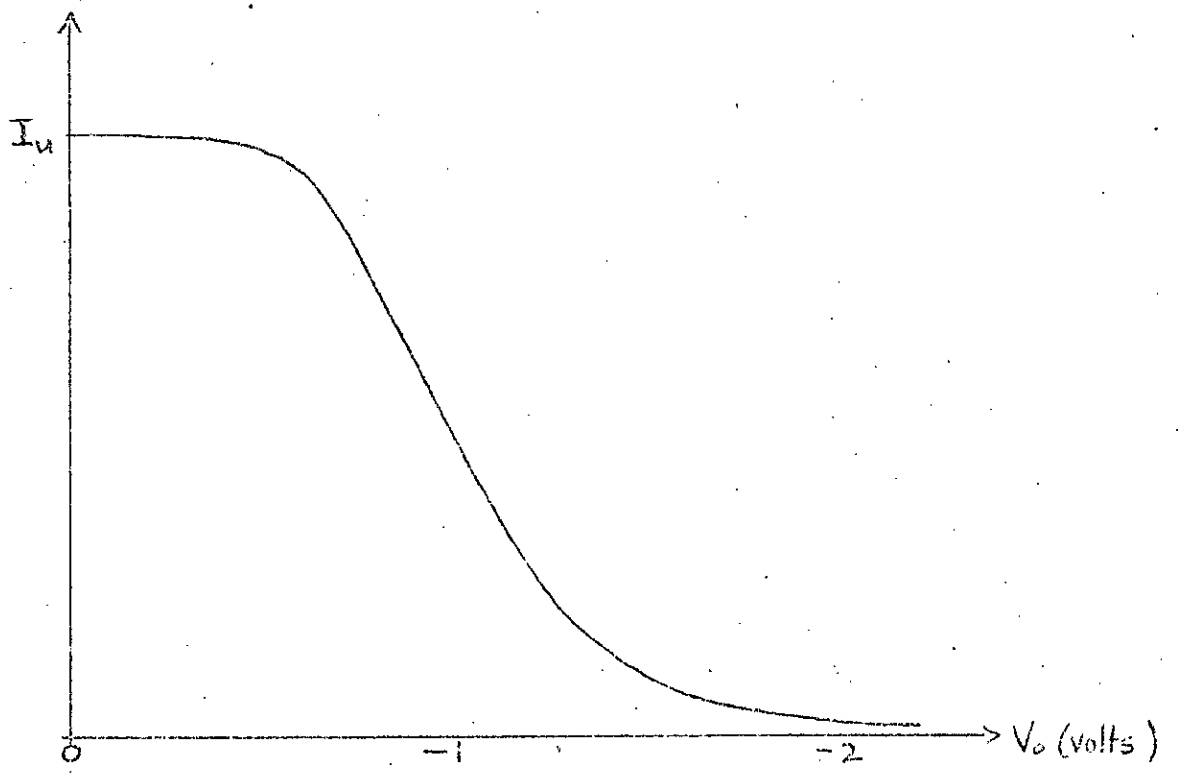

Fig.2.19: Effect of retarding potential V_o on untrapped current I_U.

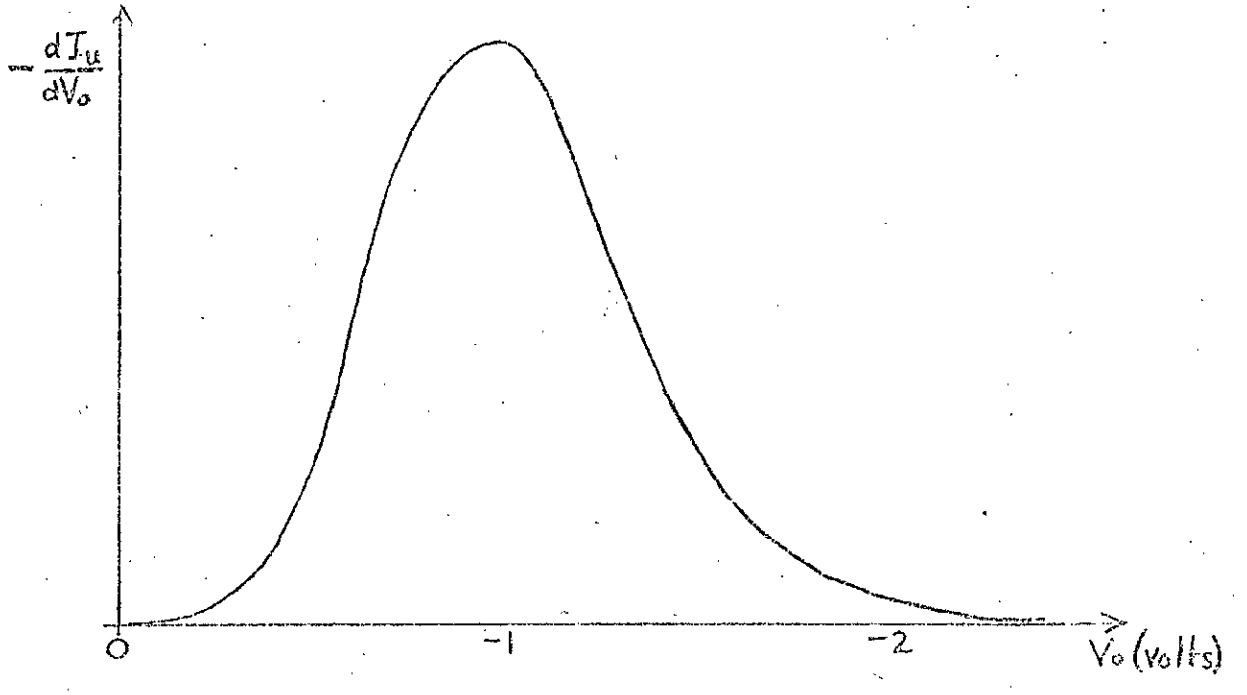

Fig. 2.20: Differentiation of curve in Fig. 2.19.

beam. In these measurements the other two electrodes were maintained at the nominal filament potential.

Since only a small fraction of the electrons emerging from the filament could have thermal energies greater than 0.5eV (corresponding to approximately 2kT), the fact that a retarding potential of over 2 volts appeared necessary to stop the electrons indicated that the region of the filament from which the electrons were principally emitted must be over 1 volt more negative than the nominal applied potential. Such an effect could be ascribed to contact or thermal E.M.F's in the electron gun; the magnitude of the apparent shift certainly increased with the temperature of the filament.

Of more serious consequence in the experimental analysis, was the observation that a more negative potential was required on the central electrode to stop the beam than sufficed on the outer electrodes (see Fig.2.21). This suggested that the potential on the axis at the centre of the trap was more positive than that applied to the central electrode (V_c). Since this electrode was in fact a fairly open structure of two discs with large apertures (Fig.2.4), the field at the centre could have been influenced by the large positive potential (80 volts) applied to the walls of the trap chamber, or by the relatively positive potential V_o applied to the outer electrodes in these measurements. In order to obtain a reasonably accurate estimate of the depth of the axial potential well, it was necessary to disentangle these effects, for although the former would remain unaltered when the electrode potentials

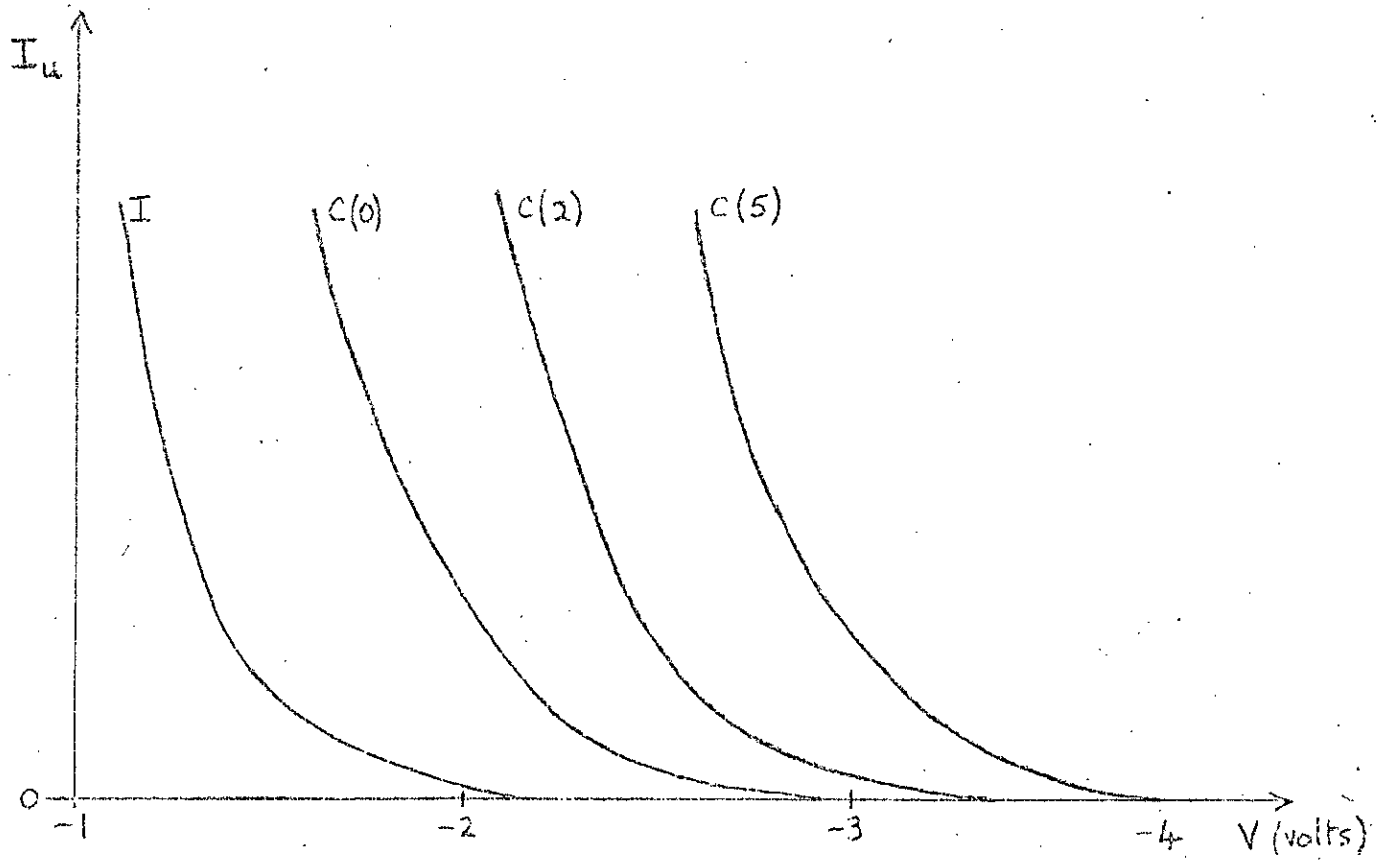

Fig. 2.21: Variation of untrapped current I_U with retarding potential V.

Curve I: $V = V_I$; $V_C = V_o = 0$

Curves C(0), C(2), C(5): $V = V_C$, $V_I = V_o = 0,2,5$.

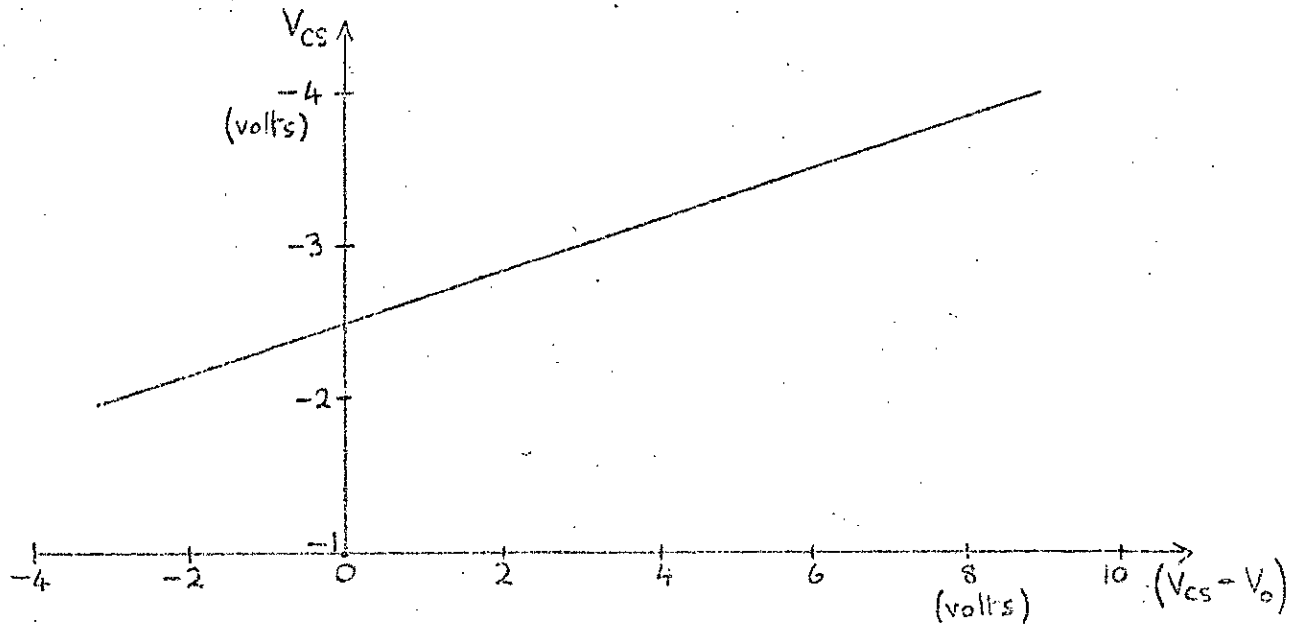

Fig. 2.22: Dependence of central electrode stopping potential V_{CS} on trap depth $V_{CS} - V_o$

were adjusted to create a trapping potential well, the latter would reverse in sign, and its magnitude would be proportional to the nominal trap depth.

To establish separately the magnitude of the effect due to the potential difference ($V_c - V_o$) between central and outer electrodes, the measurement of beam current as a function of central electrode potential was repeated, with the outer electrodes first at +2 volts, then at +5 volts (relative to the filament potential). The results are shown in Fig. 2.21. The potential V_{cs} required to completely stop the beam was plotted in Fig.2.22 against the potential difference $V_{cs} - V_o$; as expected, a linear dependence was found. By extrapolation, it was estimated that if $V_{cs} - V_o$ were equal to zero, the electron beam could have been stopped by a potential of -2.5 volts on the central electrode. In that case, of course, the outer electrodes would be at the same potential, and no correction could be necessary on their account.

The remainder of the discrepancy between the stopping potentials on central and outer electrodes, amounting to about 0.5 volts, was ascribed to the effect of the high potential on the chamber walls. It was then possible to calculate the actual depth of potential well created by a given set of electrode potentials. If, for example, these potentials were

V_I = -2 volts on the input gate,

V_c = +1 volt on the central electrode,

and V_o = -2 volts on the output gate,

further extrapolation in Fig. 2.22 showed that, for $V_c - V_o = 3$ volts, the axial potential at the centre of the trap was made 0.5 volts more negative than V_c by the influence of the outer electrodes. Taking into account also the influence of the potential on the chamber walls, which alone would have raised the axial potential by 0.5 volts, it appeared that in this case the corrections cancelled, and the actual well depth was just

$$D = V_c - V_o = 3 \text{ volts.}$$

If, on the other hand, the potentials on the electrodes were

$$V_I = -1.5 \text{ volts}$$

$$V_c = 0.0 \text{ volts}$$

$$\text{and } V_o = -1.5 \text{ volts,}$$

a similar treatment showed that the actual well depth was given by

$$D = V_c - V_o + 0.3 = 1.8 \text{ volts}$$

General confirmation of these deductions was provided by electrolytic tank and resistance paper plots of the potential distribution near the trap centre (see, for example, Fig. 2.23). More reliance was placed on the measurements quoted above, however, since the changes in potential being studied were only of the order of 0.5% of the potential difference between the central electrode and the vacuum chamber, and there were several possible sources of systematic error of this magnitude in the apparatus available for analogue measurements.

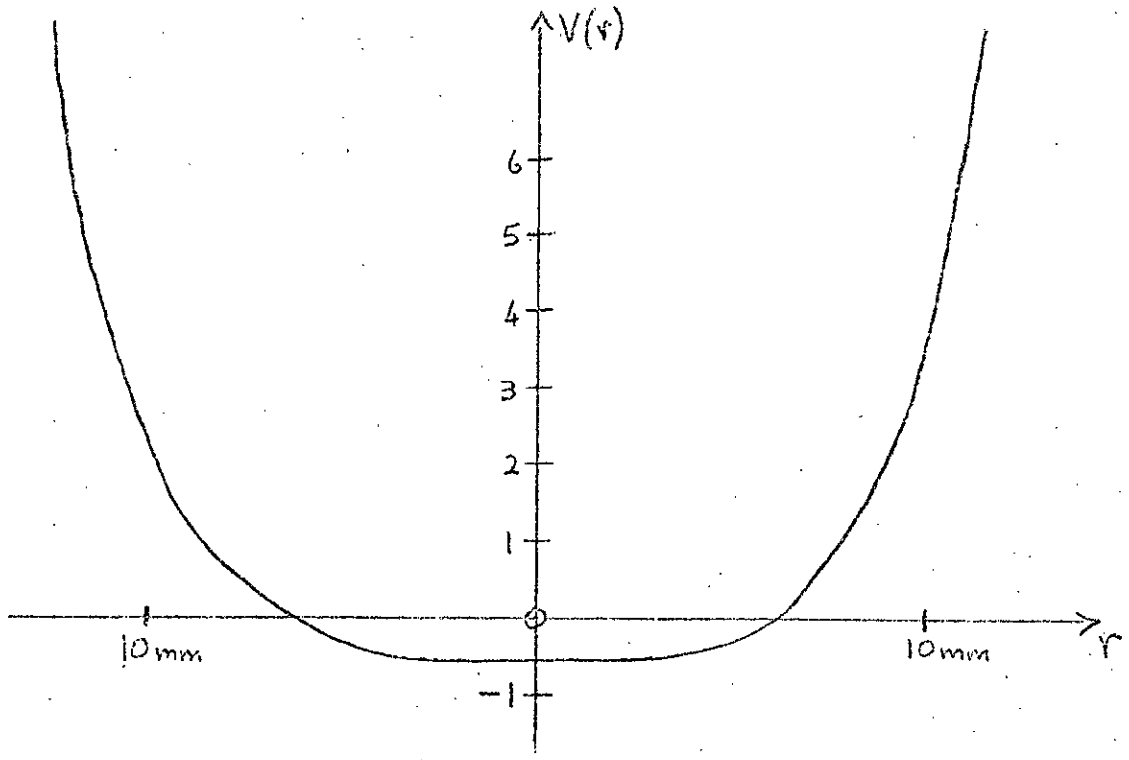

(a): $V_I = V_o = -2$volts; $V_C = -1$ volt

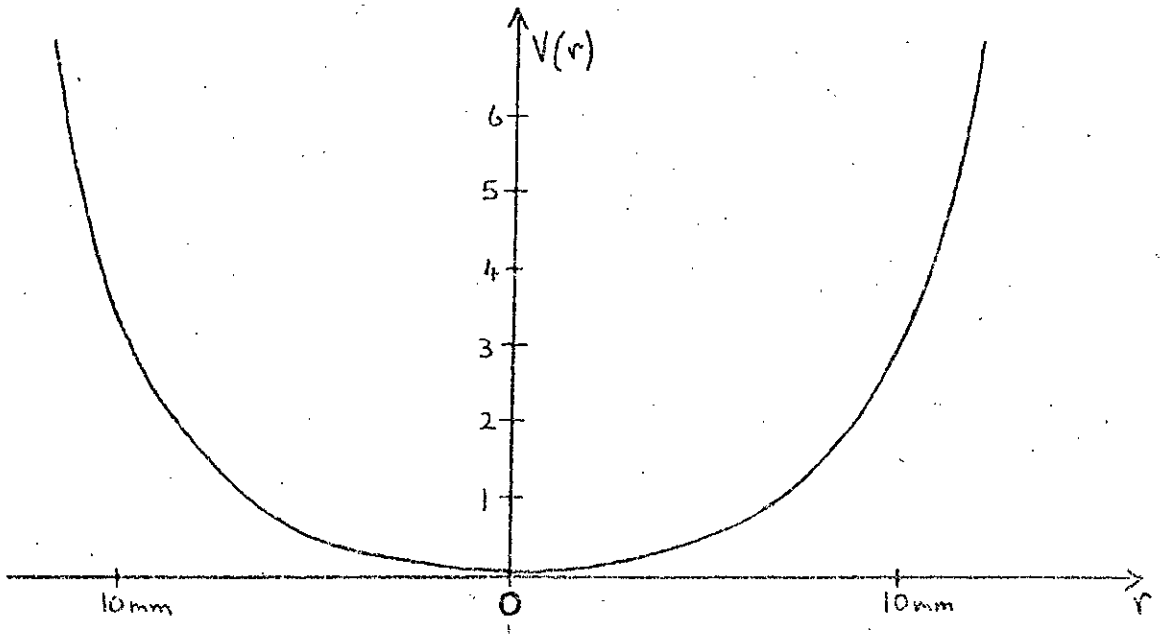

(b): $V_I = V_O = -3$ volts; $V_C = 0$ volts

Fig. 2.23: Resistance paper plots of radial potential variation at $z = 0$, with a potential of +80 volts on the chamber walls ($r = 24$mm)

2.3.3. The Effect of Closing the Input Gate

The measurements displayed in Fig. 2.20 revealed a spread of components of axial momentum in the electron beam passing through the open trap. In order to deduce the range of energy levels in the potential well which would be populated by this beam when the trap was closed, the effect of the change in the input gate potential on the energy of the electrons had to be taken into account. The nature of this effect depended on the rate at which the gate was closed; in the present case, the change was adiabatic, in the sense that the time taken to close the gate was long compared with the period of axial oscillation of a trapped electron.

To estimate the magnitude of the effect, some simplifying assumptions were made. Reverting to the convention that $V = 0$ at the centre of the trap ($z = 0$), it was assumed that at any intermediate stage in the closure of the trap, with a constant potential V_o on the output gate and an instantaneous potential $V_I < V_o$ on the input gate, the potential well was represented by two parabolic curves:

$$V = V_o\left(\frac{z}{z_o}\right)^2 \qquad \text{for} \quad z > 0$$

$$V = V_I\left(\frac{z}{z_o}\right)^2 \qquad \text{for} \quad z < 0$$

(see Fig. 2.24). When the input gate was fully open ($V_I = 0$), an electron emitted from the filament with total energy $E = e\mathcal{E}$ in such a way that it entered the region of uniform magnetic field

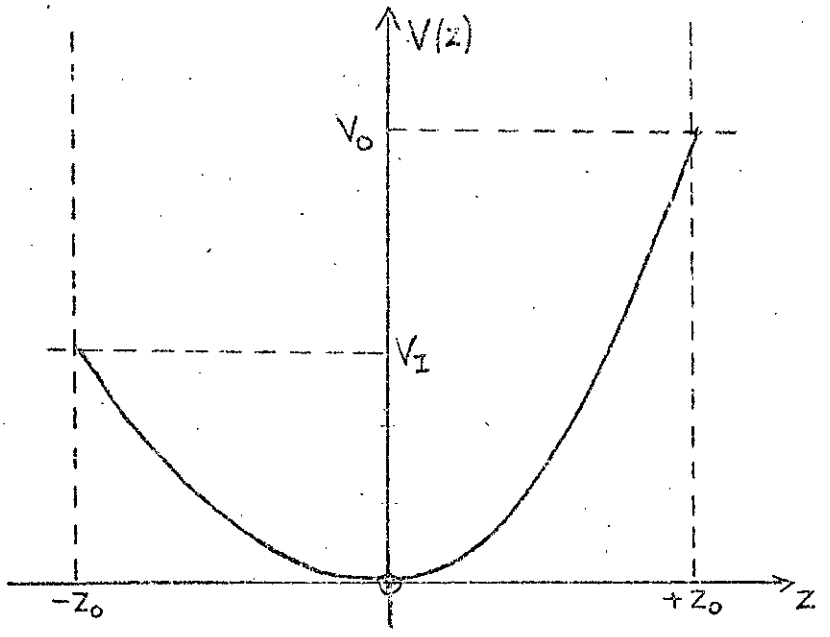

Fig. 2.24: Simplified potential distribution in partly closed trap.

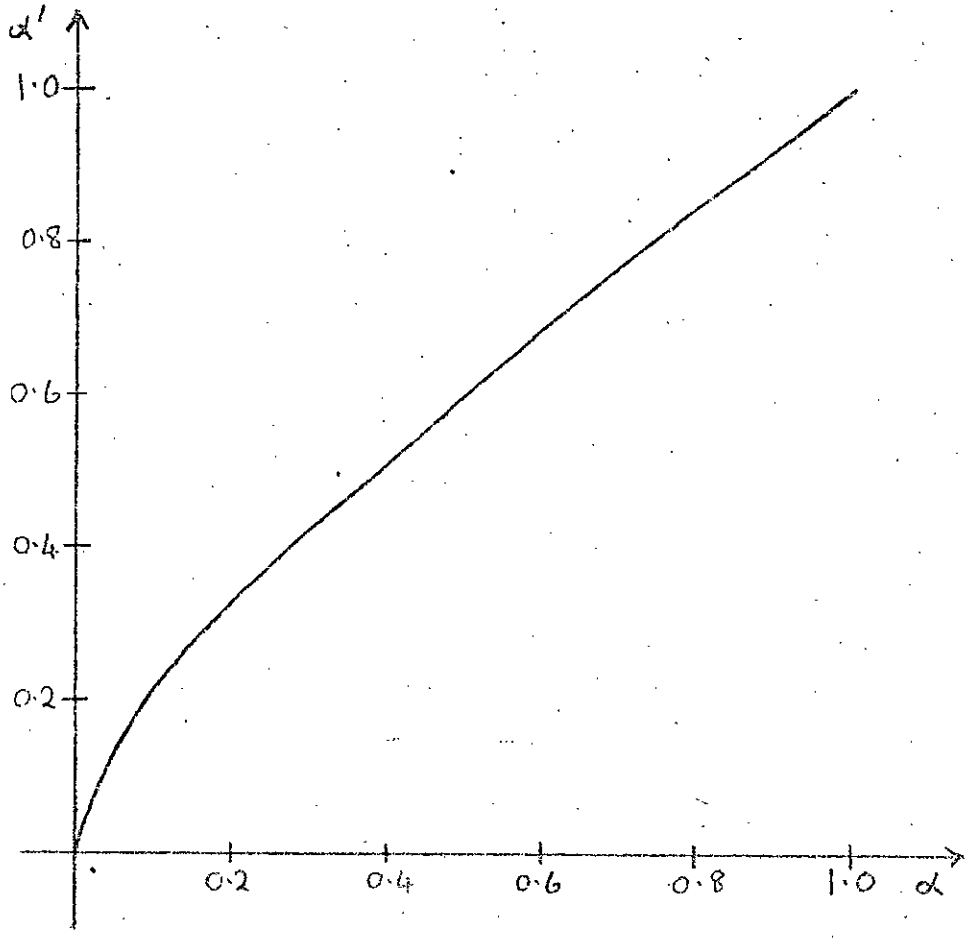

Fig. 2.25: Effect of closure of input gate on relative energy level α.

with purely axial momentum, would be reflected at the output gate if $E < eV_o$ and would oscillate between cathode and output gate. Since in this state it would spend only a small fraction of its time in the neighbourhood of the input gate, it was assumed that the changing potential on this electrode would have a negligible effect on the energy of the electron until it became trapped. This would therefore occur when $V_I = \mathcal{E}$. Subsequent to this, the electron would oscillate in the potential well between input and output gates; a considerable fraction of its time would now be spent in the region of varying potential, so that as the input gate was further closed the total energy of the electron would increase. Under the assumptions detailed above, it was shown (Appendix 1) that when the input gate was completely closed ($V_I = V_o = -D$), the total energy of the trapped electron would have increased to a value

$$E' = e\mathcal{E}' = \tfrac{1}{2} e\mathcal{E}\left[1 + \left(\frac{D}{|\mathcal{E}|}\right)^{\frac{1}{2}}\right] .$$

In terms of the parameter $\alpha = \frac{|\mathcal{E}|}{D}$, describing the total energy as a fraction of the maximum possible total energy for a trapped electron, the final energy level is given by

$$\alpha' = \frac{|\mathcal{E}'|}{D} = \tfrac{1}{2}\left(\alpha + \alpha^{\frac{1}{2}}\right) .$$

This function is plotted in Fig. 2.25; Fig. 2.26 illustrates the effect of the gate closure on a series of originally equally spaced energy levels.

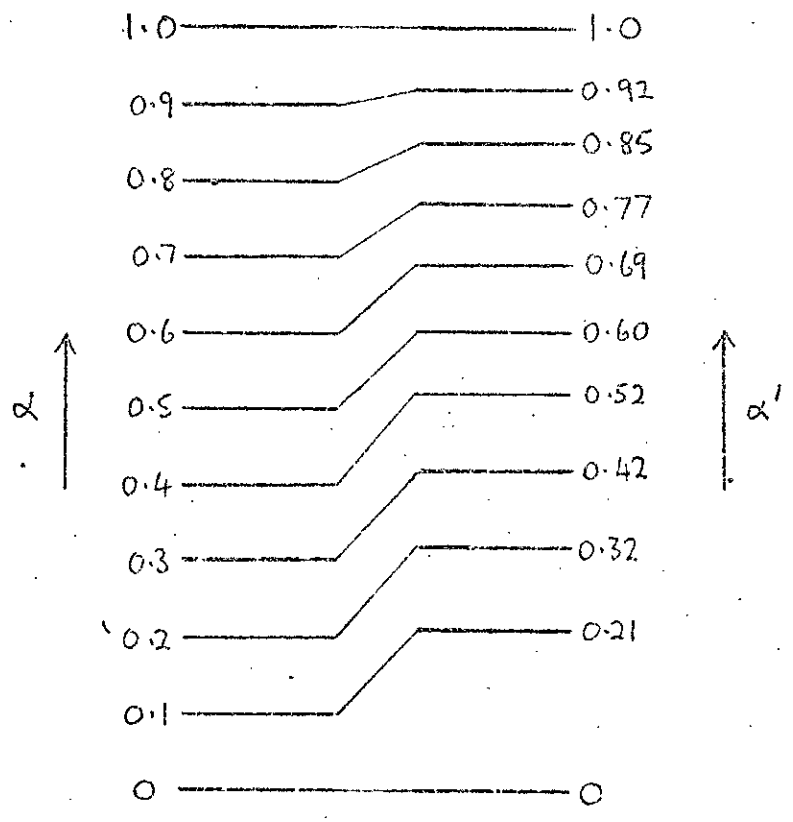

Fig. 2.26: Effect of gate closure on originally equally spaced energy levels.

These considerations were applied to the measured energy level distribution of the untrapped beam, given in Fig. 2.20, in order to predict the resulting spread of energy levels in a trap of depth D = 3 volts. The original distribution is shown as a function of α in curve A of Fig. 2.27; curve B shows the distribution to be expected after the input gate was closed. In this case the electrons may have additional energy associated with transverse momentum, and this must be borne in mind when interpreting these distributions. The average energy of axial motion at the centre of the trap corresponded to $\alpha \simeq 0{\cdot}75$, or $\bar{E} \simeq 2{\cdot}2eV$; transverse motion could increase this somewhat, but since the maximum energy in the trap was 3eV, the change in the average energy could not be large.

2.3.4 Energy Analysis of Trapped Electrons

It was desirable to establish the validity of these predictions by measuring the energy distribution of the electrons in the trap directly. To do this, a method based on that of Graff et al. (1968) was adopted. A negative pulse was applied to the central electrode of the trap at the end of the trapping period, of sufficient magnitude to reduce the trap depth to a fraction μ of its initial value D. All energy levels in the well were raised to some extent, and those above a certain level gained enough energy to escape from the trap. With the central electrode potential maintained at the new value, a small positive pulse was applied to the output gate, releasing electrons in a

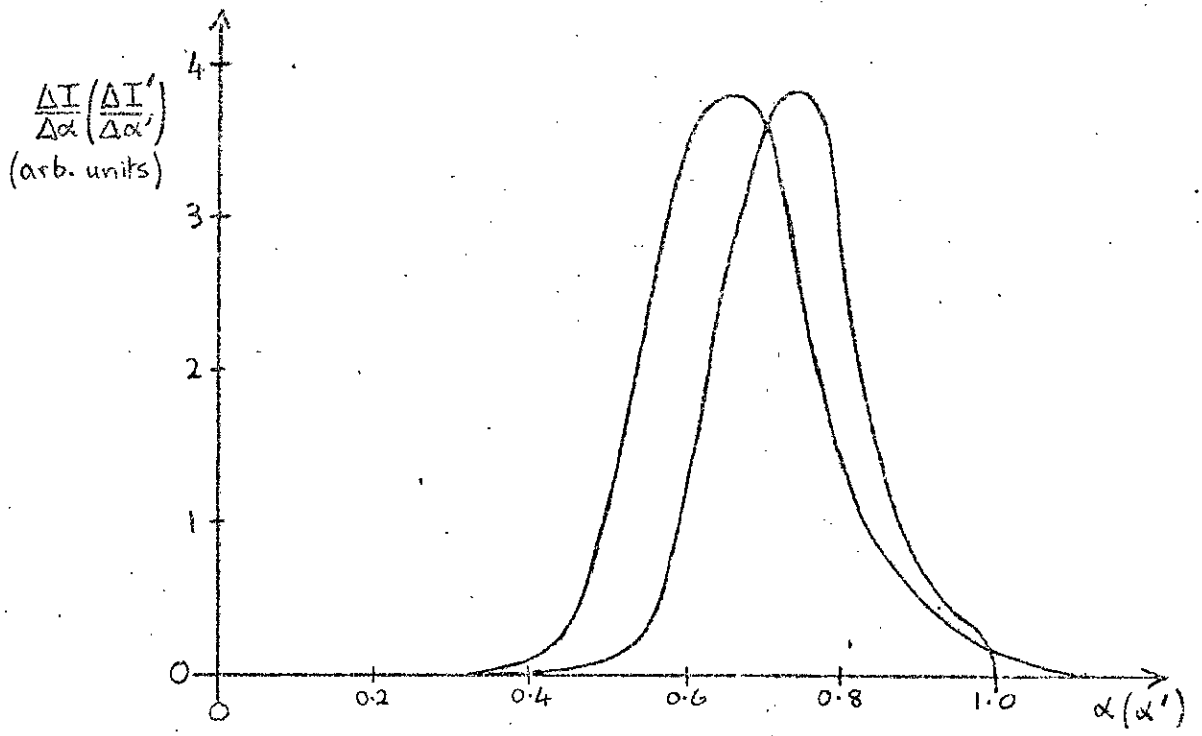

Fig. 2.27: Change in energy level distribution of Fig 20 due to closure of input gate.

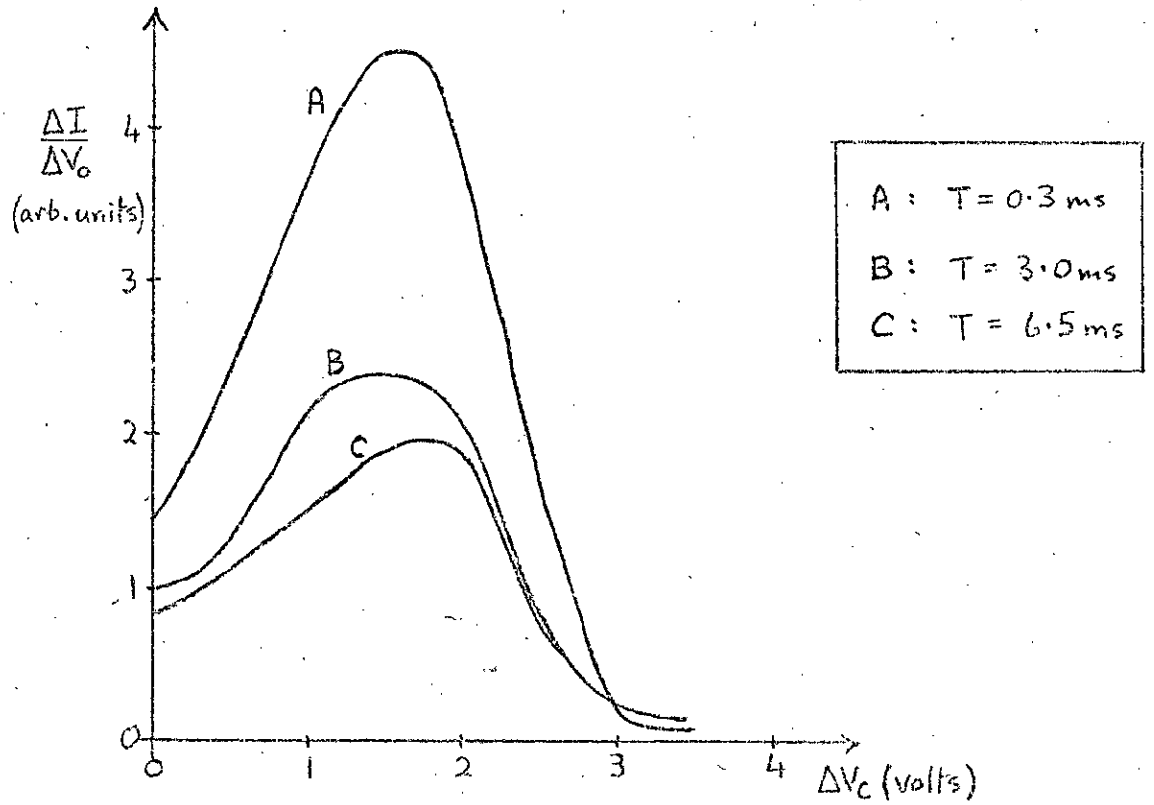

Fig. 2.28: Results of application of pulse V_C to central electrode, followed by pulse V_0 to output gate: well depth = 3·0 volts.

further narrow range of energy levels. Only these latter electrons were counted; by keeping constant the magnitude of the pulse applied to the output gate, and varying the magnitude of the pulse applied to the central electrode, the entire range of energy levels could be scanned.

The results of measurements taken in this way are shown in Fig. 2.28. In this case the nominal trap depth was 3 volts, and ΔV_o = 0.5 volts. The three curves correspond to trapping times of 0.3 ms., 3.0 ms., and 6.5 ms.; the ordinate is proportional to the number of electrons released by the 0.5 volt pulse on the output gate, after the bottom of the well had been raised by a pulse whose magnitude was given by the corresponding abscissa. From the considerations of Section 2.3.2, it was expected that the actual depth of the potential well in this case would not be significantly different from the 3 volt potential difference between central and outer electrodes. The small residue of electrons which were still apparently trapped after the central electrode had been made more negative than the outer electrodes ($\Delta V_c > 3$ volts), may have been retained in the small potential dip at the trap centre, caused by the potential on the chamber walls.

To interpret these curves in terms of the distribution of electron energies in the trap prior to the application of the pulse to the central electrode, it was necessary to consider the effect of these modifications of the potential well on the energy

of a trapped electron. The details of these considerations, which involved approximations similar to those of the previous section, are given in Appendix 2; only the results are presented here. It was found that if the pulse applied to the central electrode reduced the trap depth from D volts to μD volts, an electron whose energy level in the original well corresponded to

$$\beta = \frac{|\mathcal{E}|}{D}$$

would be raised to a level $\mathcal{E}'$ volts above the bottom of the new well, where

$$\mathcal{E}' = \mu^{\frac{1}{2}} \mathcal{E}.$$

Expressing $\mathcal{E}'$ as a fraction of the new trap depth $D' = \mu D$, the new energy level corresponded to

$$\beta' = \frac{\mathcal{E}'}{D'} = \frac{\mu^{\frac{1}{2}} |\mathcal{E}|}{\mu D} = \mu^{-\frac{1}{2}} \beta.$$

An electron at a level β in the original trap would be released from the trap by the pulse on the central electrode, if the corresponding $\beta' \geq 1$. Thus all electrons whose original energy levels were above that for which

$$\beta = \beta_1 = \mu^{\frac{1}{2}}$$

would be ejected from the trap.

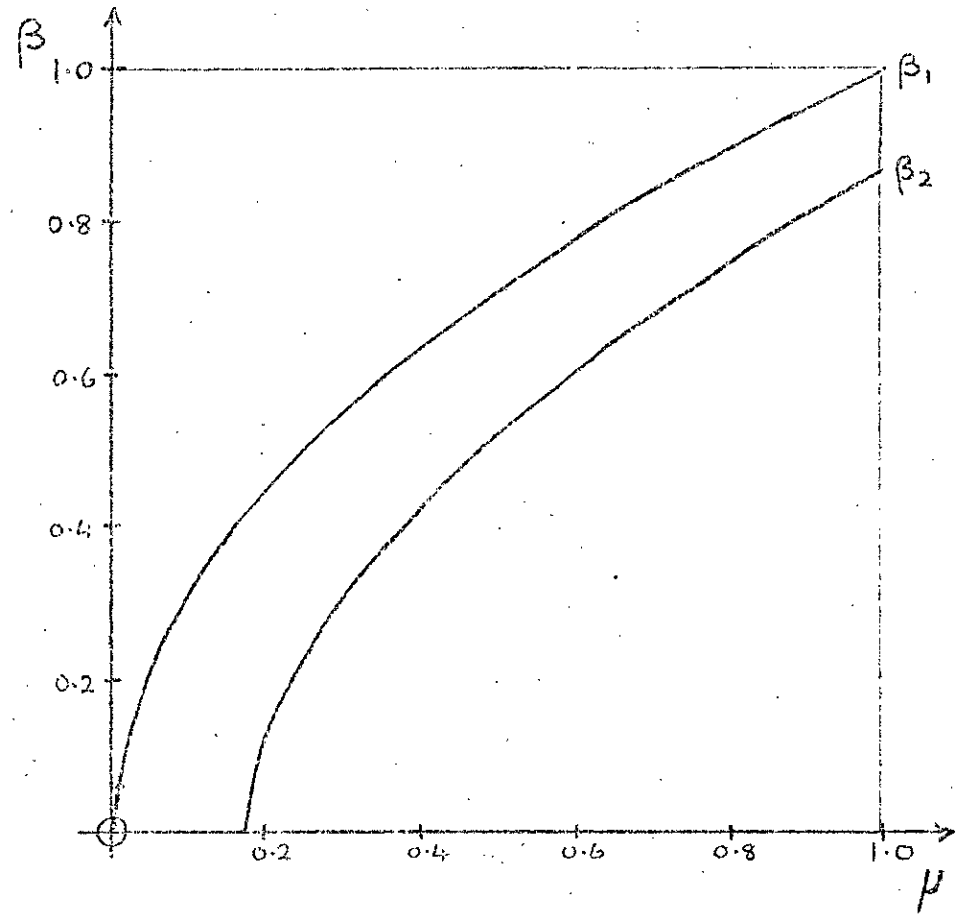

Fig. 2.29: β_1 and β_2 versus μ, for $\delta = 0.17$

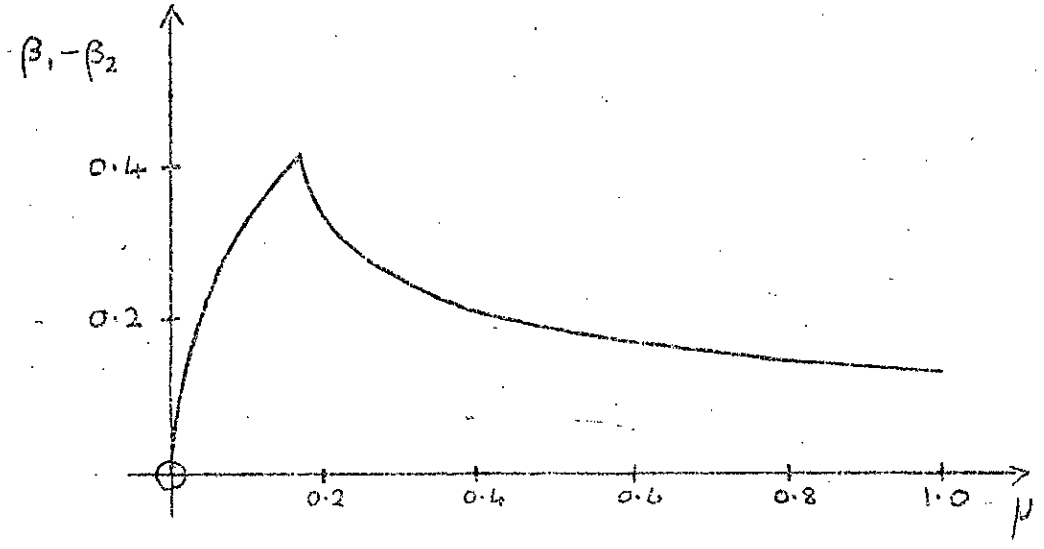

Fig. 2.30: $\beta_1 - \beta_2$ versus μ, for $\delta = -0.17$.

If the output gate were subsequently partially opened by a pulse of amplitude

$$\Delta V_o = \delta D ,$$

electrons would be released if their energy levels in the original trapping well were above that for which

$$\beta = \beta_2 = \frac{1}{2}\left[\frac{\mu - \delta}{\mu^{1/2}} + (\mu - \delta)^{1/2} \right].$$

For the measurements shown in Fig.2.28, in which D = 3 volts and ΔV_o = 0.5 volts, δ = 0.17. In Fig. 2.29, β_1 and β_2 are shown as a function of μ for this case. The width of the range of energy levels ($\beta_1 - \beta_2$) released by the pulse δD on the output gate, after the application of the pulse μD to the central electrode, was clearly dependent on μ ; this dependence is shown explicitly in Fig. 2.30.

The results given in Fig. 2.28 were reinterpreted on the basis of these considerations, to give the energy distributions over the levels of the original trap shown in Fig. 2.31. Each measured point is now represented by a bar, the length of which gives the range of energy levels released in each measurement. The ordinate is proportional to the number of electrons counted per unit range of energy levels. The curves are drawn so as to be consistent with the averages implied by the bars; they are not unique in this respect, and are merely intended to indicate the probable outline of the energy distributions. In all the

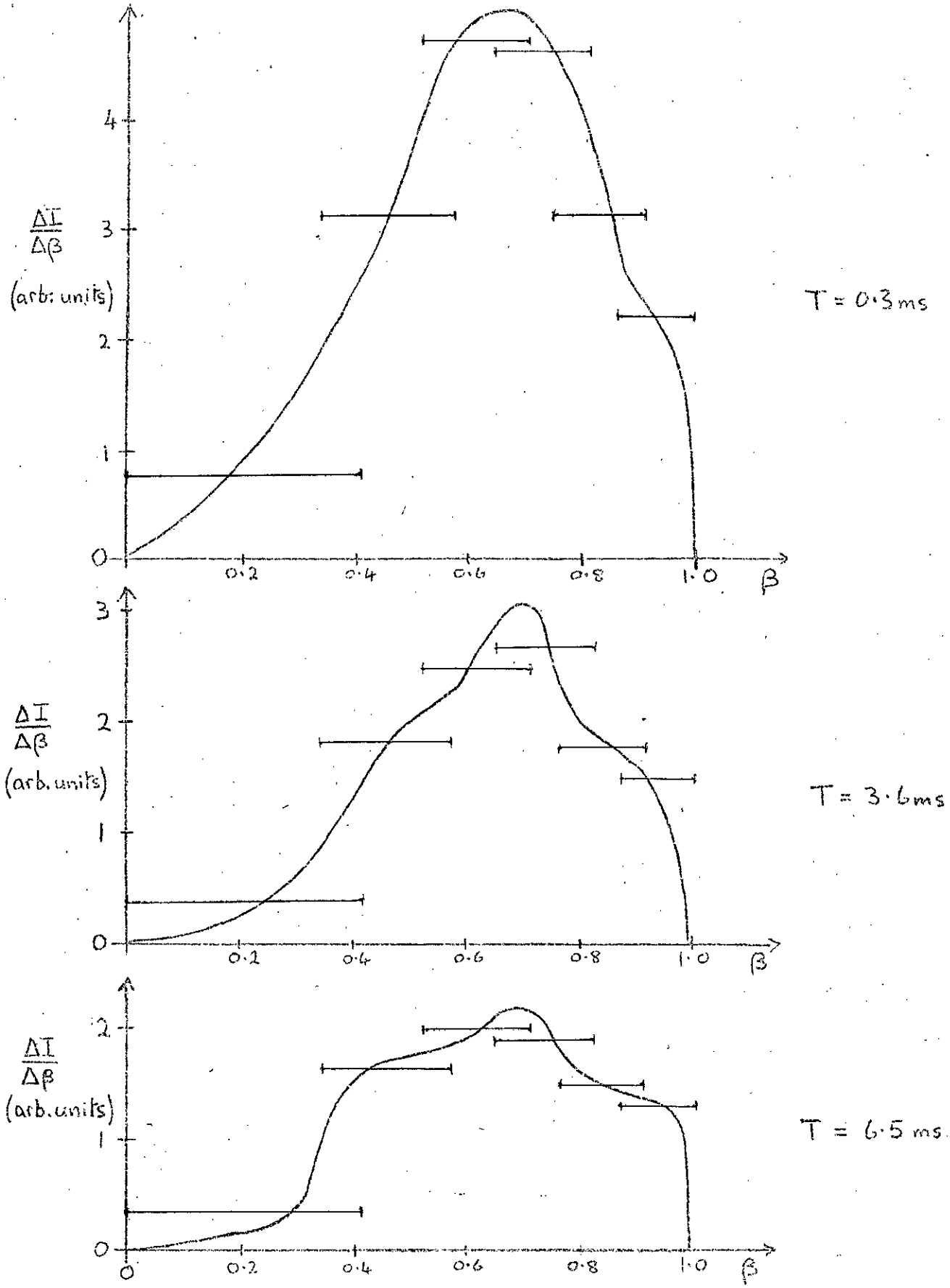

Fig. 2.31: Distribution of electron energy levels in well of depth 3·0V, derived from Fig. 2.28.

distributions, a maximum is apparent around $\beta = 0.7$, as suggested by the measurements on the untrapped beam. From the broad range of energy levels occupied in the trap, it was only possible to draw the conclusion that the average value of $e\mathcal{E}$ in the trap was

$$e\bar{\mathcal{E}} \simeq 2\,eV;$$

taking into account the additional kinetic energy associated with the transverse momentum of the electrons, the average kinetic energy at the centre of the trap was probably somewhat nearer to 3eV.

It was not found possible, in practice, to carry out an energy analysis in the manner previously described, if the amplitude of the pulse applied to the output gate was reduced below 0.5 volts. The principal limiting factor was the decrease in current as the width of the "window" was reduced. This made the method unsuitable for analysis of the energy distribution in a potential well only 1.8 volts deep. In the latter case, a modified scheme was adopted, in which, after the negative pulse had been applied to the central electrode, a pulse of +3 volts amplitude was applied to the output gate, and all the remaining electrons in the trap were ejected and counted. The curve shown in Fig. 2.32 was obtained in this way; from it, the energy distribution of Fig. 2.33 was deduced. The peak of the distribution was fairly low in this well, and the average value of was estimated to be

$$e\bar{\mathcal{E}} \simeq 0.6\,eV.$$

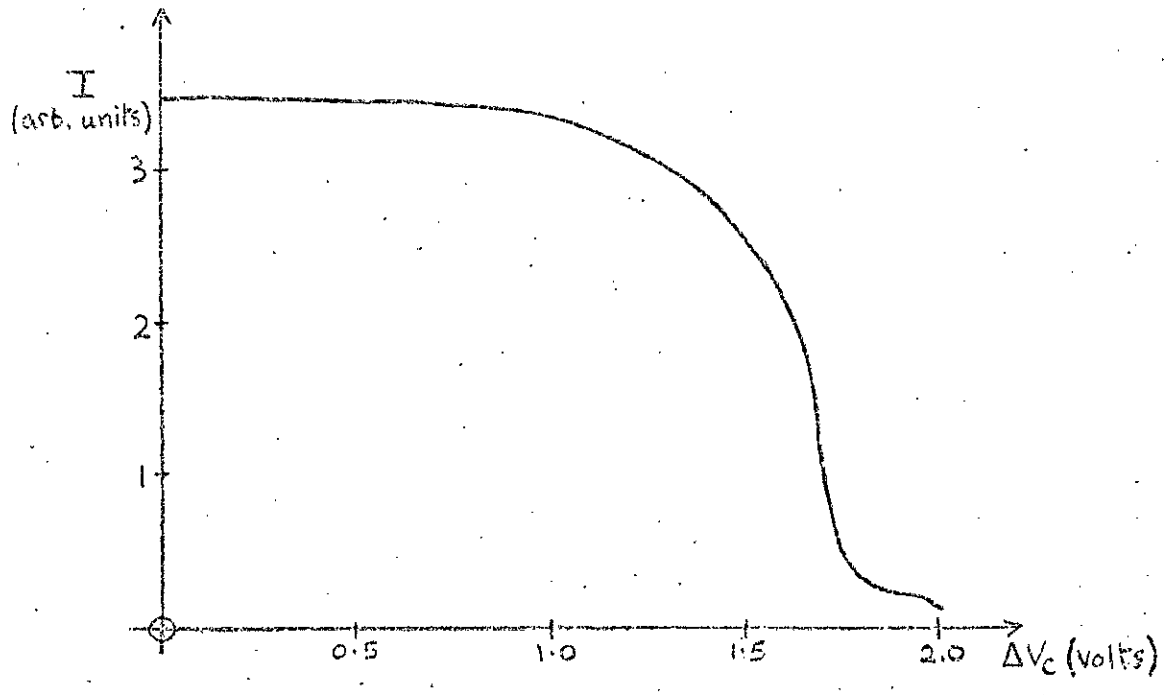

Fig. 2.32: Analysis of output from well of depth 1·8 volts.

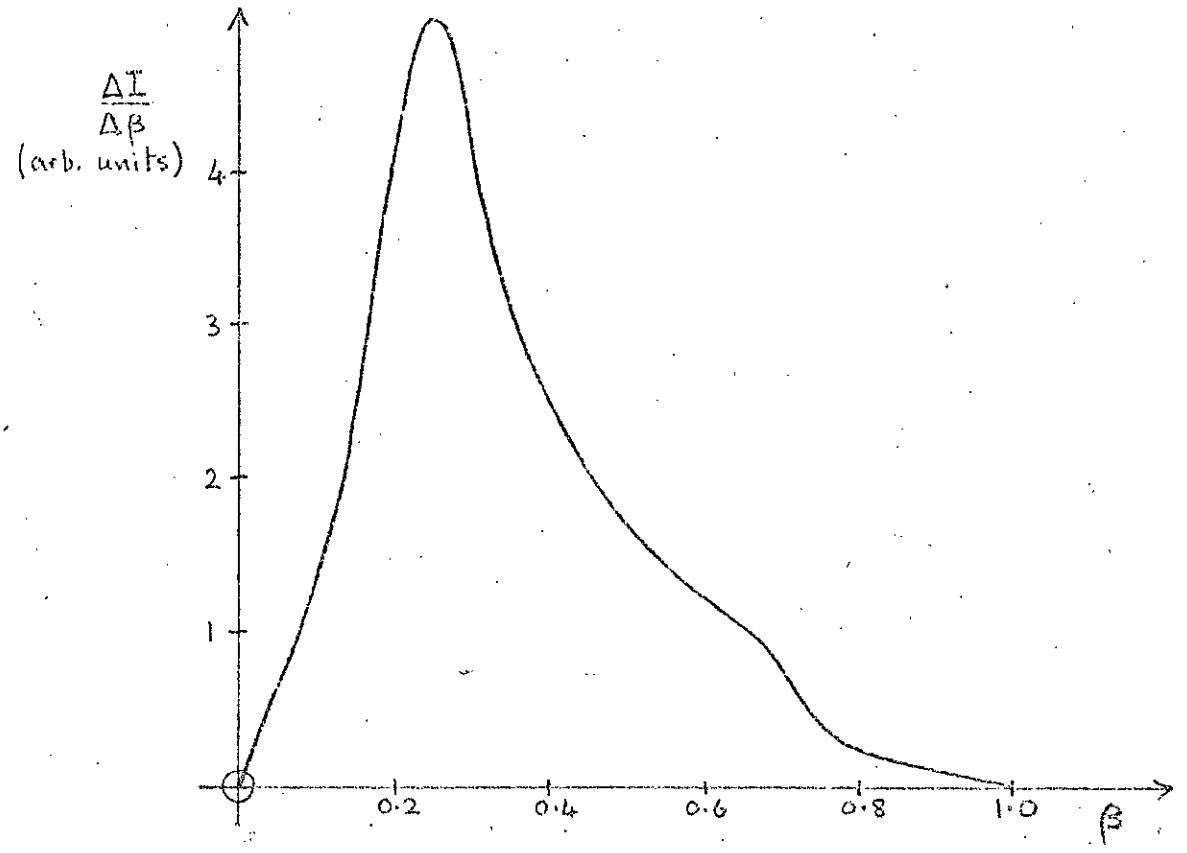

Fig. 2.33: Energy level distribution in well of depth 1·8 volts, derived from Fig. 2.32.

As in the previous case, energy of transverse motion would increase the average total energy, but it seemed probable that the average electron kinetic energy at the centre of the trap did not exceed 1 eV.

The spread in energy of electrons in the trap was perhaps best expressed by noting that over 75% of the electrons were found between levels of 1.2 and 2.7 volts in the 3 volt deep well (a range of 1.5 volts), and between 0.2 and 1.0 volts in the 1.8 volt deep well (a range of 0.8 volts). The breadth of these energy distributions allowed only a qualitative investigation of the energy dependence of the spin exchange cross-section (see Sect. 4.2). In terms of the use of the apparatus as a source of polarised electrons in further experiments, however, it may be remarked that for many experiments at somewhat higher energies, an energy resolution of under 1 volt would be quite acceptable.

2.4. LOSS OF ELECTRONS FROM THE TRAP.

2.41 Theoretical Discussion

In principle, electrons could be trapped for an indefinite time without loss in the combination of electric and magnetic fields described in Section 2.2. In practice, the maximum usable trapping time was limited by a gradual decrease in the number of trapped electrons. Measurements of the rate of this decrease are given in Section 2.42; in this section, possible causes are discussed.

In considering the loss of electrons from the trap, it is assumed that, if the radial distance from the axis of a trapped electron exceeds some limiting value R_o, the electron will be

lost, in the sense that it will not form part of the pulse of electrons extracted from the trap. The limiting radius R_o may be simply the internal radius of the cylinder forming the output gate electrode, or it may be the radius of a virtual aperture determined by the conditions governing the extraction of electrons from the trap.

Effects arising from relative misalignment of the axes of symmetry of the electric and magnetic fields in the trap were investigated theoretically by Byrne (1969). He found that such a misalignment resulted in the electrons acquiring a radial drift velocity proportional to the degree of misalignment:

$$v_{DRIFT} = -6z\omega_p \theta \sin\phi ,$$

where z and ω_p are electron axial displacement and precession frequency, as defined in Section 2.1.1, ϕ is the azimuthal angle, and θ is the angle of misalignment. Since $z = z_0 \cos\omega_z t$, the drift velocity changes sign every half period of the axial oscillation in the trap; the radial displacement is thus also an oscillatory function, with maximum amplitude

$$\Delta R = 12\theta z_0 \left(\frac{\omega_p}{\omega_z}\right).$$

For the trap previously described in Section 2.1.3, in which

$$z_0 < 8\times10^{-3}\ m, \quad \omega_p = 5\times10^6\ s^{-1}, \text{ and } \omega_z = 10^8\ s^{-1},$$

$$\Delta R < 5\times10^{-3}\theta\ m.$$

A misalignment of 1°, corresponding to $\theta = 0.02$ radians, will result in a maximum radial displacement of 10^{-4}m. It is clear that the diameter of the trapped electron cloud would not be significantly increased by this effect, unless a substantial and unsuspected degree of misalignment had occurred.

The effect of elastic electron-atom collisions on the directional distribution of electron momenta in the trap has already been mentioned (Section 2.3.1). If a trapped electron has a transverse momentum p_t, it will perform cyclotron orbits of radius:

$$r = \frac{p_t}{eB} ;$$

let the guiding centre of these orbits be a radial distance R from the trap axis. As the result of an elastic collision with an atom (assumed infinitely massive), R may be increased or decreased by up to $2r$, depending on the point in the orbit at which the collision takes place, and on the direction of the electron's velocity after the collision. The average transverse momentum of an electron, after a large number of such collisions, will depend not only on the total energy E of the electron, but also on the axial distribution of the collision probability; if the collisions all occurred at the centre of the trap, the total energy $E = p^2/2m$ would be equally shared among the three degrees of freedom of translational motion, so that

$$\frac{\langle p_t^2 \rangle}{2m} = \frac{2}{3}E .$$

The mean square radius of the cyclotron orbits would then be

$$\langle r^2 \rangle = \frac{\langle p_t^2 \rangle}{e^2 B^2} = \frac{4mE}{3e^2B^2}. \qquad 2.6.$$

The mean square displacement, in the plane perpendicular to the z axis, of the guiding centre of the cyclotron orbit as the result of a collision will be

$$\langle \Delta^2 \rangle \simeq \langle r^2 \rangle \ldots$$

As a consequence of these collisions, electrons will diffuse radially outwards from the axis, and those passing the limiting radius R_o will be lost. The rate of loss to be expected from this cause may be derived by solving the two-dimensional diffusion equation

$$\frac{\partial n}{\partial t} = D \nabla^2(r,\theta)\, n ,$$

where n is the electron concentration, and D the diffusion coefficient. For the case of two dimensional diffusion, D is given by

$$D = \frac{\nu_c}{4} \langle \Delta^2 \rangle \simeq \frac{\nu_c}{4} \langle r^2 \rangle ,$$

where ν_c is the average frequency with which a given trapped electron suffers a collision. The nature of the solution of the diffusion equation depends on the assumed initial and boundary

conditions on the electron distribution. In Appendix 2, the idealised case is considered in which the original radial electron distribution is a delta function centred on $r = 0$. It is shown there that the fraction of electrons remaining in the trap after a time t is given by

$$f(t) = 1 - e^{-R_0^2/4Dt}$$

$$= 1 - e^{-\frac{\nu_c}{t}\cdot\frac{\langle r^2\rangle}{R_0^2}}$$

The function $f(t)$ is shown in Fig. 2.34. The time taken for the population of electrons in the trap to decrease to half of its initial number is

$$T_{1/2} = \frac{1\cdot 44}{\nu_c}\,\frac{R_0^2}{\langle r^2\rangle}\,.$$

In a potential well of depth 1.8 volts, with an axial magnetic field of 6×10^{-3} T, the maximum electron energy corresponds to a mean square cyclotron orbit radius

$$\langle r^2\rangle_{max.} \simeq 4 \times 10^{-7}\ m^2.$$

For a limiting radius $R_0 = 3 \times 10^{-3}$ m (the internal radius of the gate electrodes),

$$\frac{R_0^2}{\langle r^2\rangle_{max.}} \simeq 23\ ;$$

$$\therefore T_{1/2} \gtrsim 33\,\nu_c^{-1}\ s.$$

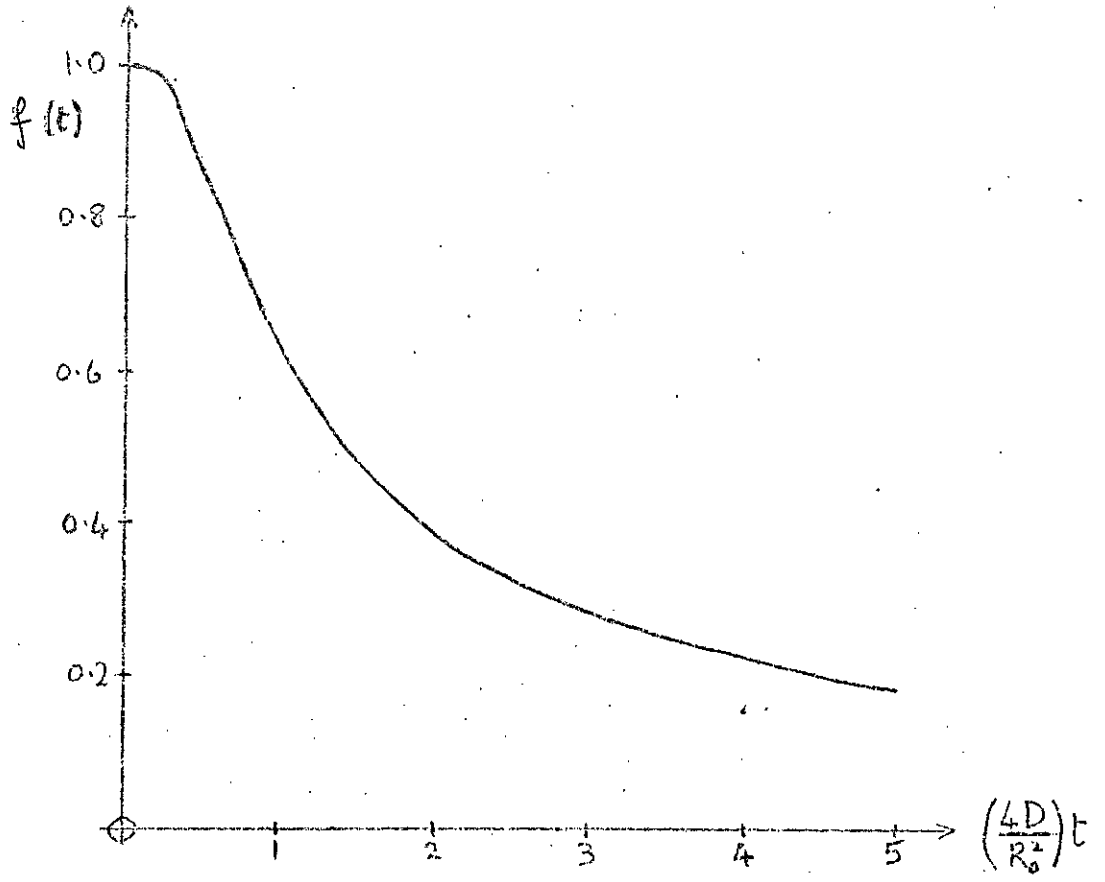

Fig. 2.34: Fraction $f(t)$ of electrons remaining in trap after time t.

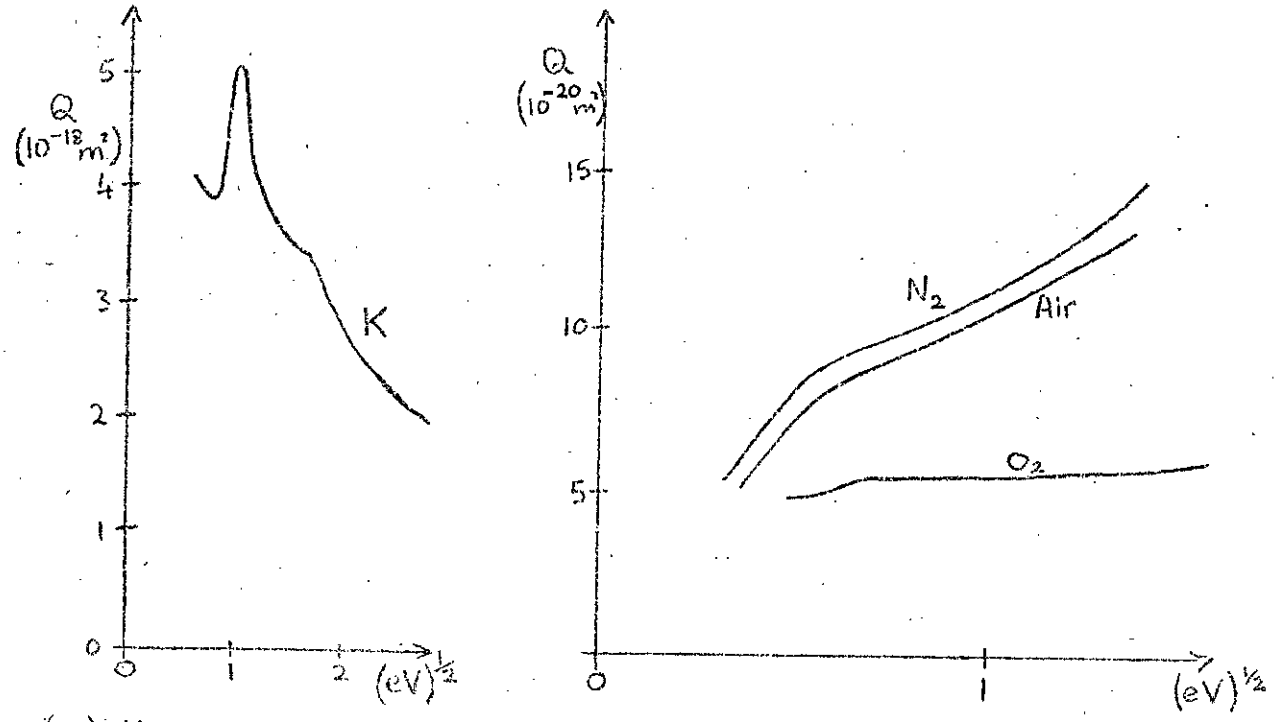

(a): Massey and Burhop, p30. (b): Hasted, p.179.

Fig. 2.35: Total electron collision cross-sections.

The trapped electrons may collide either with atoms in the atomic beam, or with atoms of the residual gas. If the corresponding collision frequencies are ν_B and ν_R respectively, then

$$\nu_c = \nu_B + \nu_R .$$

The normal density of the potassium beam was $\sim 3 \times 10^{14}$ atoms m^{-3}, and the width of the interaction region $\sim$ 4mm; the total cross-section for potassium-electron collisions at an electron energy of 1.8eV is $\sim 5 \times 10^{-18}$ m^2 (see Fig. 2.35), so that

$$\nu_B \simeq 3.5 \times 10^{-6} \omega_z \simeq 350\ s^{-1}.$$

If the residual gas pressure were low enough so that $\nu_B \gg \nu_R$, the diffusion of the electrons would be characterised by a time

$$T_{1/2} \gtrsim 100\ ms$$

From Equation 2.6, $\langle r^2 \rangle \propto E$. The diffusion rate might therefore be expected to increase with increasing trap depth. However, ν_c is proportional to the collision cross-section, which is also energy dependent. For example, if the trap depth were increased to 4.5 volts, so that the maximum electron energy was increased by a factor 2.5, the corresponding cross-section would be reduced by a factor 1.5; the diffusion rate would therefore only increase by a factor 1.7.

2.4.2 Measurements of Trapped Current as a Function of Trapping Time

The most striking fact to emerge from an experimental investigation of the loss of trapped electrons was that the rate of loss appeared to be unaffected by whether or not the atomic beam was passing through the trap. The curves in Fig.2.36 show the average trapped current as a function of trapping time for several different trap depths, with an atomic beam passing through the trap; in each case, measurements were also made with the atomic beam shut off, and the resulting curves were not significantly different. This implied that, if radial diffusion were indeed the dominant mechanism for electron loss, collisions must occur predominantly with residual gas atoms. The theoretical considerations of the previous section showed that a collision frequency $\nu_B \simeq 350\ s^{-1}$ with beam atoms would correspond to $T_{1/2} \gtrsim 60$ ms in a trapping well of depth 4.5 volts; the situation revealed by curve B in Fig. 2.36, for which $T_{1/2} < 6$ms, required a collision frequency ν_R at least an order of magnitude greater than ν_B .

Estimation of ν_R was difficult, since the nature and partial pressures of the constituents of the residual gas were not known. Measurement with an ionisation gauge indicated a total pressure in the trap of the order of 10^{-7} Torr, corresponding to a number density of residual gas atoms of $\sim 3 \times 10^{15}$ atoms m^{-3}. This was an order of magnitude greater than the atomic beam number density; however, if the residual gas is assumed to be composed

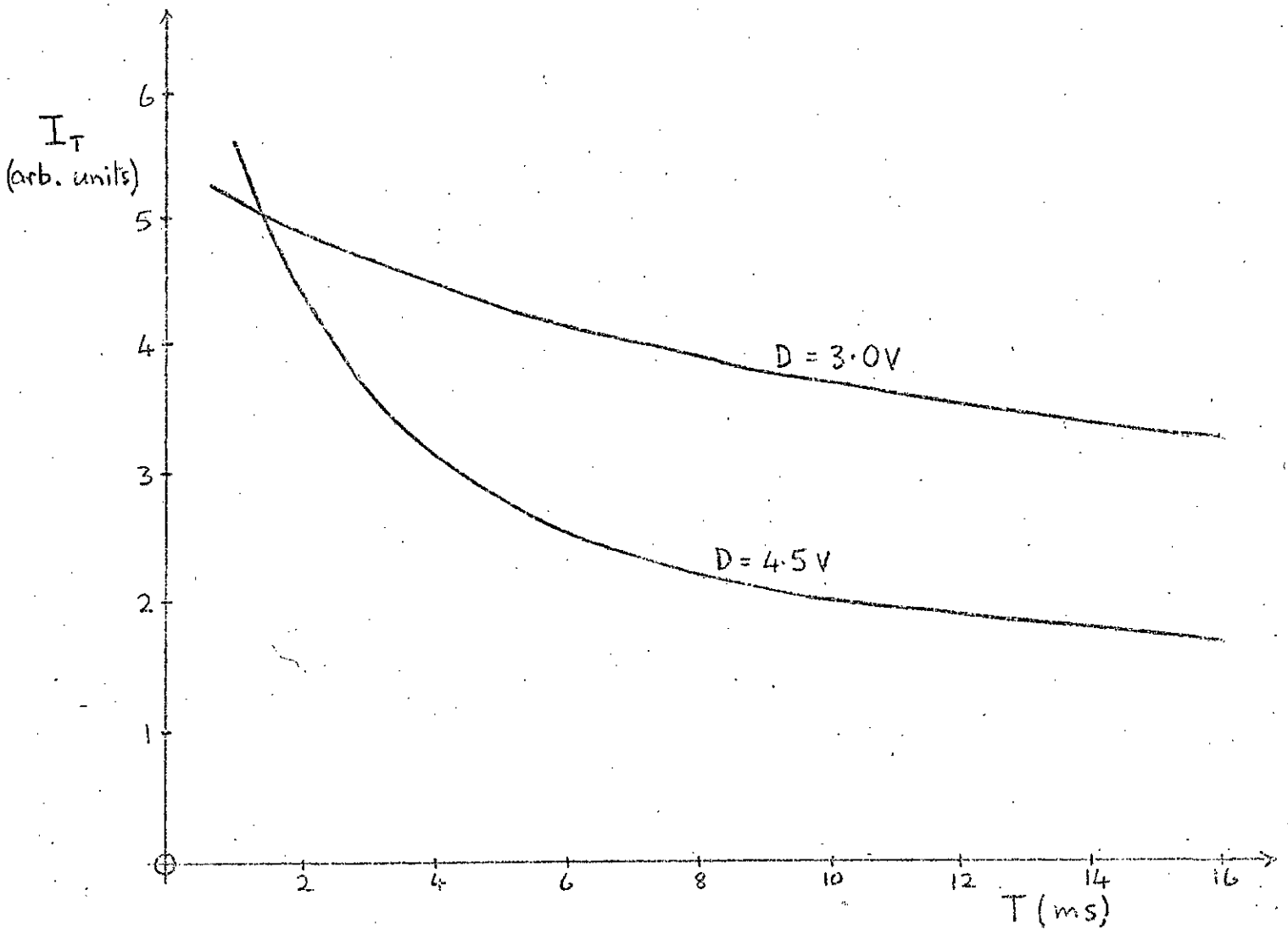

Fig. 2.36: Trapped electron current I_T versus trapping time T: well depths 3·0 and 4·5 volts.

of atmospheric proportions of oxygen and nitrogen, the cross-section in the relevant energy region is smaller than that of potassium by a factor of about 40 (see Fig. 2.35). When the increase in the length of the interaction region is taken into account, a collision frequency $\nu_R \simeq \nu_B$ could be explained. The fact that the collision rate with the residual gas appeared to be an order of magnitude greater than expected might be due either to an underestimate of the pressure in the trap, or to the presence of an appreciable density of molecules of large cross-section due to backstreaming from the (oil) diffusion pumps.

In general, the trend towards increasing diffusion rate with increasing trap depth was observed. The measurements on a potential well of 1.8 volts depth showed some curious features: three typical examples are shown in Fig. 2.37. Normally, the usual pattern of increasing loss with increasing trapping time was found, as shown in curve A; on occasion, however, it appeared that more electrons were extracted from the trap after a long trapping time than after a brief confinement, as evidenced by curves B and C. Presumably the losses were in such cases being masked by larger variations in either injection or extraction efficiency; the explanation might lie in the fact that the energy distribution of the trapped electrons changes with increasing trapping time.

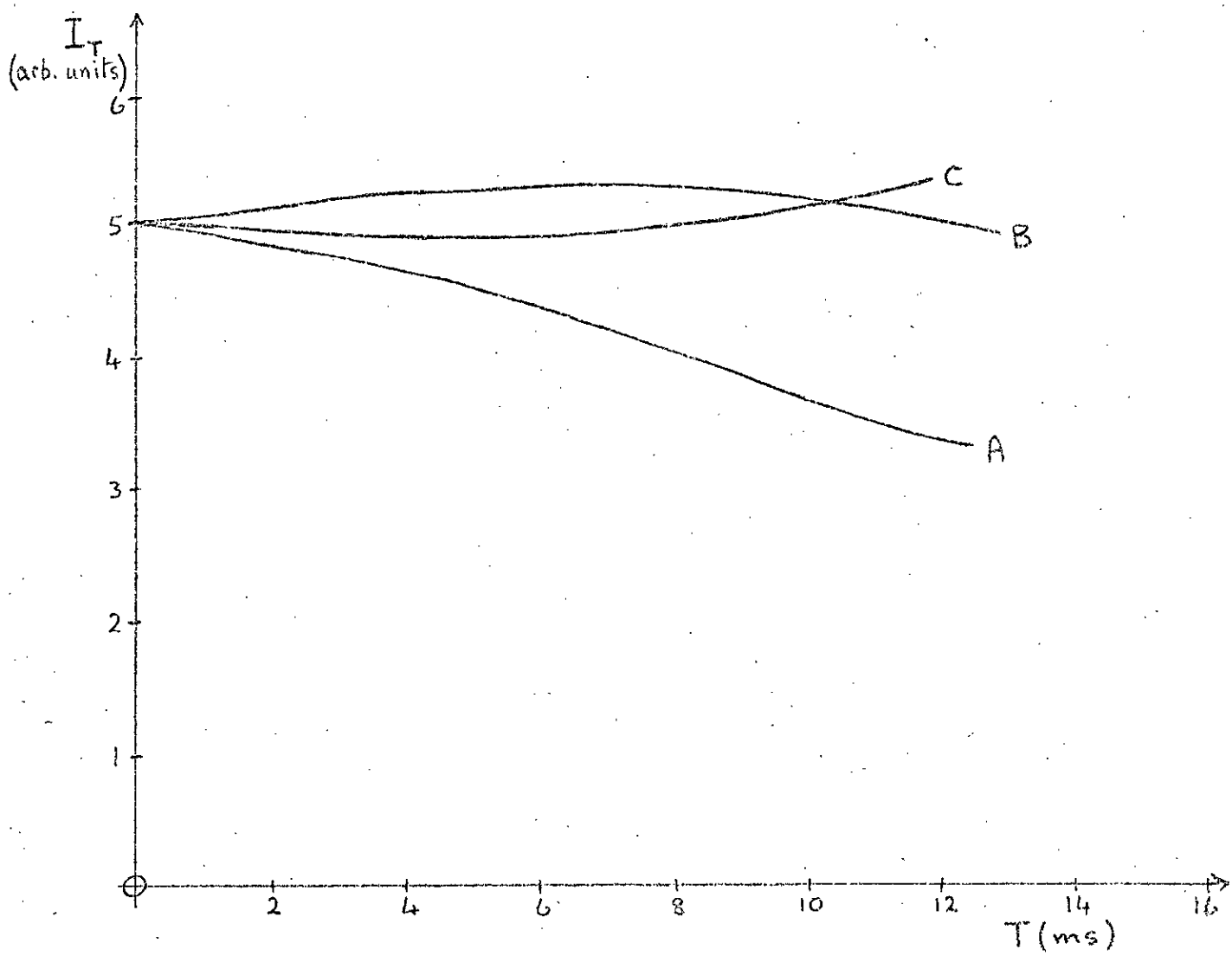

Fig. 2.37: Trapped electron current I_T versus trapping time T: well depth 1·8 volts.

CHAPTER 3

INTERACTION BETWEEN TRAPPED ELECTRONS AND A POLARISED ATOMIC BEAM

3.1. THE ATOMIC BEAM

3.1.1. Properties of the six-pole magnet.

The early experiments of Stern and Gerlach (Stern, 1921; Gerlach, 1924) established the feasibility of producing a highly polarised beam of atoms by passing them through a region of strong magnetic field gradient transverse to the beam. If the atoms have a magnetic moment μ, they will experience a deflecting force

$$F = \pm \mu VB$$

an atom whose magnetic moment is aligned with the magnetic field will be deflected in one direction, and one whose magnetic moment is antiparallel to the field will be deflected in the opposite direction. By insertion of suitable apertures, it is possible to achieve almost 100% polarisation of the output beam.

The principal disadvantage in using a straightforward dipole magnet of the Stern-Gerlach type (Fig. 3.1) is that the collimation necessary in order to totally exclude one spin state results in a rather low transmission. Much more intense polarised beams can be produced by using a magnetic field of the "six-pole" type (Fig. 3.2). In this type of field the magnetic field gradient VB is proportional to the radial distance r from the symmetry axis, and is in the direction of $\underline{r}$. Consequently, an atom with magnetic

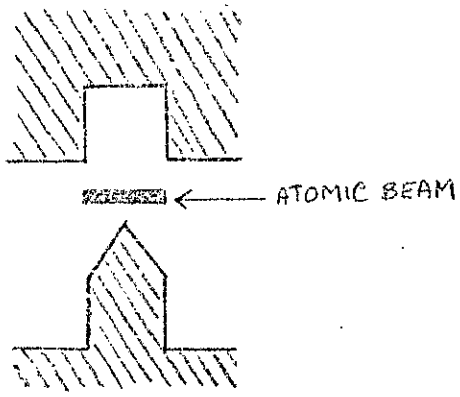

Fig. 3.1: Cross-section through pole-pieces of Stern Gerlach magnet.

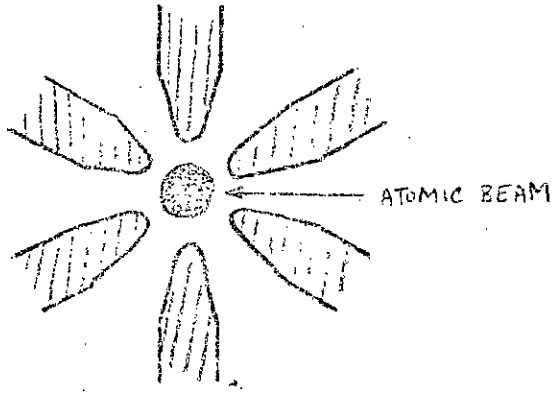

Fig. 3.2: Cross-section through polepieces of six-pole magnet.

moment parallel to B will experience a force away from the axis, increasing linearly with r, while an atom with magnetic moment antiparallel to B will experience a linear restoring force towards the axis. One spin state will be defocussed, the other spin state will be focussed at some point on the axis.

Arguments can be developed by analogy with optical focussing systems to predict quantitatively the behaviour of such a "lens" (Brash et al., 1969). The power of the lens will clearly be a function of the velocity of the atoms along the axis, since the net deflection will be proportional to the time that the atom spends in the field. This "chromatic aberration" means that it is impossible to focus at one point on the axis all the atoms in one spin-state emanating from a point source. Nevertheless, by adjusting the value of the magnetic field so that the peak of the velocity distribution is focussed at the centre of the interaction region, high atomic densities can be achieved.

3.1.2. Details of the six-pole magnet used.

The six-pole magnet used in the present investigation was an electromagnet manufactured by Newport Instruments. The length of the magnet was 250 mm., and the poletips were at a distance of 3.5 mm. radius from the axis. The magnetic field at the pole tips could be varied, by adjusting the current through the windings, from zero up to the saturation value of about 0.7 T. (at a current of about 8 A.).

Using the formulae given in Brash et al., (1969), Brash has calculated (Brash, 1969) the total flux, number density, and polarisation which can be expected from a potassium beam

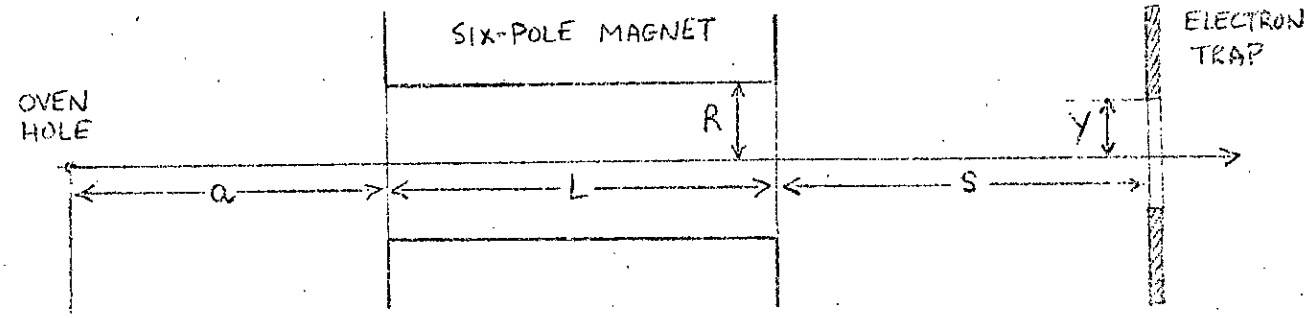

a = 0·27m

L = 0·25m

S = 0·27m

R = 3·0mm

Y = 2·8mm

Fig. 3.3: Dimensions of atomic beam focusing system.

focussed by such a magnet under the conditions of the present experiment (Fig. 3.3). It was assumed that the atomic beam was produced by a point source at a temperature of 583K. The results of these calculations are shown in Fig. 3.4. For a poletip field of 0.5T., corresponding to a current of about 3A., the polarisation is close to 100%.

3.1.3. Measurement of atomic beam density.

In the analysis of the results of the present experiment, two properties of the atomic beam are significant: the number density of atoms in the region of interaction with the trapped electrons, and the polarisation of the atomic beam in this region. Basically these quantities are found by using the computed curves shown in Fig. 3.5, normalised by a measurement of the atomic beam flux on a Langmuir-Taylor hot wire detector. The details of this normalisation procedure are given by Brash (Brash, 1969), and only an outline is presented here.

The use of a hot-wire detector is the most convenient method of measuring the flux of an alkali atomic beam. It relies on the fact that the work function for an incandescent platinum surface is greater than the ionisation potential of the alkali atom; an atom falling on such a surface has therefore a high probability - approaching unity for a clean surface (Schroen, 1963) - of losing its electron to the metal and being re-emitted as a positive ion. By applying a suitable electric field the ion current can be collected on an anode, and a measure obtained of the number of atoms per second falling on the exposed surface of the wire.

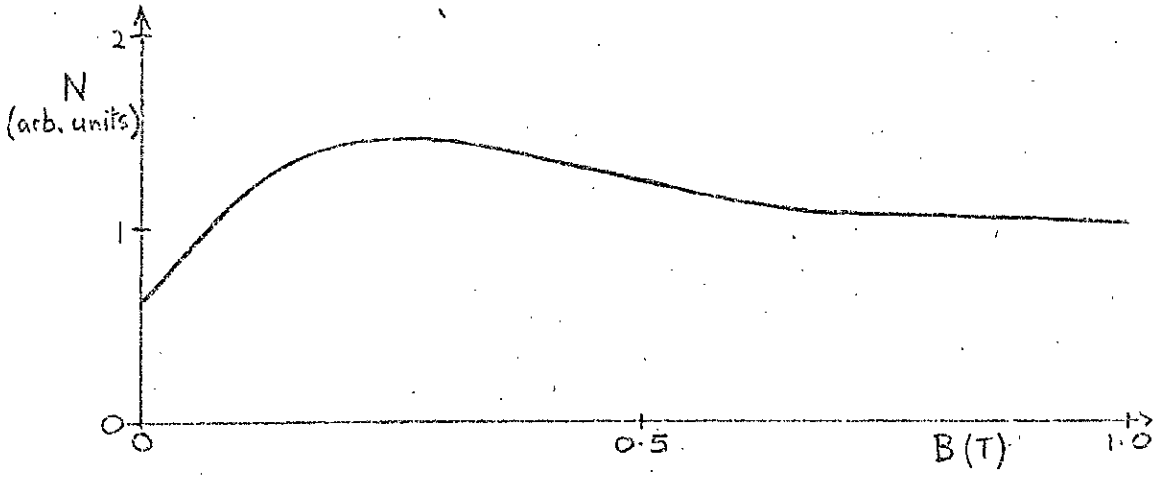

Fig.3.4: Calculated average atomic number density in trap (Brash)

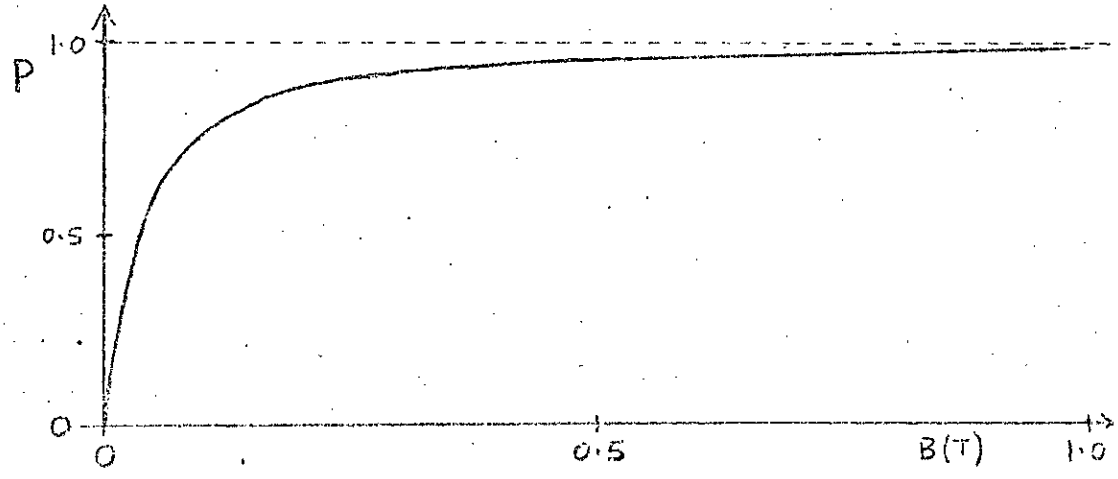

Fig.3.5: Calculated average atomic beam polarisation in trap (Brash)

In the detector used here the wire had a diameter of 0.1 mm., and a slit in front of it exposed a 0.62 mm. length to the atomic beam. Because of the geometry of the ion collectors (Fig. 3.6), only a fraction 0.53 of the emitted ion current was collected when a potential difference of 90 volts was applied between filament and collectors. The relationship between measured ion current i and incident atomic flux density Φ was therefore

$$i = 5.3 \times 10^{-27} \Phi \ .$$

It was not possible to place the hot wire detector in the centre of the trap, for obvious reasons; the actual experimental arrangement is shown in Fig. 3.7. However, for a given current through the six-pole magnet, and a fixed beam source temperature, there is a unique relationship between the flux density measured at the detector and the particle density in the interaction region. For a six-pole current of 3A., corresponding to a poletip field $B_0 = 0.44T$, this is given by

$$N = 1.88 \times 10^{-3} \Phi_m \ ,$$

where Φ_m is the maximum flux density measured at the detector. In terms of ion current, this can be written

$$N = 3.58 \times 10^{23} i_m \ ,$$

where i_m is the corresponding maximum ion current from the detector.

The source of the atomic beam in the present experiment was a conventional oven (Fig. 3.8), in which potassium was vaporised at a temperature of about 300°C. The vapour issued

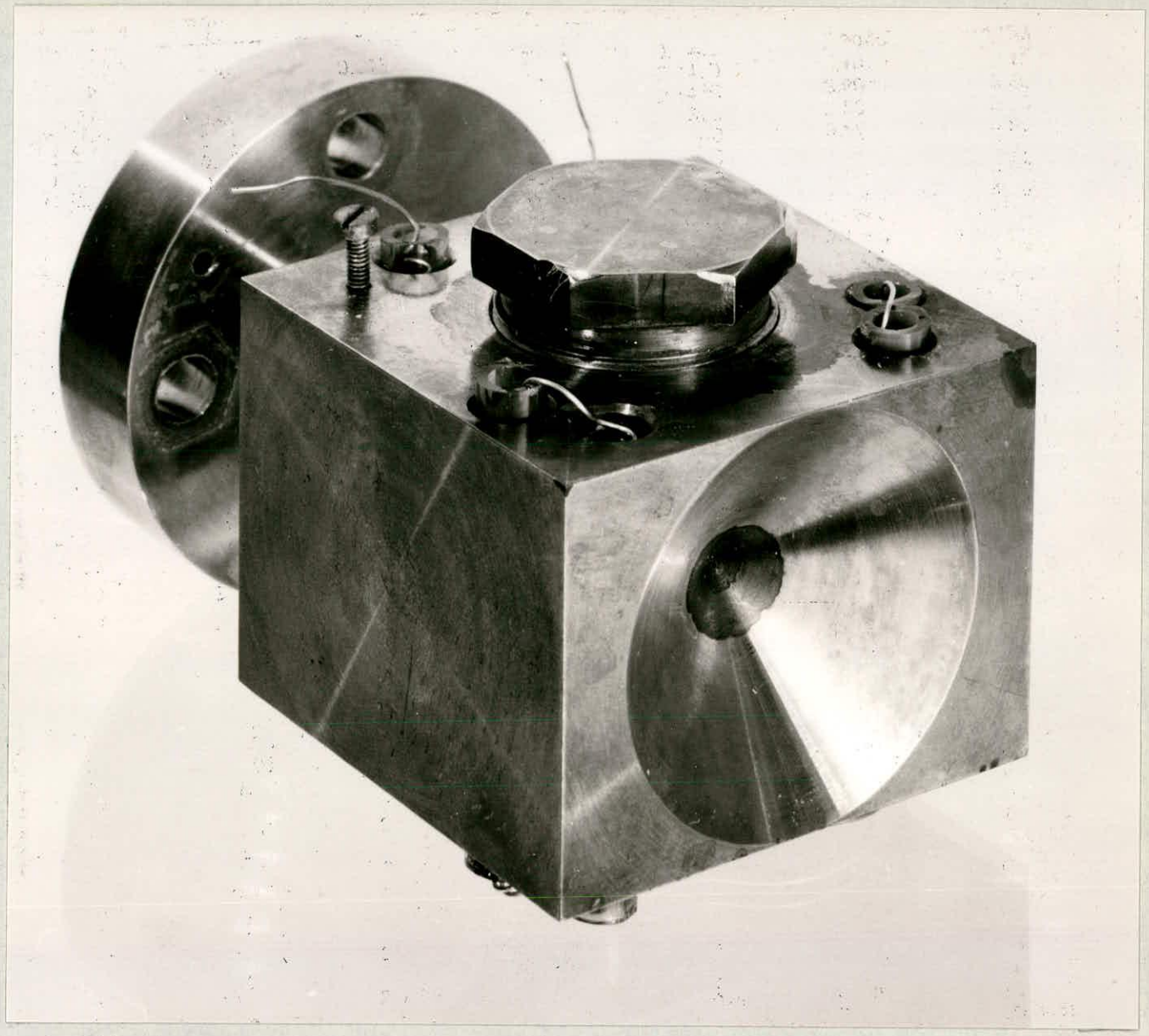

Fig. 3.8: Atomic beam oven.

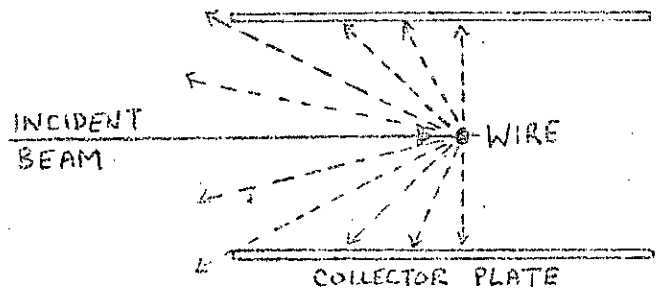

Fig. 3.6: Collection geometry of hot-wire detector.

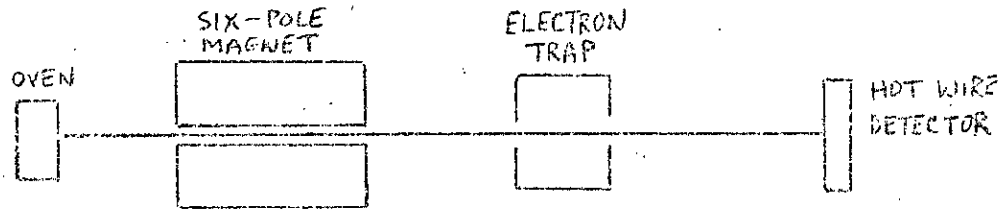

(a) Intensity measurement

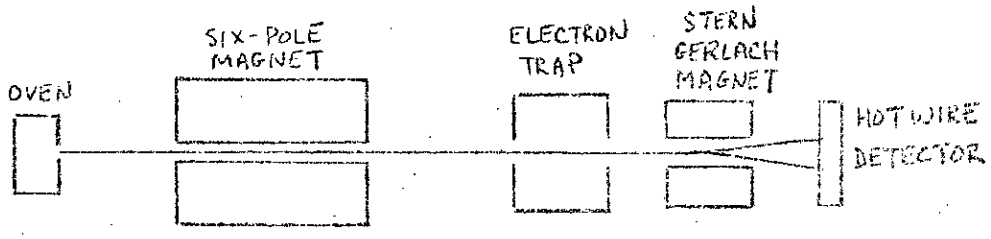

(b) Polarisation measurement

Fig. 3.7: Measurements on the atomic beam.

through a cylindrical channel 0.4mm diameter, 1.5mm long. Since the mean free path in saturated potassium vapour at this temperature is

$$\lambda \simeq 0{\cdot}1 \text{ mm},$$

it could not be expected that molecular flow would occur in this channel. However, it was found that a much higher beam intensity could be obtained by such a source than was possible from a conventionally sized aperture. The maximum beam intensities used gave a maximum detector current of 10^{-9} A, corresponding to a number density in the trap of $\frac{1}{3} \times 10^{14}$ atoms m^{-3}.

The calculated atomic beam polarisation in the trap for a sixpole current of 3A was

$$P = 0.95 .$$

A fairly crude confirmation of the high degree of polarisation of the beam was obtained by inserting a small Stern-Gerlach magnet immediately in front of the detector. By traversing the wire across the emergent beam, the plots of ion current against displacement in the Stern-Gerlach field shown in Fig. 3.9 were obtained. The resolution of the two peaks corresponding to the two spinstates can be clearly seen in Fig. 3.9(A), for the unpolarised beam; for sixpole currents greater than 2 A, one peak completely disappears, indicating a polarisation greater than 85%. There are, however, several important qualifications to this result.

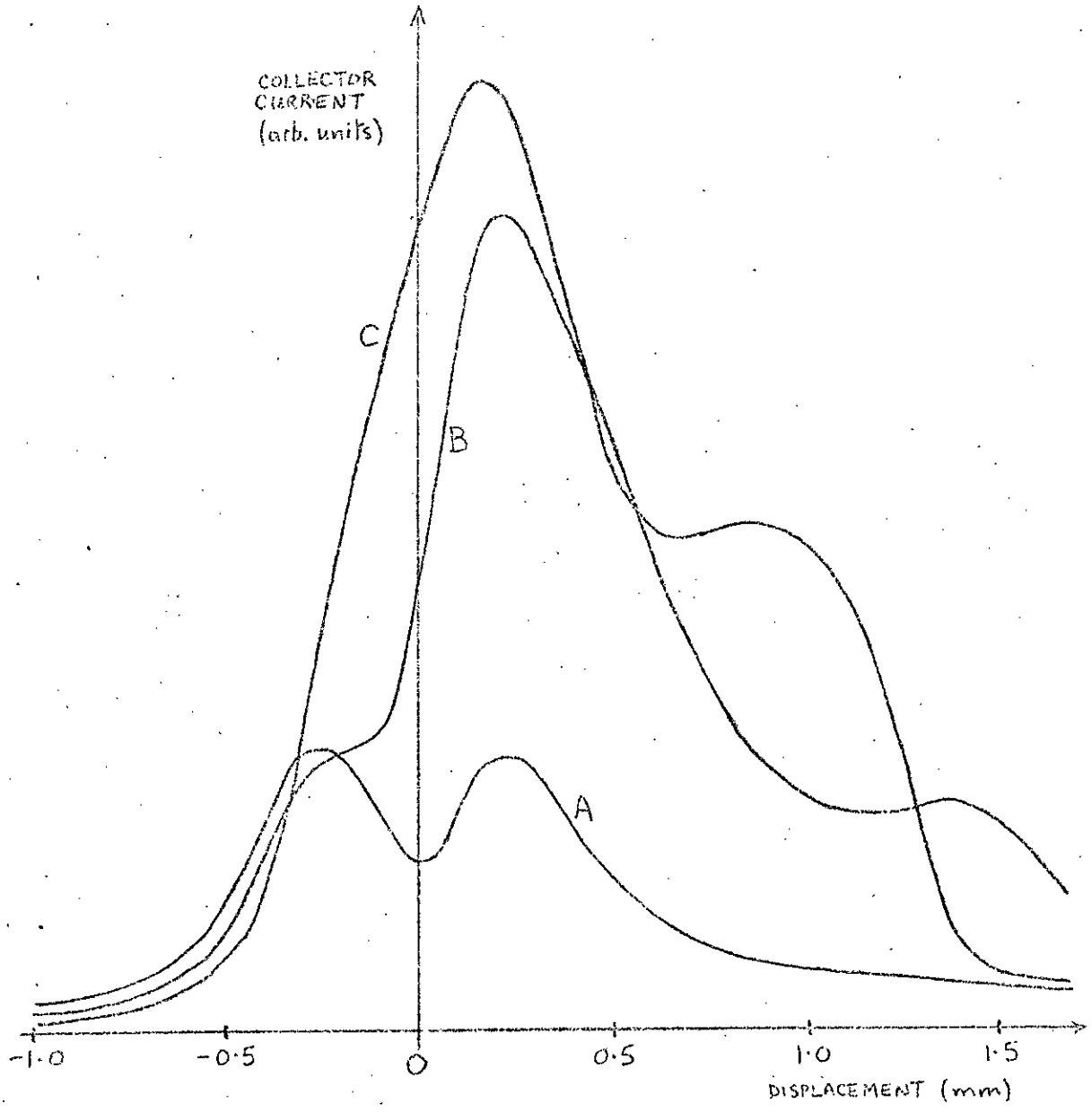

Fig. 3.9: Analysis of atomic beam polarisation using Stern Gerlach magnet, with sixpole current of (A) 0A, (B) 1A, (C) 2A

In order to achieve the required resolution, a very narrow slit (0.1mm) was placed in front of the Stern-Gerlach magnet. The measured polarisation is therefore not the average polarisation over the whole beam cross-section but the polarisation of a small segment of the beam. If the aperture is on the axis, this could give a misleadingly high figure. The "polarisation" measured by the Stern-Gerlach magnet is furthermore a relationship between the fluxes of the two spin states, rather than their number densities, and the measurement takes place at a quite different position on the axis to that of the interaction region. Taking these factors into account, however, the results confirm that high polarisations are obtained, as predicted by the theoretical treatment.

So far, the coupling of nuclear and atomic angular momenta in the potassium atom has been neglected. In the sixpole magnet, the magnitude of the magnetic field is large enough to render the effects of coupling insignificant, except for atoms travelling within 0.5mm of the axis. The result of the coupling is that the effective magnetic moment of the atom becomes different for each of the hyperfine states of the atom; for all the hyperfine states except those with total magnetic quantum number $m = \pm 2$ the magnetic moment is field dependent (Fig. 3.10). The consequence is that the lens is weakened for paraxial rays. A central axial stop of 0.5mm radius would eliminate this section of the beam, which will of course have a reduced polarisation. However, the solid angle involved is of the order of 1/40th of the total acceptance of the magnet, and the resulting complication of alignment procedure was

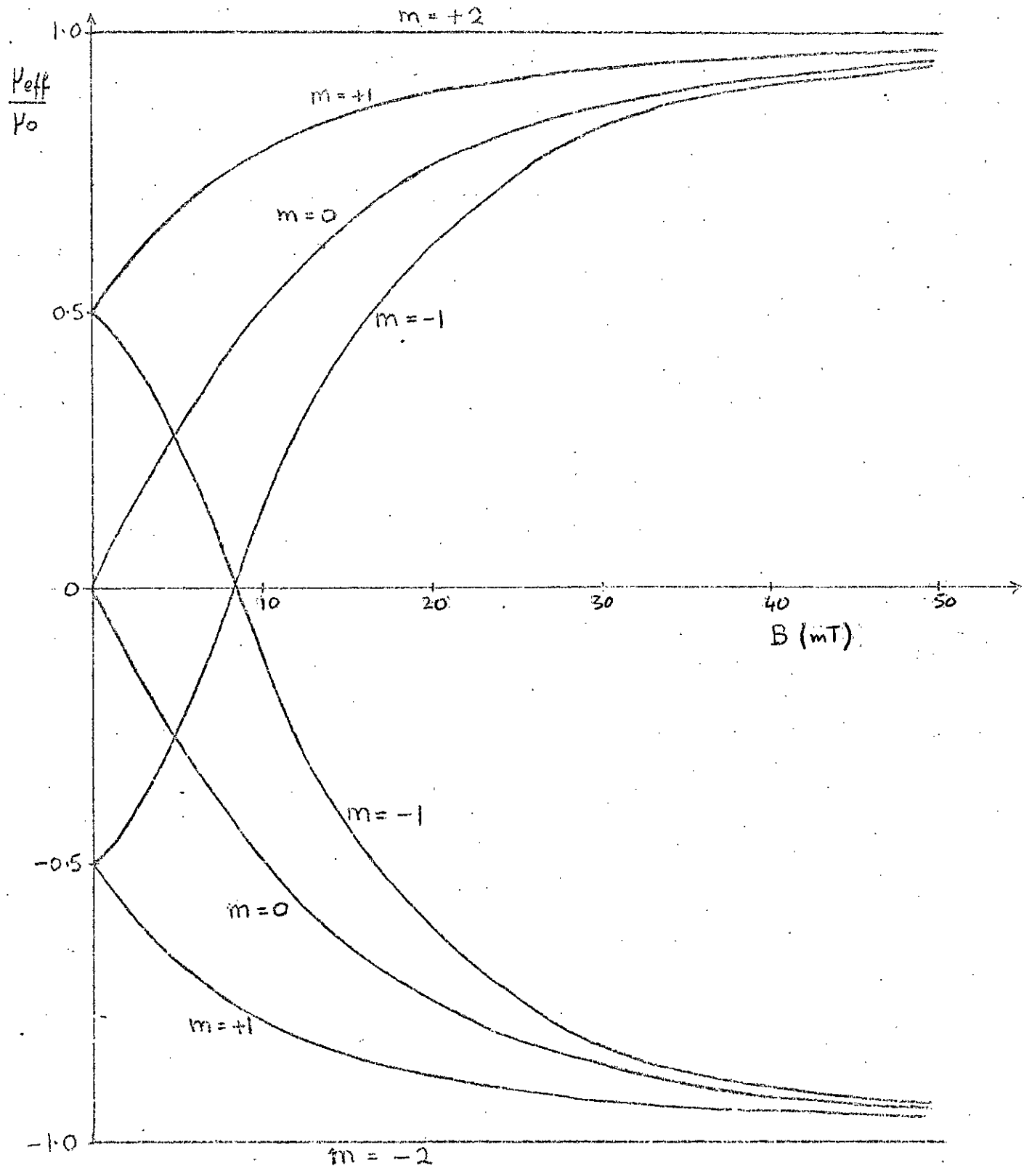

Fig. 3.10: Magnetic moments of hyperfine states of potassium in intermediate magnetic field.

not considered worth the small increase in polarisation which might be expected.

In the Stern-Gerlach magnet the atoms once again find themselves in a strongly decoupling magnetic field, and the polarisation measured will be that corresponding to the complete absence of coupling. The situation is very different in the electron trap, where, for reasons already described (Sect. 2.2.1), the magnetic field had to be restricted to under 10^{-2}T. The effective polarisation of the beam will be much reduced by the fairly strong coupling between nuclear and atomic electron spins. The extent of the reduction in polarisation can be found by expressing each hyperfine state of the atom as a summation of $|m_J, m_I\rangle$ states and calculating the effective polarisation, subsequently averaging over all hyperfine states present in the beam. If a particular hyperfine state $|F, m\rangle$ is written in terms of $|m_J, M_I\rangle$ states as

$$|F, m\rangle = a\,|+\tfrac{1}{2},\ m-\tfrac{1}{2}\rangle + b\,|-\tfrac{1}{2},\ m+\tfrac{1}{2}\rangle,$$

the effective polarisation of this state is

$$P_{F,m} = \frac{a^2 - b^2}{a^2 + b^2}$$

An atomic beam which is completely polarised in a strongly decoupling field will be composed of equal populations of those hyperfine states which in the strong field limit tend to the form $|+\tfrac{1}{2}, m_I\rangle$. The effective polarisation of these states as a function of magnetic field is shown in Fig. 3.11; Fig. 3.12 gives the effective polarisation of the whole beam. It will be seen that in a magnetic field of 6×10^{-3}T, the polarisation of

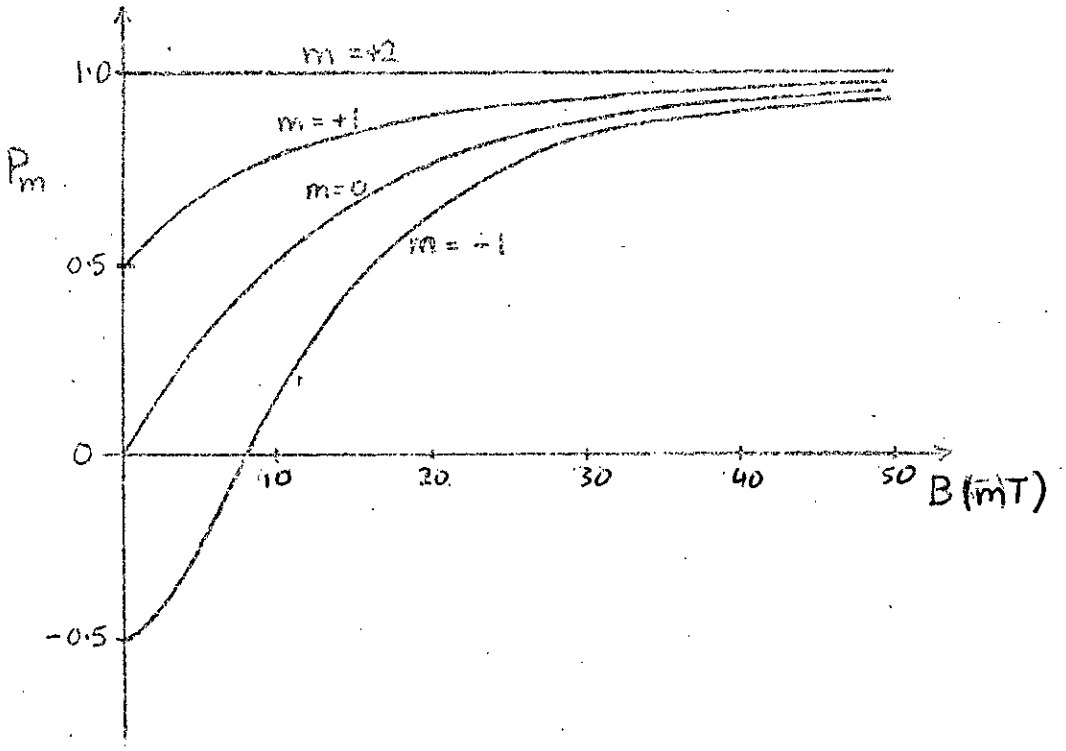

Fig. 3.11: Effective polarisation in intermediate field of hyperfine states corresponding to strong field polarisation 1.

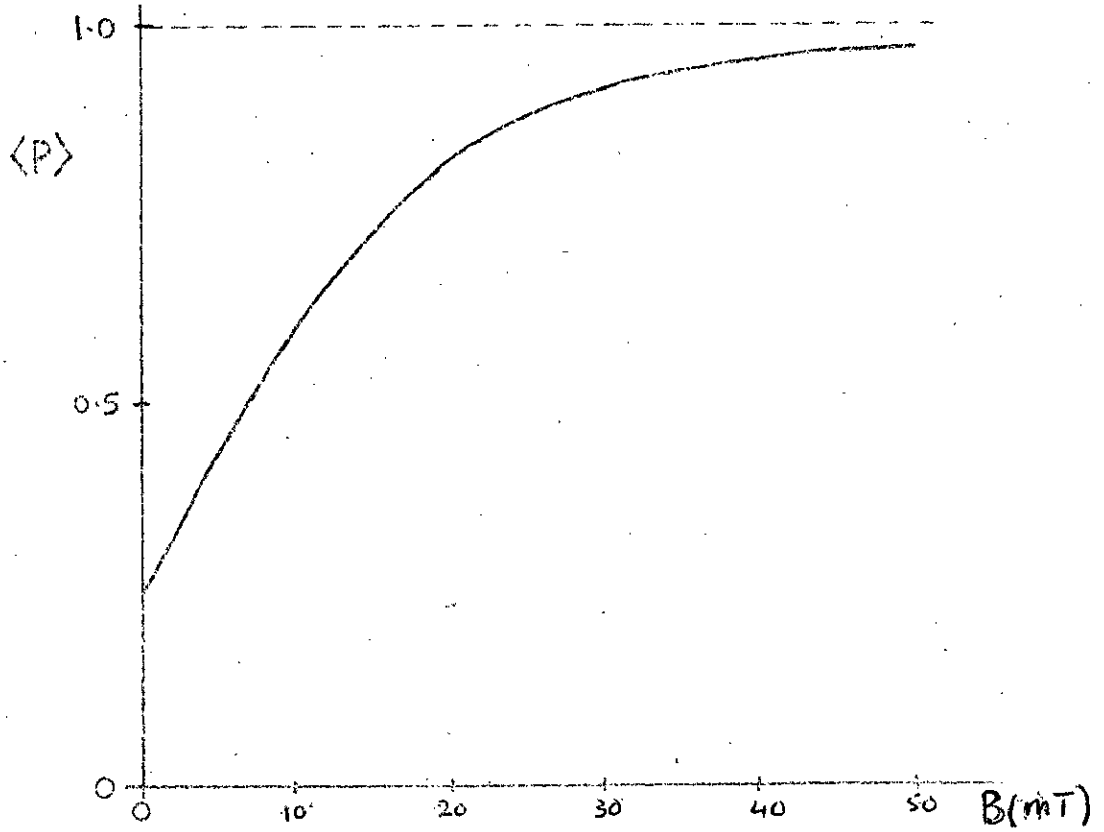

Fig. 3.12: Effective polarisation in intermediate field of atomic beam with strong field polarisation 1.

a beam of atoms initially all in one spin state is reduced to 47%. This effective depolarisation must be taken into account in discussion of the interaction between the atomic beam and the trapped electrons.

3.2. MATHEMATICAL DESCRIPTION OF THE INTERACTION

3.2.1. The Interaction Matrix.

We consider a beam of electrons interacting with an atomic beam in a region of uniform atomic density. Let there be N_+ atoms per unit volume with spin component $+\frac{1}{2}\hbar$ in the direction of the magnetic field, and N_- with spin component $-\frac{1}{2}\hbar$. Let the densities of electrons in the two spin states be likewise n_+ and n_-. It is useful also to consider the effect of a typical unpolarised residual gas, of density N' molecules/unit volume.

The population n_+ of electrons with spin $+\frac{1}{2}\hbar$ can change as a result of three processes during the interaction with the atomic beam:

(i) A spin-exchange collision between a "spin-up" electron and a "spin-down" atom will result in a loss to n_+.

(ii) A spin exchange collision between a "spin-down" electron and a "spin-up" atom will result in a gain to n_+.

(iii) Electrons will be lost from the trap during the interaction by radial diffusion (see Sect.2.4). We will consider a simplified case in which the rate of loss of electrons is proportional to the total collision frequency. This is expressed by allowing a probability α that after a collision an electron will be lost from the trap.

An interaction with a molecule of the residual gas may also lead to a change in electron spin state. Since spin-orbit interaction, negligible in the case of low energy scattering from

potassium, may make a significant contribution in the case of a residual gas molecule, we will define a total spin-flip cross-section Q'_{sf} to allow for both spin-exchange and spin-orbit interactions. The residual gas will also contribute to radial diffusion, with a total cross-section Q' .

If Q_1, Q_3, Q_d, and Q_e are singlet, triplet, direct and exchange cross-sections respectively for collision between an electron and a potassium atom, the changes in n_+ and n_- after an interaction time δt are given by:

$$n_+(t+\delta t) = n_+(t) - \alpha n_+ v\delta t\left[N_+Q_3 + N_-(Q_d+Q_e) + N'Q'\right] + (1-\alpha)v\delta t\left[Q_e(N_+n_- - N_-n_+) + \tfrac{1}{2}Q'_{sf}N'(n_- - n_+)\right]$$

$$n_-(t+\delta t) = n_-(t) - \alpha n_- v\delta t\left[N_-Q_3 + N_+(Q_d+Q_e) + N'Q'\right] + (1-\alpha)v\delta t\left[Q_e(N_-n_+ - N_+n_-) + \tfrac{1}{2}Q'_{sf}N'(n_+ - n_-)\right]$$

Writing

$$n = n_+ + n_-\,, \quad m = n_+ - n_-\,, \quad N = N_+ + N_-\,, \quad M = N_+ - N_-\,:$$

$$n(t+\delta t) = n(t) - \alpha v\delta t\left[\tfrac{1}{2}Q_3(Nn+Mm) + \tfrac{1}{2}(Q_d+Q_e)(Nn-Mm) + N'nQ'\right]$$

$$m(t+\delta t) = m(t) - \alpha v\delta t\left[\tfrac{1}{2}Q_3(Nm+Mn) + \tfrac{1}{2}(Q_d+Q_e)(Nm-Mn) + N'mQ'\right] + (1-\alpha)v\delta t\left[Q_e(Mn-Nm) - Q'_{sf}N'm\right]\,;$$

therefore

$$\delta n = \left[-\alpha v\delta t.\tfrac{1}{2}\left\{(Q_3+Q_d+Q_e)N + 2Q'N'\right\}\right]n + \left[-\alpha v\delta t.\tfrac{1}{2}\left\{(Q_3-Q_d-Q_e)M\right\}\right]m$$

$$\delta m = \begin{bmatrix} -\alpha v\delta t.\tfrac{1}{2}\left\{(Q_3-Q_d-Q_e)M\right\} \\ +(1-\alpha)v\delta t\left\{Q_eM\right\} \end{bmatrix}n + \begin{bmatrix} -\alpha v\delta t.\tfrac{1}{2}\left\{Q_3+Q_d+Q_e\right\}N + 2Q'N' \\ -(1-\alpha)v\delta t\left\{Q_eN + Q'_{sf}N'\right\} \end{bmatrix}m$$

It is convenient to describe the polarisation state of the trapped electrons by a two component vector $\begin{bmatrix} n \\ m \end{bmatrix}$ (Byrne and Farago, 1965).

In terms of this vector, the interaction can be described by a matrix A:

$$\begin{bmatrix} n(t+\delta t) \\ m(t+\delta t) \end{bmatrix} = (I + A\delta t) \begin{bmatrix} n(t) \\ m(t) \end{bmatrix}$$

or

$$\frac{d}{dt}\begin{bmatrix} n \\ m \end{bmatrix} = A\begin{bmatrix} n \\ m \end{bmatrix}. \qquad 3.1.$$

The elements of the matrix A are given by

$$\begin{aligned}
a_{11} &= -\tfrac{1}{2}\alpha v\{(Q_3 + Q_d + Q_e)N + 2Q'N'\} \\
a_{12} &= -\tfrac{1}{2}\alpha v\{(Q_3 - Q_d - Q_e)M\} \\
a_{21} &= -\tfrac{1}{2}\alpha v\{(Q_3 - Q_d - Q_e)M\} + (1-\alpha)v\{Q_e M\} \\
a_{22} &= -\tfrac{1}{2}\alpha v\{(Q_3 + Q_d + Q_e)N + 2Q'N'\} - (1-\alpha)v\{Q_e N + Q'_{SF}N'\}.
\end{aligned}$$

Defining $Q = \frac{1}{4}(Q_1 + 3Q_3)$

and $S = \frac{1}{4}(Q_1 - Q_3)$

and bearing in mind that $Q_d + Q_e = \frac{1}{2}(Q_1 + Q_3)$,

the elements of A can be written as

$$\begin{aligned}
a_{11} &= -\alpha v\{QN + Q'N'\} \\
a_{12} &= +\alpha v\{SM\} \\
a_{21} &= +\alpha v\{SM\} + (1-\alpha)v\{Q_e M\} \\
a_{21} &= -\alpha v\{QN + Q'N'\} - (1-\alpha)v\{Q_e N + Q'_{SF}N'\}.
\end{aligned}$$

Integration of Equation 3.1 yields the result

$$\begin{bmatrix} n(t) \\ m(t) \end{bmatrix} = e^{-tA}\begin{bmatrix} n(0) \\ m(0) \end{bmatrix}$$

This can be expanded by matrix methods to give the development of n and m with time. However, the result we require here is the development of the electron polarisation $p = \frac{m}{n}$, and this can be found without recourse to matrix algebra.

3.2.2. Development of Polarisation

Equation 3.1 implies two component equations:

$$\frac{dn}{dt} = a_{11} n + a_{12} m$$

$$\frac{dm}{dt} = a_{21} n + a_{22} m .$$

Now $p = \frac{m}{n}$;

$$\therefore \frac{dp}{dt} = \frac{dp}{dm} \cdot \frac{dm}{dt} + \frac{dp}{dn} \cdot \frac{dn}{dt}$$

$$= \frac{1}{n} \cdot \frac{dm}{dt} - \frac{m}{n^2} \cdot \frac{dn}{dt} ,$$

$$= a_{21} + (a_{22} - a_{11}) p - a_{12} p^2$$

This can be written:

$$\frac{dp}{dt} = - a_{12} (p - \mu)(p - \rho)$$

with $\mu, \rho = \frac{1}{2a_{12}} \left\{ -(a_{11} - a_{22}) \pm \left[(a_{11} - a_{22})^2 + 4 a_{12} a_{21} \right]^{\frac{1}{2}} \right\}.$

$$\therefore \int \frac{dp}{(p-\mu)(p-\rho)} = -a_{12}t + c$$

$$\therefore \frac{1}{\mu-\rho} \ln\left|\frac{p-\mu}{p-\rho}\right| = -a_{12}t + c$$

$$\therefore \left|\frac{p-\mu}{p-\rho}\right| = e^{-a_{12}(\mu-\rho)t + c(\mu-\rho)}.$$

If $p = 0$ when $t = 0$,

$$\left|\frac{p-\mu}{p-\rho}\right| = \frac{\mu}{\rho} e^{-a_{12}(\mu-\rho)t} = \nu e^{-\lambda t}$$

where $\nu = \mu/\rho$

$\lambda = a_{12}(\mu-\rho)$

$$\therefore p(1-\nu e^{-\lambda t}) = \mu(1-e^{-\lambda t})$$

$$\therefore p = \frac{\mu(1-e^{-\lambda t})}{1-\nu e^{-\lambda t}} \qquad 3.2.$$

where $\lambda = \left[(a_{11}-a_{22})^2 + 4a_{12}a_{21}\right]^{\frac{1}{2}}$

$\mu = \frac{1}{2a_{12}}\left[\lambda - (a_{11}-a_{22})\right]$

$\nu = \frac{a_{11}-a_{22}-\lambda}{a_{11}-a_{22}+\lambda}$.

Thus the polarisation of the electron beam tends asymptotically to a value

$$p_\infty = \mu .$$

In general this is a complicated function of the matrix elements; some special cases which lead to simplified results are interesting.

3.2.3. No Atomic Beam (M=N=0):

$$a_{11} = -\alpha v Q' N'$$
$$a_{12} = 0$$
$$a_{21} = 0$$
$$a_{22} = -\alpha v Q' N' - (1-\alpha) v Q'_{SF} N' .$$

The equation for p reduces to

$$p = p_0 e^{-\lambda_R t} ,$$

where $v Q'_{SF} N' (1-\alpha) = \lambda_R$, the reciprocal of the relaxation time constant due to the depolarisation of the electron beam by the residual gas. In the presence of several such gases, with number densities $N'_1, N'_2, \ldots$,

$$\lambda_R = \sum_i (1-\alpha) v (Q'_{SF\,i} N'_i) .$$

3.2.4. No Losses from Trap ($\alpha = 0$).

$$a_{11} = 0$$

$$a_{12} = 0$$

$$a_{21} = \nu Q_e M$$

$$a_{22} = -\nu(Q_e N + Q'_{SF} N')$$

$\lambda = \lambda_P + \lambda_R$, where $\lambda_P = \nu Q_e N$, $\lambda_R = \nu Q'_{SF} N'$

$\nu = 0$

$\mu = \frac{\nu Q_e M}{\nu Q_e N + \nu Q'_{SF} N'} = P\left(1 + \frac{\lambda_R}{\lambda_P}\right)^{-1}$,

where P is the atomic beam polarisation $(= \frac{M}{N})$.

Thus $$p = \frac{P}{\left(1 + \frac{\lambda_R}{\lambda_P}\right)}\left(1 - e^{-(\lambda_P + \lambda_R)t}\right).$$

In the absence of losses, the electron polarisation approaches an equilibrium value

$$p_\infty = \frac{P}{(1 + \lambda_R/\lambda_P)}$$

with a time constant $\tau = (\lambda_P + \lambda_R)^{-1}$. The relaxation effects due to the residual gases reduce the ultimately attainable polarisation, and increase the rate at which it is achieved.

It may be noted here that $\lambda_R/\lambda_P = \frac{Q'_{SF} N'}{Q_e N}$. Since most residual gases appear to have spin flip cross-sections several orders of magnitude below that of the alkalis (cf. Bernheim, 1969, p.59) relaxation effects are likely to be small unless the residual gas density is considerably greater than the density of the atomic beam.

3.2.5. Small Loss Rate ($\alpha \ll 1$)

A curious result emerges from a consideration of the equilibrium electron polarisation achieved when there is a small but finite rate of loss from the trap. From Equation 3.2

$$p_\infty = \mu = \frac{\lambda - (a_{11} - a_{22})}{2a_{12}}$$

and

$$\lambda = (a_{11} - a_{22})\left[1 + \frac{4a_{12}a_{21}}{(a_{11} - a_{22})^2}\right]^{\frac{1}{2}}.$$

If $\frac{4a_{12}a_{21}}{(a_{11} - a_{22})^2} \ll 1$,

$$\lambda \simeq (a_{11} - a_{22})\left[1 + 2\frac{a_{12}a_{21}}{(a_{11} - a_{22})^2} - 2\left(\frac{a_{12}a_{21}}{(a_{11} - a_{22})^2}\right)^2 \ldots\right]$$

$$\therefore \mu \simeq \frac{a_{21}}{(a_{11} - a_{22})}\left[1 - \frac{a_{12}a_{21}}{(a_{11} - a_{22})^2}\right]$$

$$\simeq \frac{P}{\left(1 + \frac{\lambda_R}{\lambda_P}\right)}\left[1 + \frac{\alpha}{(1-\alpha)}\left(\frac{S}{Q_e}\right)\left\{1 - \left(\frac{P}{\left(1 + \frac{\lambda_R}{\lambda_P}\right)}\right)^2\right\}\right] \qquad 3.3(a).$$

$\frac{P}{(1 + \lambda_P/\lambda_R)}$ is the equilibrium polarisation that would obtain if $\alpha = 0$; call this P_o.

Then

$$\mu \simeq P_o\left[1 + \alpha\left(\frac{S}{Q_e}\right)(1 - P_o^2)\right] \qquad 3.3(b).$$

In the case of potassium, it appears that $Q_3 > Q_1$; thus $S/Q_e < 0$, and the equilibrium polarisation is reduced by losses. However, it is interesting to note that if $Q_1 \gg Q_3$ (e.g. for hydrogen), $S/Q_e \simeq +1$. Thus the equilibrium polarisation attained by the electrons can be greater than that of the atomic beam, if relaxation effects are negligible. This apparent paradox can be understood by considering the case of a completely polarised atomic beam. If the triplet cross-section is negligible, electrons in the same spin state as the atoms will suffer no collisions; those in the opposite spin state will therefore be preferentially lost. The polarised atomic

beam acts as a spin-sensitive filter.

Of course, if the atomic beam is completely polarised, the spin-exchange process will eventually yield complete electron polarisation in any case. A partially polarised beam will still preferentially filter out one spin state, and this effect will augment the polarisation of the electrons due to spin exchange.

It can easily be shown that the above result (Equation 3.3(a)) remains valid up to fairly high values of α, if the effective atomic beam polarisation P_o is low. For instance, if $P_o = 0.1$ and $\alpha = 0.5$, the equilibrium polarisation of the electron ensemble is

$$p_\infty = \mu_o = 0.2\left(\frac{S}{Q_e}\right) = 0.2 \text{ if } \frac{S}{Q_e} = 1.$$

This is not of practical significance, however, as such a high loss factor would deplete the electron population to an unacceptable degree.

3.2.6. Initial Rate of Increase of Electron Polarisation.

The development of the electron polarisation with time is given by equation:-

$$p = \frac{\mu\left(1 - e^{-\lambda t}\right)}{1 - \nu e^{-\lambda t}}$$

When $\lambda t \ll 1$, the exponentials in this expression can be written out as rapidly converging power series. Taking only the first order of λt, we obtain the result

$$p \simeq \left(\frac{\mu\lambda}{1-\nu}\right) t.$$

A graph of p against t should initially be linear, with slope given by

$$\dot{p}(0) = \frac{\mu\lambda}{1-\nu}$$

If losses are neglected,

$$\lambda = \lambda_P + \lambda_R, \quad \mu = \frac{P\lambda_P}{\lambda_P + \lambda_R}, \quad \nu = 0.$$

$$\therefore \frac{\mu\lambda}{1-\nu} = P\lambda_P ; \quad \lambda_P = \frac{\dot{p}(0)}{P} . \qquad 3.4.$$

The fact that the initial slope of the polarisation curve is independent of λ_R is important, since measurements in this region will yield information directly about λ_P. If the equilibrium polarisation (as $t \to \infty$) can also be measured, an estimation of relaxation effects can be made, since

$$p(\infty) = \frac{P}{\left(1 + \frac{\lambda_R}{\lambda_P}\right)} . \qquad 3.5$$

Combining Eqns. 3.4, 3.5, we have:

$$\lambda_R = \dot{p}(0)\left(\frac{1}{p(\infty)} - \frac{1}{P}\right) .$$

3.3. MEASUREMENT OF ELECTRON POLARISATION

3.3.1. Theory of Mott Scattering.

The theory of what has subsequently become known as Mott scattering was first given by Mott in 1929. His application of the Dirac electron theory to the case of fast electron scattering by a heavy bare nucleus (a Coulomb field) showed that, if a beam of electrons travelling in the x direction with transverse polarisation P in the z direction is incident on a target containing heavy nuclei, the intensity of scattering through an angle θ in the x,y plane will in general be different from the intensity of scattering through an angle $-\theta$. If $I(\theta)$ and $I(-\theta)$ denote these respective scattering intensities, a scattering asymmetry A will be observed, defined by

$$A(\theta) = \frac{I(\theta) - I(-\theta)}{I(\theta) + I(-\theta)} .$$

The scattering asymmetry can be written as

$$A = SP ,$$

where P is the polarisation of the incident beam, and S (the Sherman function) is a function of the scattering angle, the charge on the nucleus, and the energy of the incident electron.

This asymmetry in the distribution of scattered electrons arises from the fact that an electron approaching a positively charged nucleus with velocity $\underline{v}$ experiences a magnetic field $\underline{B} = \frac{1}{c^2}(\underline{v} \wedge \underline{E})$ in its own frame of reference, due to its motion in the nuclear field $\underline{E}$. If the magnetic moment of the electron is $\underline{\mu}$,

it will have a potential energy $U = \underline{\mu}.\underline{B}$ in the field $\underline{B}$; since $\underline{B}$ will be a rapidly varying function of position in the region of the nucleus, the electron will experience a force (in its own reference frame) given by $\underline{F} = -\nabla U = -\frac{1}{c}\nabla\left(\underline{\mu}.\underline{v}\wedge\underline{E}\right)$. The sign of this force will depend on the orientation of $\underline{\mu}$ relative to $\underline{v}\wedge\underline{E}$; the scattering must therefore be spin-dependent. This simple classical argument, which is confirmed by the quantum mechanical treatment of Mott, provides a useful check on the sign of the asymmetry expected in a given situation. For example, if the electron approaches the nucleus with velocity $\underline{v}$ in the x direction with positive spin component in the z direction, its magnetic moment will have a negative z component, and the spin-orbit interaction will result in a force with a negative y component (Fig.3.13). The effect of this force will be to increase the number of electrons scattered "to the right" in the diagram, at the expense of those scattered "to the left".

Detailed calculations of the value of S as a function of the various parameters involved were performed by Sherman (1956). The experimental verification of these calculations presented great difficulties, since it involved measurement of the absolute scattering asymmetry in a double scattering experiment, in which intensities were inevitably low, and many potential sources of systematic error were present. Careful measurements performed by Mikaelyan et al (1963) indicated that for high energies agreement between theory and experiment was adequate, but that with

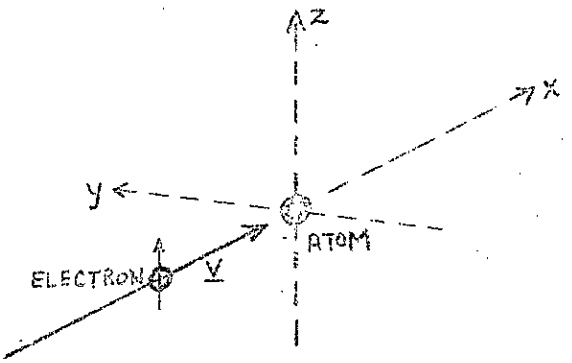

Fig. 3.13: Sketch illustrating Mott scattering situation.

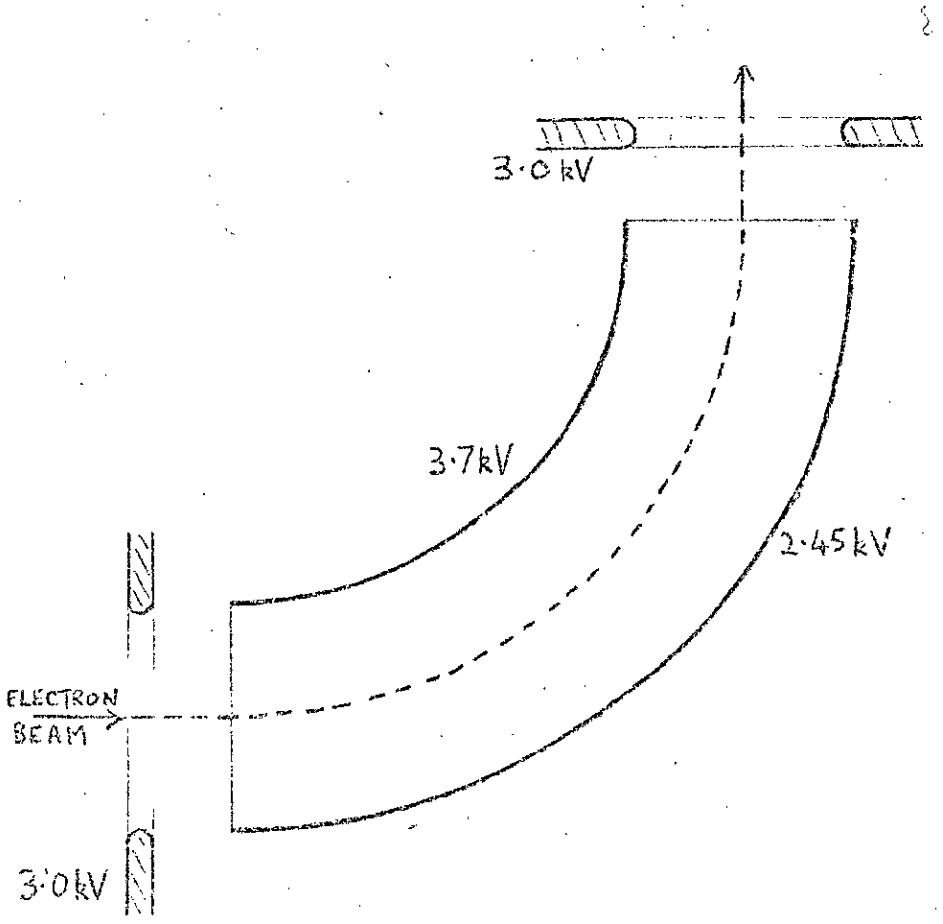

Fig. 3.14: Electrostatic deflector (spin twister).

decreasing energy the experimental values for S were systematically lower than predicted by Sherman.

Holzwarth and Meister (1964) considered various possible sources of error in the theoretical derivation, and concluded that only the neglect of the screening effect of the atomic electrons on the Coulomb field of the nucleus could cause an error comparable to the observed discrepancy. They therefore allowed for this effect by using a relativistic Hartree potential for the scattering field instead of the Coulomb potential. The results of their calculations provide the best available theoretical estimation of the scattering function, but still do not give agreement within experimental uncertainty with the results of Mikaelyan et al. Holzwarth and Meister concluded that the exceptional difficulties involved in the experiments were likely to account for these remaining differences.

For scattering from a gold target at an angle $\theta = 120^{\circ}$ and energy 50 KeV, the value of S calculated by Holzwarth and Meister is 0.34. The experimental value given by Mikaelyan is 0.29 + 0.01. Because of the arguments advanced by Holzwarth and Meister, the theoretical value was considered more reliable, and was used in the evaluation of the results of the present experiments.

3.3.2 Design of Mott Scatterer

In considering the design of an apparatus to measure the electron polarisation of the beam emerging from the trapping region, the first point to note was that the beam would be longitudinally polarised, the electrons being radially confined by an axial magnetic field. In order to use Mott scattering analysis, this longitudinal polarisation must be converted into transverse polarisation. There are two straightforward ways of doing this. The beam may be passed through uniform electric and magnetic fields $\underline{E}$ and $\underline{B}$ which are perpendicular to each other and to the velocity $\underline{v}$ of the electrons. If the ratio of the magnitudes of $\underline{E}$ and $\underline{B}$ is given by

$$\frac{E}{B} = v ,$$

the Lorentz force on the electrons vanishes, and the trajectory of the beam is unaffected. The magnetic moment of the electron will, however, precess about the magnetic field direction with angular velocity $\omega = \frac{egB}{2m}$, where e,m, and g are the charge, mass, and g factor of the electron respectively. After the electron has travelled a distance $l = \frac{\pi}{2\omega v}$ in the crossed fields, the magnetic moment will have precessed through an angle $\pi/2$ and the original longitudinal polarisation will have become transverse. Such a "spintwister" is known as a "Wien filter" and was originally developed as a velocity selector.

An alternative means of converting longitudinal polarisation into transverse is the use of an electrostatic beam deflection.

If the beam is injected into the space between two concentric cylinders with a potential difference V applied between them, as shown in Fig. 3.14, an electron entering with a tangential velocity $v = \sqrt{\frac{2eV_o}{m}}$ at a radius r_o will experience an electrostatic force eE, where E is the electric field at radius r_o. If the potentials on the cylinders are adjusted such that

$$E = \frac{2V_o}{r_o}$$

the trajectory of the electron will be the circumference of the circle of radius r_o, and after traversing one quadrant the electron beam will emerge with its momentum vector rotated through 90°. It can easily be shown that electrons entering the deflector with a small spread of angles about the tangential direction will experience an additional deflection towards the central trajectory: that is, there is a focussing effect in the plane perpendicular to the symmetry axis of the cylinders. Since there is no field perpendicular to this plane there will obviously be no focussing effect on electrons diverging from the plane of incidence perpendicular to the symmetry axis; as an electron lens, the cylindrical deflector is astigmatic. (This astigmatism can be removed by using sections of two concentric spheres as deflectors.)

In the absence of any magnetic field, the direction in space of the magnetic moment will remain constant, and the angle between momentum and magnetic moment will be increased by $\frac{\pi}{2}$ in the deflector. The electron will, however, experience a magnetic field in its frame of reference, due to its motion in the electric field $\underline{E}$, given by $\underline{B} = \frac{1}{c^2}(\underline{v} \wedge \underline{E})$.

Tolhoek and DeGroot,who first considered the use of the electrostatic deflector as a polarisation transformer (Tolhoek and DeGroot, 1951), pointed out that this relativistic effect would result in an electron emerging after 90° deflection with its magnetic moment rotated (relative to the original momentum vector) by an angle

$$\psi = \frac{\pi}{2}\left[1 - (1-\beta^2)^{1/2}\right] \qquad 3.6.$$

Since the transverse polarisation P_t is the expectation value of the electron spin measured in the transverse direction, it will clearly be given by

$$P_t = P_\ell \cos\psi ,$$

where P_ℓ is the original longitudinal polarisation. The electrostatic deflector was chosen in the present experiment, partly because of its simplicity of construction and operation, but principally because it was desired to introduce a bend into the electron path in order to shield photomultipliers in the Mott scatterer from the radiation from the electron gun filament. One particularly useful facility was denied by this choice: with the electrostatic deflector, the direction in space of the emergent magnetic moment was determined by the direction of the field in the trap, whereas with the Wien filter this direction could have been varied by rotating the entire filter about the beam axis. The elimination of instrumental asymmetries in the Mott scatterer would have been greatly facilitated by this possibility. Reversing the sign of the electron polarisation by reversing the magnetic field in the trap was not a practicable

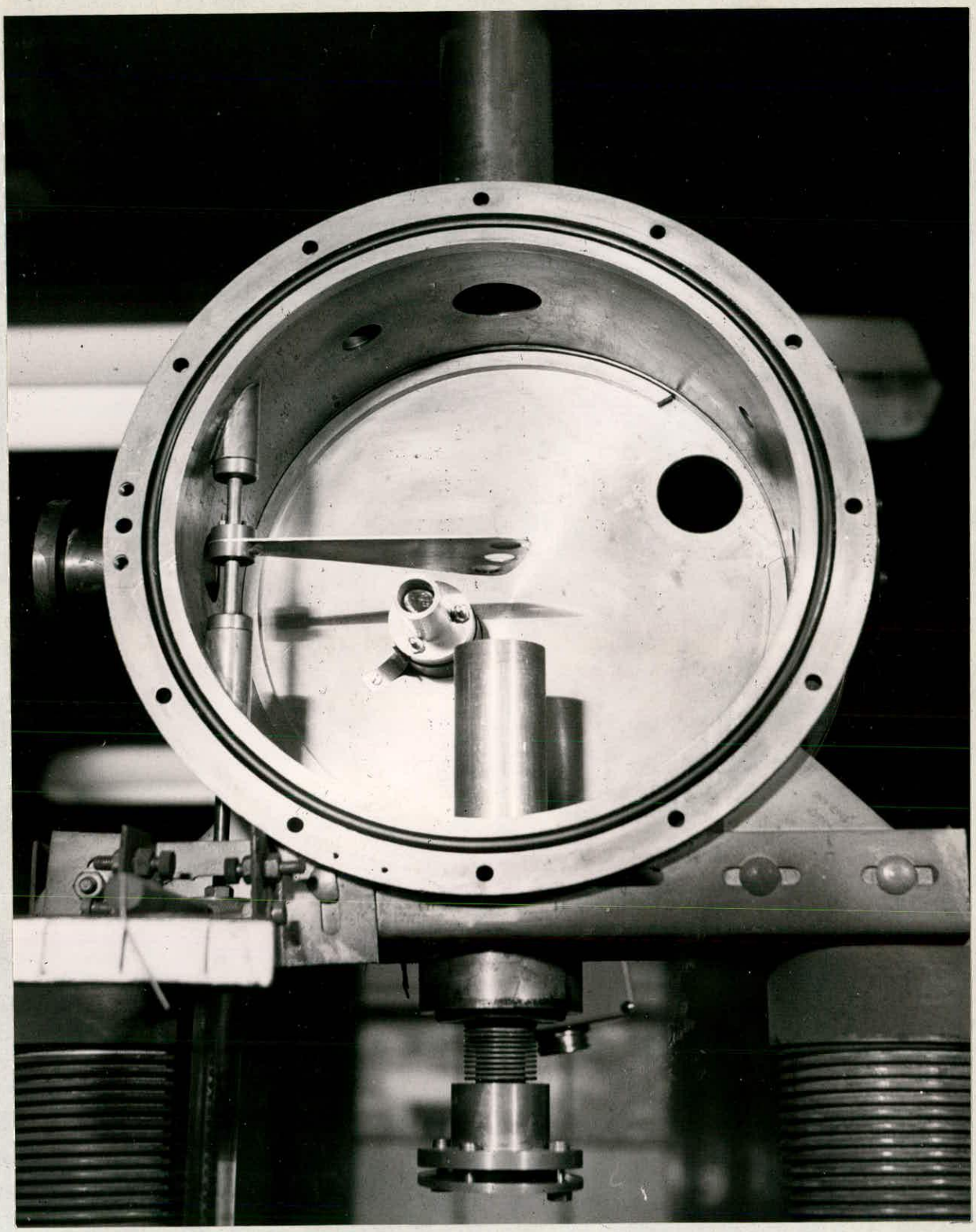

Fig. 3.15: Mott Scattering chamber.

alternative, because the properties of the trap depended strongly on the sign as well as the magnitude of the magnetic field (See Sect. 2.2.1).

The electrons were accelerated to 3 kV before deflection. This voltage was considered high enough to minimise the effects of contact potentials, stray magnetic fields, and other such plagues of low energy electron work, but low enough for the relativistic effect described by Equation 3.6 to be negligible ($\psi \simeq 0.5°$). Potentials of 3,700V and 2,450V were applied to the cylindrical plates, so that the 3,000V equipotential surface lay midway between the plates. Apertures at 3kV were inserted at input and output ends to reduce fringing field effects. The whole deflector was enclosed in a magnetic shroud.

On emergence from the deflector the beam was accelerated to 50kV in 8 stages. A large number of stages was desirable in order that each stage should be a weakly focussing lens, resulting in beam confinement without overfocussing and consequent divergence. At the exit of the accelerator, the beam was collimated by a series of aluminium apertures, and entered the Mott scattering chamber. This was a brass cylinder of 250mm diameter (Fig.3.15). In the diametral plane perpendicular to the direction of incidence was an aluminium target-holder (Fig.3.16), rotatable in this plane so that one of three targets could be inserted into the beam. The gold foil target used in Mott scattering was made by evaporating a known thickness of gold (See Sect.3.3.4) on to a thin film of cellulose nitrate ("Zapon"). Another target, consisting only of this backing film, could be inserted in place of the gold foil target to assess the

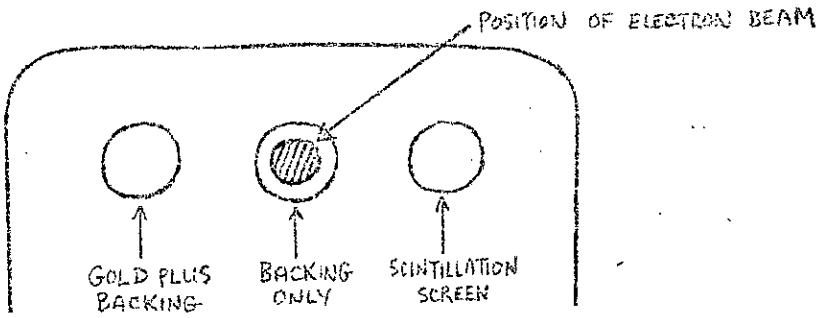

Fig. 3.16: Sketch of target holder.

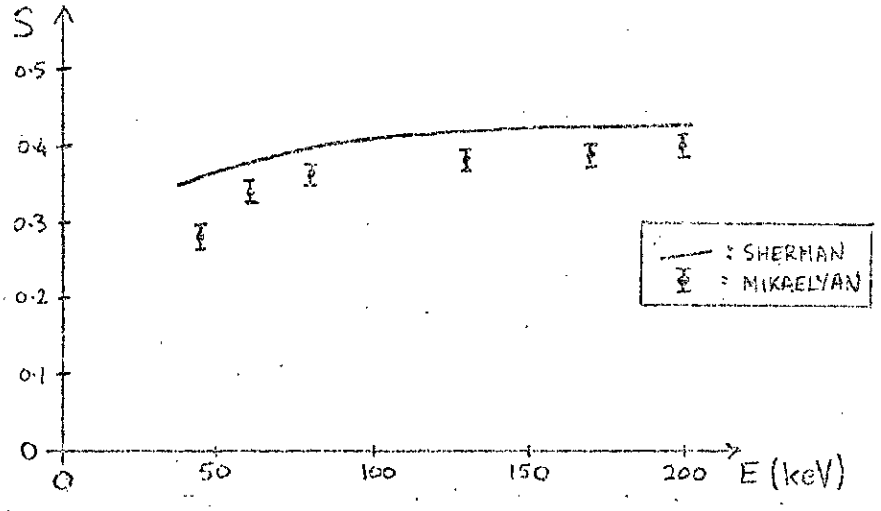

Fig. 3.17: Variation of Sherman function with energy (θ = 120°)

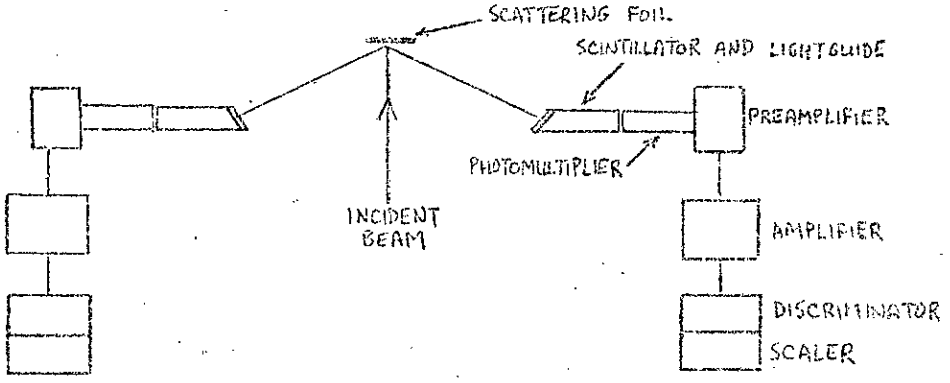

Fig. 3.18: Counting channels.

effects of scattering from the backing. In addition, a scintillating screen was available to examine the beam profile (see Sect.3.3.3). The chamber was evacuated to a pressure of $\sim 2 \times 10^{-6}$ Torr.

Electrons back-scattered from the target through an angle of $\pm 120^{\circ}$ (see Fig. 3.15) were incident on two circular discs of plastic scintillator (NE102A) mounted on cylindrical light guides of polyvinyltoluene. The lightguides passed out of the vacuum chamber through Wilson seals; inside the scattering chamber they were surrounded by aluminium shields containing apertures to define the solid angle of acceptance of the scintillators. Polyvinyltoluene was chosen because its refractive index matched that of the NE102A plastic scintillator, and reflections at the interfaces were therefore avoided. At the other end of the light guide, similar attention was paid to achieving good optical contact with the face of the 20th Century Electronics BMS 10/14A photomultiplier, used in conjunction with a Nuclear Enterprises "Edinburgh Series" counting system. One of the major practical difficulties of Mott-scattering lies in the necessity for the scatterer to be at high voltage relative to source. The frequently adopted solution of placing the entire counting system at high voltage (and taking readings with a telescope!) was avoided here by dropping the high voltage along the lightguides. This too has its disadvantages; experience has shown that electrical discharges in such a sensitive region can be very troublesome. However, it has the advantage that everything from the photomultiplier onwards is at ground potential.

Problems associated with discharges along the lightguides precluded the use of a higher scattering energy than 50 keV. This limitation was not serious as far as the magnitude of the Mott scattering effect was concerned - the variation of the Sherman functions S with energy (Fig.3.17) is fairly slow at the energies involved here - but proved troublesome for other reasons. One problem which was much magnified by the restriction to relatively low energy scattering was the estimation of the effect of multiple scattering in the gold foil, which is dealt with in detail in Section 3.3.4. Another disadvantage was that the energy was not high enough to give a resolved peak in the pulse-height distribution of the photomultiplier output, and a considerable amount of noise had to be accepted in order to be sure of counting all the genuine scattering events.

3.3.3. Electron Optics of Mott Scatterer.

It has already been stated that the spin twister behaved as a cylindrical lens, and that it was expected that the accelerator should have a small overall focussing effect. Detailed calculations were not attempted on the electron optics of the system. Instead, the electron beam cross-section at the scatterer was examined experimentally for a range of accelerating voltages, deflecting voltages, and currents. This was done by covering one of the holes in the scattering foil holder (Fig.3.16) with a scintillating screen made by depositing a uniform layer of silver-activated zinc sulphide on a mica backing. The gold foil normally used as the scattering target could thus be replaced by a scintillating screen of identical

position and size, and the beam cross-section observed through a viewing port in the scattering chamber (Fig.3.15).

Several significant results emerged from this study. The normal image observed on the scintillation screen was a circular disc, of considerably smaller diameter than the scattering foil, crossed by a much more intense bar in the plane of scattering. A photograph of such an image, taken through the viewing port, is shown in Fig.3.21. The diameter of the image was consistent with the diameter of the beam collimators, and confirmed that the electron beam was being adequately confined by these. The intense bar was interpreted as being the result of focussing by the electrostatic deflector, having the appearance of the astigmatic image produced by a cylindrical lens.

One odd effect which had been previously noticed in measurements on counting rates was elucidated by using the scintillating screen. The electrostatic deflector was adjusted by first setting the potentials to the theoretically derived values, and then maximising the transmission of the deflector by further fine adjustments. It was found that two such maxima occurred, for two different values of the deflecting field, and it was not clear which to choose. On examining the image on the scintillating screen, it was found that one maximum (in fact, that corresponding to maximum scattering intensity) had the appearance of an astigmatic image previously described, whereas the other was a more diffuse pattern. It was concluded that the latter was the spurious maximum, possibly arising from a setting of the deflector for which electrons hit the outer plate at such a point that the reflected beam could emerge with considerable intensity through the exit aperture of the deflector.

Periodic beam instability was noticed for certain values of accelerating voltage at high beam currents. The image drifted slowly across the screen, returning abruptly to its original position. The periodicity was a function of accelerating voltage. The effect seemed likely to result from charging and discharging of insulators in or near the beam path (the scintillating screen was coated with a thin layer of aluminium to minimise such effects there). It was less noticeable at low beam currents, and was not therefore likely to be significant when dealing with trapped electrons, the average current of which was always several orders of magnitude lower than the "straight-through" currents ($\sim 10^{-8}$A) used in this investigation.

While investigating the instrumental asymmetries in the Mott scatterer (see Section 3.3.6), it was desired to check on whether the beam cross-section at the scatterer was the same for each trapping time. Since the average current was much too small to give a visible image, long-exposure photographs were taken through the viewing port (Fig.3.15). By this method it was confirmed that for all trapping times used, the beam cross-section retained the "bar" shape previously described, and that its position relative to the scattering foil remained unchanged.

3.3.4 Effect of Scattering Foil Thickness

The theory of Mott scattering given in Section 3.3.1 assumed that electrons were scattered from a single target atom. In practice, a gold foil of a finite thickness (~ 500 Å) is used, and

a fraction of the electrons scattered through a given angle will do so as a result of more than one collision in the scattering foil. Since the magnitude of the Sherman function is in general small for small angle scattering, electrons scattered through 120°. by a series of collisions each resulting in a small angle scattering event will display a negligible asymmetry regardless of their initial polarisation; the overall asymmetry will therefore be reduced. This corresponds to a decrease in the effective Sherman function.

It has been established both by theoretical considerations (Wegener, 1958) and from experimental measurements (Mikaelyan et al, 1963) that for sufficiently small thicknesses of foil, the effective Sherman function is decreased by a fraction proportional to the foil thickness (t); that is,

$$\frac{\Delta S}{S_o} = \alpha t \qquad (3.7)$$

where S_o is the Sherman function corresponding to zero foil thickness. Measuring asymmetries for several foil thicknesses, and extrapolating the asymmetry linearly to zero foil thickness, is therefore a justifiable procedure within the range of thicknesses for which Equation 3.7 is valid. According to Mikaelyan et al., this can be done for values of $\Delta S/S_o$ up to $\sim$ 0.3.

Unfortunately, α is a function of scattering energy which increases rapidly as the energy becomes less than 100 KeV. For scattering of 50 KeV electrons, $\alpha \simeq 6 \times 10^{-3}$, and linear extrapolation can be justified for foil thicknesses up to 50 $\mu g/cm^2$. Since the total scattered intensity is proportional to foil thickness,

this imposes an undesirable restriction on the maximum available count rate. If thicker foils are to be used, however, a different method of extrapolation must be used, and there is no consensus as to the most reliable function of the asymmetry which may be linearly extrapolated to zero foil thickness.

In the present experiment a foil of 100 $\mu g/cm^2$ was used in order to achieve reasonable counting rates at long trapping times. The effective Sherman function was found by extrapolating a graph of A^{-1} against t to zero thickness, a procedure used by Cavanagh (1957) with success. It was not possible to perform polarisation measurements in the present case for thinner foils, so the gradient of the graph was estimated from the data of Mikaelyan in similar circumstances. This results in a value of $\frac{\Delta S}{S_o} = 0.38$, and an effective Sherman function

$$S_{eff.} \simeq 0{\cdot}21 .$$

3.3.5 Instrumental Asymmetry in Mott Scatterer.

Ideally, an asymmetry in the counting rates in the two channels, measuring scattering through $\pm$ 120° respectively, should appear only when the incident electron beam is polarised. In practice, a range of factors may give rise to a spurious asymmetry even when the beam is unpolarised, and this purely instrumental asymmetry must be allowed for in estimating the electron beam polarisation.

In order to see where spurious asymmetries can arise, we may consider Fig. 3.18, showing the two counting channels, and follow the signals through. Starting with the beam incident on the

scattering foil, the beam axis may not be perpendicular to the foil, resulting in different scattering angles on either side. Since the Sherman function varies slowly around $\theta = 120^{\circ}$, this source of error may safely be neglected. The scattered electrons are then incident on scintillators, which may have different conversion efficiencies. The light pulses travel down the light guides to the photocathodes of the photomultipliers, and the two optical systems will probably have different transmission characteristics. The gains of the two photomultipliers will in general be different, and there is the additional possibility that the overall gain of the preamplifiers and amplifiers may be different. The net result of these effects is that the pulse-height distributions due to a monoenergetic incident electron beam can be different in the two channels. The signals then pass through discriminators; unless the pulse-height spectra are identical, equal settings of discriminator level will result in different fractions of the total count rate passing to the scalers; the net result will be that an instrumental asymmetry appears. An additional possible source of error arises from the fact that the scalers are gated to accept input only for a short period after each trap ejection, in order to reduce background; differences in the gating in each channel could produce an apparent asymmetry.

The procedure adopted in allowing for these effects was to set the discriminator levels to the same value by feeding into both the output from the amplifier of one channel, and adjusting for equal count rates; the amplifier gains were then equalised by feeding

the output from one preamplifier to both amplifiers; the pre-amplifier gain was not variable. It was then assumed that with an unpolarised electron beam incident on the target, equal numbers of electrons were falling on each scintillator, and the gains of the photomultipliers were adjusted until equal count rates were achieved in the two channels.

One disadvantage of the Mott scatterer used here was its inability to rotate about the incident beam axis. This facility would have enabled the entire counting channels, from scintillators onwards, to be interchanged. The sign of any instrumental asymmetry arising due to differences in the counting channels would then have changed, whereas that of the genuine assymmetry would not; the two could therefore have been distinguished. It should be noted, however, that the present scatterer was not designed as a high precision instrument, capable of absolute measurements. Essentially, it was designed to measure the difference in asymmetry between a polarised electron beam (when a polarised atomic beam was flowing through the trap) and an unpolarised beam (when the atomic beam was off). Since instrumental asymmetries in the Mott scatterer were unlikely to depend on the presence of an atomic beam in a quite different part of the apparatus, the instrumental asymmetries were expected to be the same in the two cases. By simply subtracting the measured asymmetry in an "atomic beam off" experimental run, the genuine polarisation dependent asymmetry would be found.

In order to ensure that only electrons scattered from the gold foil were counted, and that spurious counts from electrons scattered by the chamber walls, or from photomultiplier noise, did not dilute the asymmetry, one of the holes in the target holder was covered only by the cellulose nitrate backing on which the 100 $\mu g/cm^2$ gold film was normally evaporated. The effect of substituting this for the gold target was therefore effectively to remove the gold atoms from the backing, leaving everything else unaltered. Every measurement with a gold foil was normally accompanied by such a background measurement, which was subtracted before calculation of the asymmetries.

3.3.6. Instrumental Asymmetry with Trapped Beams

With the first results from tests of the Mott scatter with an unpolarised but trapped electron beam, a major problem presented itself. It was found that the instrumental asymmetry was systematically dependent on the trapping time. The details of this dependence were liable to change considerably between experimental runs; but for a given run the measured asymmetry, calculated after subtraction of background, increased (or decreased) regularly with increasing trapping time.

In order to understand the full implications of this fact, it must be recalled that the effect which the experiment was primarily designed to study, namely the polarisation of the electron beam by spin-exchange collisions with the atomic beam, manifests itself in just the same way as does this trapping-time dependent instrumental effect. The polarisation of the electron beam was expected to

increase regularly with trapping time in accordance with Equation 3.2, the time constant depending on the spin-exchange cross section. Any instrumental asymmetry which was independent of the trapping time would not affect the form of this curve, but would merely shift the abscissa. If had therefore been hoped that the asymmetry corresponding to genuine polarisation would have been readily distinguished from instrumental effects by just this dependence on trapping time which the instrumental effects now appeared to demonstrate.

The magnitude of the effect varied considerably, but a typical set of results is given in Table 3.1 and Fig. 3.19, showing an instrumental asymmetry change of nearly 4% for a variation in trapping time of 15 ms.

A considerable time was spent in attempting to identify the experimental factors which determined the size of the effect, and various possible causes were considered and discarded. The possibility that the gating of the scalers might vary with trapping time in such a way as to cause an asymmetry was ruled out by interchanging the two channels from preamplifiers onwards, which did not change the sign of the asymmetry. Another obvious possible explanation arose from the dependence of trap losses on trapping time, resulting in a smaller number of electrons in each output pulse at long trapping times than at short trapping times. The "dead-time" correction arising from the finite resolution time of the counting system would therefore be more significant for short trapping times. An estimate of the upper limit of such a correction may be made by assuming that if two electrons from a single trap output pulse

Trapping time T (ms)	Asymmetry A (10^{-2})	Uncertainty ΔA (10^{-2})
0.3	-4.5	$\pm$ 0.4
3.1	-6.3	$\pm$ 0.7
15.5	-8.4	$\pm$ 1.0

Table 3.1: Dependence of instrumental asymmetry on trapping time - a typical set of measurements.

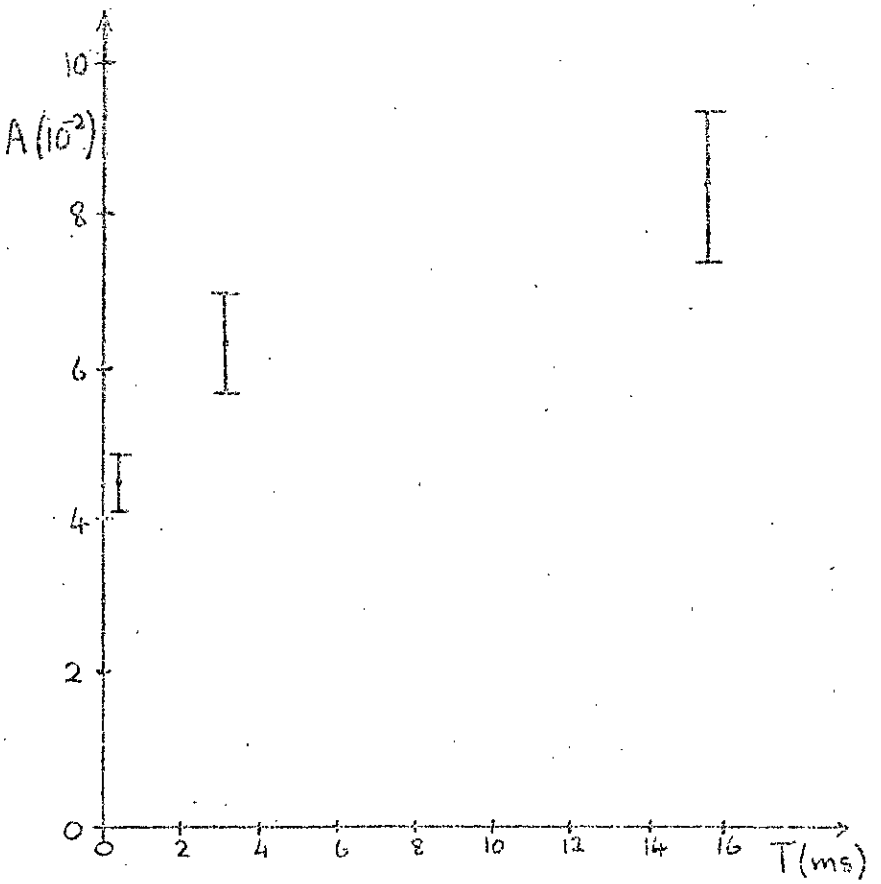

Fig. 3.19: Instrumental asymmetry A versus trapping time T.

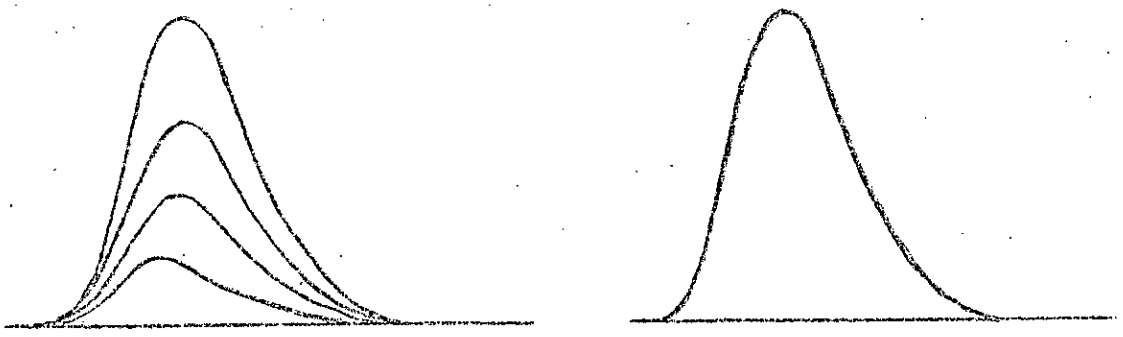

(a): low count rate (b): high count rate

Fig. 3.20: Oscilloscope traces of photomultiplier pulses due to trap output.

arrive at one of the scintillators, only one count will be recorded. (In fact, since most of the electrons in a given output pulse appear to leave the trap within one microsecond of the opening of the output gate of the trap, this is probably a fairly realistic estimate.) For small asymmetries, it can be shown that the correction ΔA which must be made to the measured asymmetry A is approximately

$$\Delta A = \beta A,$$

where β is the probability of a count being registered in a given channel due to a single output pulse from the trap. If the correction is to be negligible in comparison with the uncertainty in measuring A (normally of the order of $\pm$ 1%), the maximum count rate per pulse in each channel must be restricted to a value

$$\beta < 0.1.$$

The maximum correction necessary for a measured asymmetry of 5% would then be less than 0.5%.

The effect of increasing β above this limit was observed by displaying the output from one of the photomultipliers on an oscilloscope. The oscilloscope was triggered by the pulse which opened the output gate of the trap, and thus displayed superimposed the pulses resulting from several hundred openings of the trap. For relatively low currents the heights of these pulses formed a continuous spectrum (Fig.3.20 (a)), for although the electrons arriving at the scintillator were all the same energy, the number of light quanta received by the photomultiplier per incident electron fluctuated. When the beam current was increased, the

oscilloscope trace assumed the appearance of Fig.3.20(b). The pulses were of a more or less uniform height, corresponding to limiting in the amplifier, and no small pulses were observed. Clearly, under these circumstances, the probability of only one electron arriving at the scintillator during an output pulse was small, and it would be meaningless to perform asymmetry measurements by comparing the counting rates in the two channels. It was therefore essential to restrict β to reasonably low values.

In practice, values of β up to 0.15 have been used in order to accumulate a significant number of counts without unduly long runs. Even so, the difference between the corrections required for asymmetries measured at short and long trapping times could not approach the observed differences in the instrumental asymmetry. The final nail in the coffin of this explanation was the observation that altering the gain of one channel (by adjusting the photomultiplier voltage), so that the sign of the measured asymmetry changed, did not reverse the sign of the asymmetry difference between long and short trapping times.

The possibility that the pulses which were applied to the trap might be influencing the counting system was carefully investigated, and it was in fact discovered that such pulses were being picked up and transmitted through the power supplies to the amplifiers and discriminators. Eliminating these did not however eliminate the dependence on trapping time of the instrumental asymmetry.

A series of experimental runs was performed, during which various experimental parameters were varied in order to identify those to which the effect was sensitive. The results were not wholly conclusive, since the magnitude appeared to vary when everything under experimental control remained constant, but the effect was found to depend on the depth of the trap: the difference between long and short trapping time asymmetries increased as the trap depth was reduced.

It is difficult to see how such a dependence could arise. The electron optics of the trap varied with trap depth, and it seemed possible that the orientation of the electron beam entering the deflector might be different for different trap depths. This could result in the beam being steered to one side or another during acceleration; if it arrived considerably off-centre at the scatterer, this could give rise to an asymmetry in the counting rate of the two scintillators, since the scattering geometry would no longer be symmetrical. If this were the explanation of the effect, however, the orientation of the beam would have to be dependent on the trapping time as well as on the trap depth. To check this, the scattering foil was replaced by the scintillating screen, and the photographs shown in Fig. 3.21 taken. There is certainly no obvious difference between the cross-sections of the untrapped beam and either of the beams corresponding to short and long trapping times. This explanation was therefore also discarded.

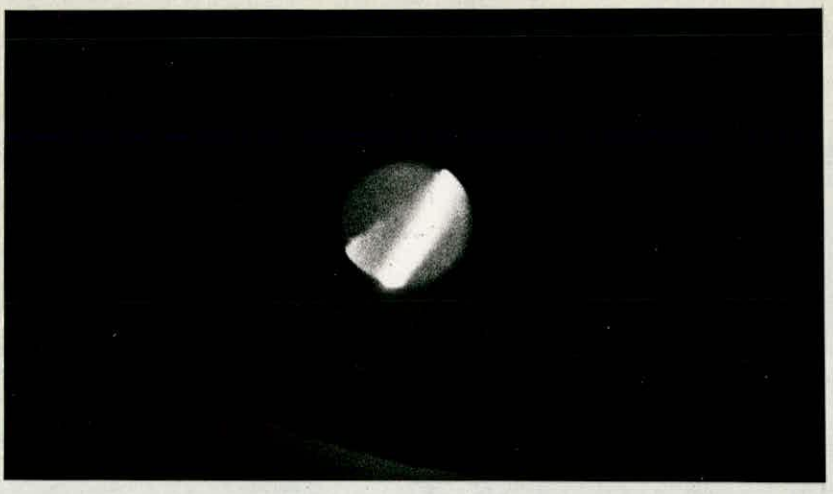

(a):
untrapped

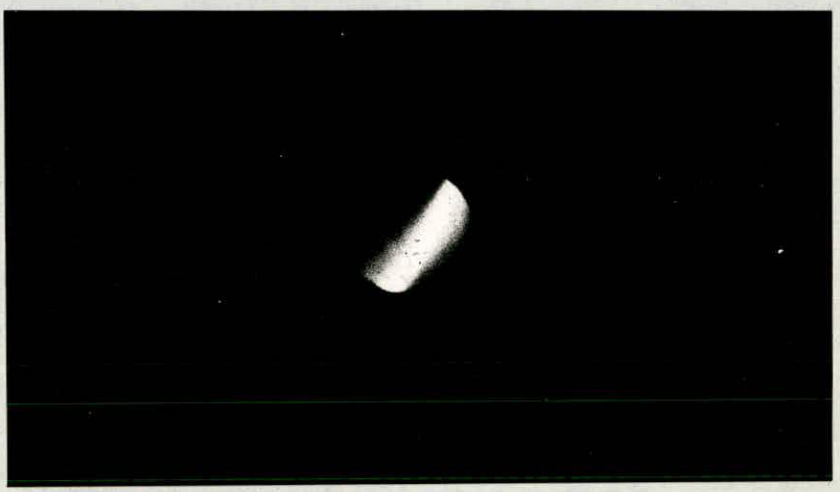

(b)
TT = 0·3ms

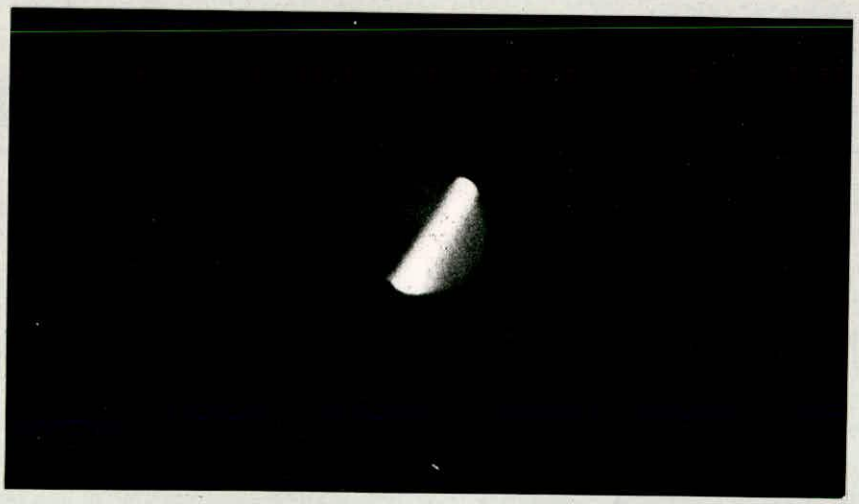

(c)
TT = 10ms

Fig. 3.21: Beam cross-section at scattering foil.

3.3.7 Measurement Procedure

The method of taking measurements was based on the automatic repetition of a cycle of measurements at different trapping times. The timer of the counting system was modified to count the pulses applied to the output gate of the trap instead of those from its internal oscillator. One cycle of measurement involved (i) selecting a given trapping time; (ii) counting for a fixed number of trapping cycles (usually 2×10^4); (iii) printing out the number of counts accumulated at the two scalers; (iv) replacing the foil by a backing film and repeating (ii) and (iii); (v) selecting a different trapping time, replacing the gold foil, and repeating from (ii) for as many trapping times as was desired (usually six). When the cycle was complete, the original trapping time was selected, and the cycle repeated a sufficient number of times to give adequately low uncertainties. The asymmetries were then derived by summing the corresponding terms in each cycle output, subtracting the total "foil in" counts from the corresponding "foil out" counts, and calculating the asymmetries in corresponding pairs of corrected totals.

The number of cycles required to achieve a given uncertainty in the asymmetry was determined by the limit on β. Normally each element of a cycle consisted of 2×10^4 output pulses of the trap, and the maximum number of counts allowed by restricting to 0.15 was therefore 3×10^3 in each channel. Since for small asymmetries the absolute uncertainty in an asymmetry measurement is

$$\Delta A \simeq N^{-\frac{1}{2}},$$

where N is the sum of the two counts, the restriction on β implied that at least seven cycles would be required in order to reduce the uncertainty in the asymmetry to 0.5%. In fact, the count rate for long trapping times was usually much lower than for short trapping time due to losses, and longer series of cycles were necessary.

The reason for choosing a large number of fairly short cycles, rather than a single cycle whose elements were each long enough to accumulate significant numbers of counts, was that the instrumental asymmetry showed long term fluctuations. These seemed to be due to variations in the gains of the photomultipliers, which were of course highly dependent on applied voltage. It was therefore not possible to do a significant measurement over a period greater than about an hour; in order to reduce the effect to insignificance the repetition period of the cycles was reduced to about 10 minutes, the exact time depending on the choice of trapping times.

These precautions did not affect the trapping time dependence of the instrumental asymmetry. Since it was not found possible to find the cause of this effect, or to eliminate it by a suitable choice of experimental circumstances, it was necessary to allow for it in the treatment of the results. The method at first adopted was to precede and follow each experimental run in which an atomic beam was present, and polarisation therefore expected, with a run in which the atomic beam was switched off, and the electron beam unpolarised. The unpolarised runs were used to estimate the variation of instrumental asymmetry which would have occurred in

the central run if the atomic beam had been switched off; the difference between this variation and that which actually occurred was taken as the asymmetry variation due to the presence of the beam, corresponding to genuine polarisation. Experience showed that this method of allowing for the trapping-time dependence of the instrumental asymmetry was not entirely satisfactory. It has already been pointed out that the value of the instrumental asymmetry for a fixed trapping time drifted noticeably over the length of time necessary for an experimental run (usually about four hours); it appeared that the difference in instrumental asymmetry for different trapping times also showed this kind of fluctuation.

It was therefore common to find that the difference in asymmetry for short and long trapping times in the run preceding the polarisation measurement was substantially different from that in the run following the polarisation measurement, and there was some doubt that a simple averaging provided a valid estimate of the instrumental effect in the polarisation run.

Eventually it was decided that the only way to be sure that the instrumental effect was being properly measured and allowed for, was to interlace measurements on polarised and unpolarised electron beams (atomic beam on and off respectively), at such a frequency that the instrumental effect was effectively constant during each pair of measurements. It might then be expected that the average instrumental asymmetry, obtained from the summations of the "unpolarised" counts in a complete run consisting of many such

pairs, would correspond fairly accurately to that part of the average asymmetry in the "polarised" counts due solely to instrumental effects.

To assess the validity of this scheme a series of measurements on an unpolarised beam was analysed in the way described above. The results for a typical run are shown in Table 3.2 and Fig.3.22. This run contained 24 cycles, each consisting of measurements at three different trapping times with gold foil in and out, as previously described. Each cycle lasted just under ten minutes. Cycles numbered 1, 2, 5, 6, 9, 10, etc. were labelled "series A", cycles numbered 3, 4, 7, 8, 11, 12, etc., were labelled "Series B". The average asymmetries at each trapping time, corrected for background, were computed separately for the two series. It was found that for each series the asymmetry tended to increase with trapping time as expected, the asymmetry at the long trapping time in each case being about 1.5% greater than that at short trapping time. The difference between the average asymmetry at a given trapping time in Series A and the asymmetry at the same trapping time in Series B was found to be zero within the uncertainty expected from statistical considerations.($\pm 0.8\%$)

The deduction may therefore be made with reasonable confidence that if the atomic beam had been passed through the trap only during the cycles of Series A, and had been switched off during those of Series B, an accurate estimate of the instrumental asymmetry for each trapping time in the Series A measurements could be found by using the asymmetries calculated from the measurements of Series B. This conclusion was confirmed by many such

Trapping time T (ms)	Asymmetry A with uncertainty ΔA (10^{-2})		
	Series A	Series B	A(A) - A(B)
0.3	0.4 ± 0.5	0.3 ± 0.5	0.1 ± 0.7
3.0	0.9 ± 0.6	0.8 ± 0.6	0.1 ± 0.8
6.5	2.1 ± 0.6	1.7 ± 0.6	0.4 ± 0.8

Table 3.2: Asymmetry measurements with an unpolarised beam (see p.101).

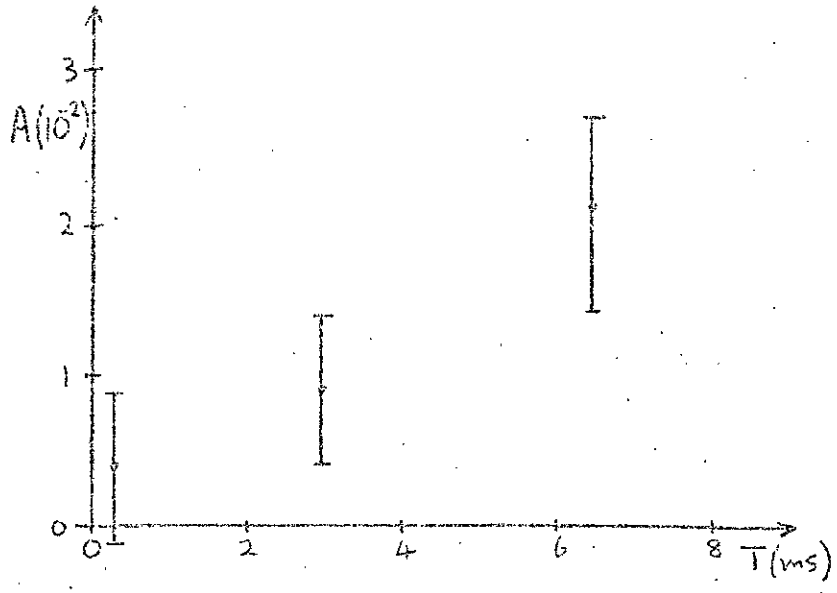

(a): Series A.

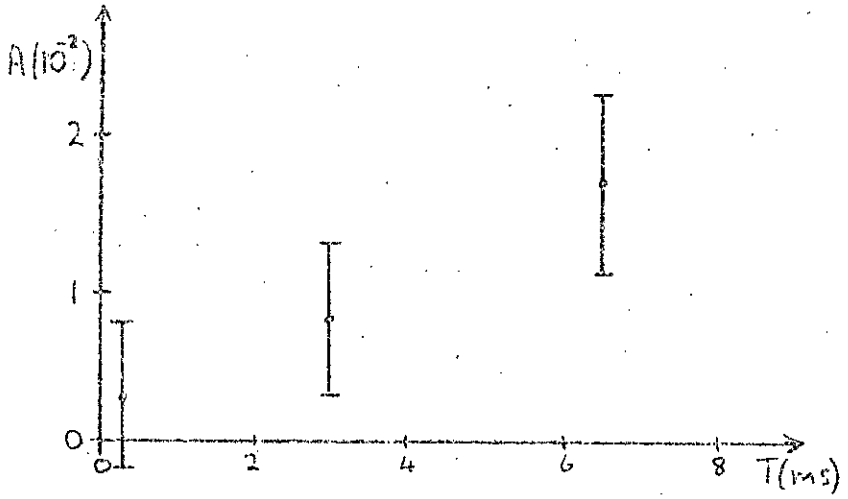

(b): Series B.

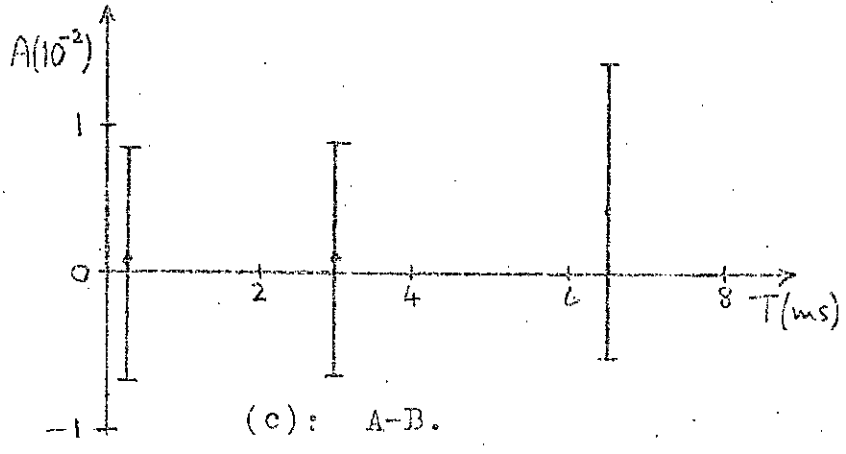

(c): A-B.

Fig. 3.22: Instrumental asymmetry in interleaved series.

measurements of the type shown in Table 3.2.

This method of measurement was nevertheless adopted with reluctance, because it involved "wasting" half of the output of the atomic beam oven. In order to achieve a stable atomic beam the oven had to be heated up and cooled down slowly, and it was not possible to do this in the twenty minute intervals prescribed above. The atomic beam was therefore running continuously, but was shut off from the trap for half of its life. The increased frequency of oven filling was finally accepted as the price of accounting for the trapping time dependence in the instrumental asymmetry.

CHAPTER 4

4.1. MEASUREMENTS OF ELECTRON POLARISATION AT FIXED TRAP DEPTH

4.1.1. Nature of the Measurements

The results presented and discussed in this chapter are measurements of the polarisation of the pulsed electron beam extracted from the electron trap after interaction with a polarised potassium beam. The measurements were made in accordance with the procedure outlined in Section 3.3.7, except that the regular accompaniment of every measurement of scattering from the gold target by a similar measurement using only the backing film was replaced by an occasional check on the magnitude of the signal to background ratio. Justification of this change was provided by the observation that, while the correction to the absolute value of the asymmetry resulting from the subtraction of the background counts could be significant, the relevant quantity in the experimental analysis was in fact the difference between the asymmetry measured with the atomic beam on, and the corresponding asymmetry with the atomic beam off. The change in this difference occasioned by the background corrections was invariably found to be insignificant in comparison with the statistical uncertainties (see, for example, Table 4.1). It can be seen that this will be the case if the signal to background ratio is much greater than 1, as long as neither the signal to background ratio nor the asymmetry in the background changes by more than a few per cent

Trapping time T (ms)	Asymmetry A with uncertainty ΔA (10^{-2})					
	with background correction			without background correction		
	Series A	Series B	A(A)-A(B)	Series A	Series B	A(A)-A(B)
	$\Delta A=\pm 0.5$	$\Delta A=\pm 0.5$	$\Delta A=\pm 0.7$	$\Delta A=\pm 0.5$	$\Delta A=\pm 0.5$	$\Delta A=\pm 0.7$
0.3	5.0	6.0	-1.0	5.6	6.6	-1.0
3.0	4.1	6.6	-2.5	4.6	7.0	-2.4
6.5	2.0	6.1	-4.1	2.6	6.6	-4.0

Table 4.1: Measurements on polarised electron beam, illustrating effect of background corrections.

due to the introduction of the atomic beam. Since the scalers were gated to coincidence with the trap output pulse, the signal to background ratio was always >10; the validity of the other conditions was confirmed by the occasional background measurements.

This change in procedure enabled a more rapid accumulation of data. When the full procedure was used with alternations of both "atomic beam on - atomic beam off" and "foil in - foil out" measurements, only a quarter of the total running time of the atomic beam oven was in fact available for the actual polarisation measurements. By elimination of the "foil out" measurements, it was possible to repeat a cycle of six trapping times, ranging from 1.5 ms to 17 ms, with and without the atomic beam, five times in an hour. About 30 hours of such measurements were necessary in order to accumulate a sufficient number of counts to reduce the statistical uncertainty in the asymmetry difference discussed above to $\pm 5 \times 10^{-3}$; it was normally possible to carry out such a run without having to refill the atomic beam oven.

4.12. Confirmation of Equation 3.2

In Section 3.2, the interaction between trapped electrons and polarised atoms was discussed, and a formula derived which predicted the polarisation of the emergent electrons as a function of time:

$$P = \frac{\mu(1 - e^{-\lambda t})}{1 - \nu e^{-\lambda t}} \qquad 3.2.$$

(the parameters μ, λ and ν being defined in Sect.3.2.2).

The form of this function depends on the magnitude of ν, which in turn is governed by the parameter α characterising the rate of loss of electrons from the trap. It can be shown (Appendix 4) that if $\alpha \ll 1$, then $\nu \ll 1$. In the present case, $\alpha \simeq 0.1$ (see Appendix 3), so that the exponential term in the denominator of Equation 3.2 can be neglected:

$$p \simeq P(1 - e^{-\lambda t}). \qquad 4.1$$

The first experimental task was to verify that the electron polarisation was validly described by Equation 4.1.

For reasons previously given (Sect.2.1.3), these initial measurements were done using a nominal trap depth of 1.5 volts. The results obtained are shown in Table 4.2; in Fig. 4.1 the asymmetry is plotted as a function of trapping time. The continuous curve in Fig. 4.1(a) is a least mean squares fit of the exponential function

$$A = A_0 (1 - e^{-\lambda t});$$

the best fit was obtained with

$$A_0 = 8.5 \times 10^{-2},$$
$$\lambda = 87\ s^{-1}.$$

The confirmation of the functional dependence predicted by Equation 4.1 which these results afford is perhaps best illustrated

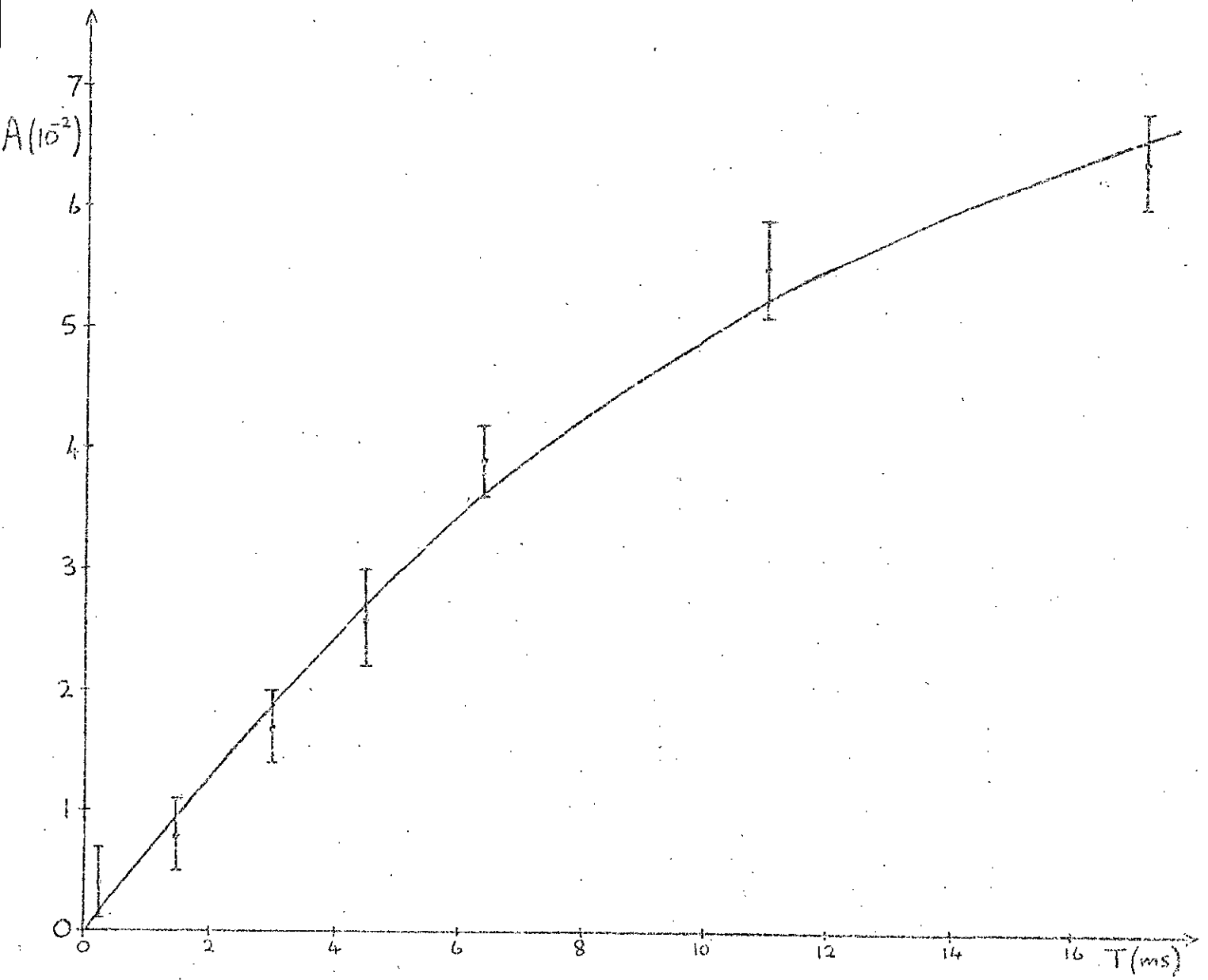

Fig. 4.1(a): Electron asymmetry versus trapping time (D = 1.8V).

Trapping time T (ms)	Asymmetry $A(10^{-2})$	Uncertainty $\Delta A\ (10^{-2})$
0.3	0.4	$\pm$ 0.3
1.5	0.8	$\pm$ 0.3
3.0	1.7	$\pm$ 0.3
4.5	2.6	$\pm$ 0.4
6.4	3.9	$\pm$ 0.3
11.0	5.5	$\pm$ 0.4
17.2	6.4	$\pm$ 0.4

Table 4.2: Electron scattering asymmetry versus trapping time (well depth 1.8V).

by Fig. 4.1(b), in which $\ln (A_o - A)$ is plotted against t. According to Equation 4.1,

$$\ln (A_o - A) = \ln A_o - \lambda t \; ;$$

the straight line in Fig. 4.1(b) is the previously derived least mean squares fit.

Having established the functional dependence, it remained to confirm that the magnitudes of μ and λ were consonant with theoretical predictions. The equilibrium electron polarisation,

$$p(\infty) = \mu ,$$

is obtained from A_o through the relationship

$$p(\infty) = A_o S^{-1} ,$$

where S is the Mott scattering Sherman function. A considerable disagreement between theoretical and experimental values of S at the electron scattering energy used here (50 keV) was pointed out in Section 3.3.4; coupled with the uncertainty arising from multiple scattering in the target foil, this disagreement led to some doubt as to the correct value of S to be used in the present circumstances. Adopting the value S = 0.21 proposed in Section 3.3.4 gave a value for the equilibrium electron polarisation

$$p(\infty) = 0{\cdot}40.$$

According to the discussion in Section 3.2.4, if losses can be neglected, $p(\infty)$ should be given by

$$p(\infty) = P_A \left(1 + \frac{\lambda_R}{\lambda_P}\right)^{-1} , \qquad 4.2.$$

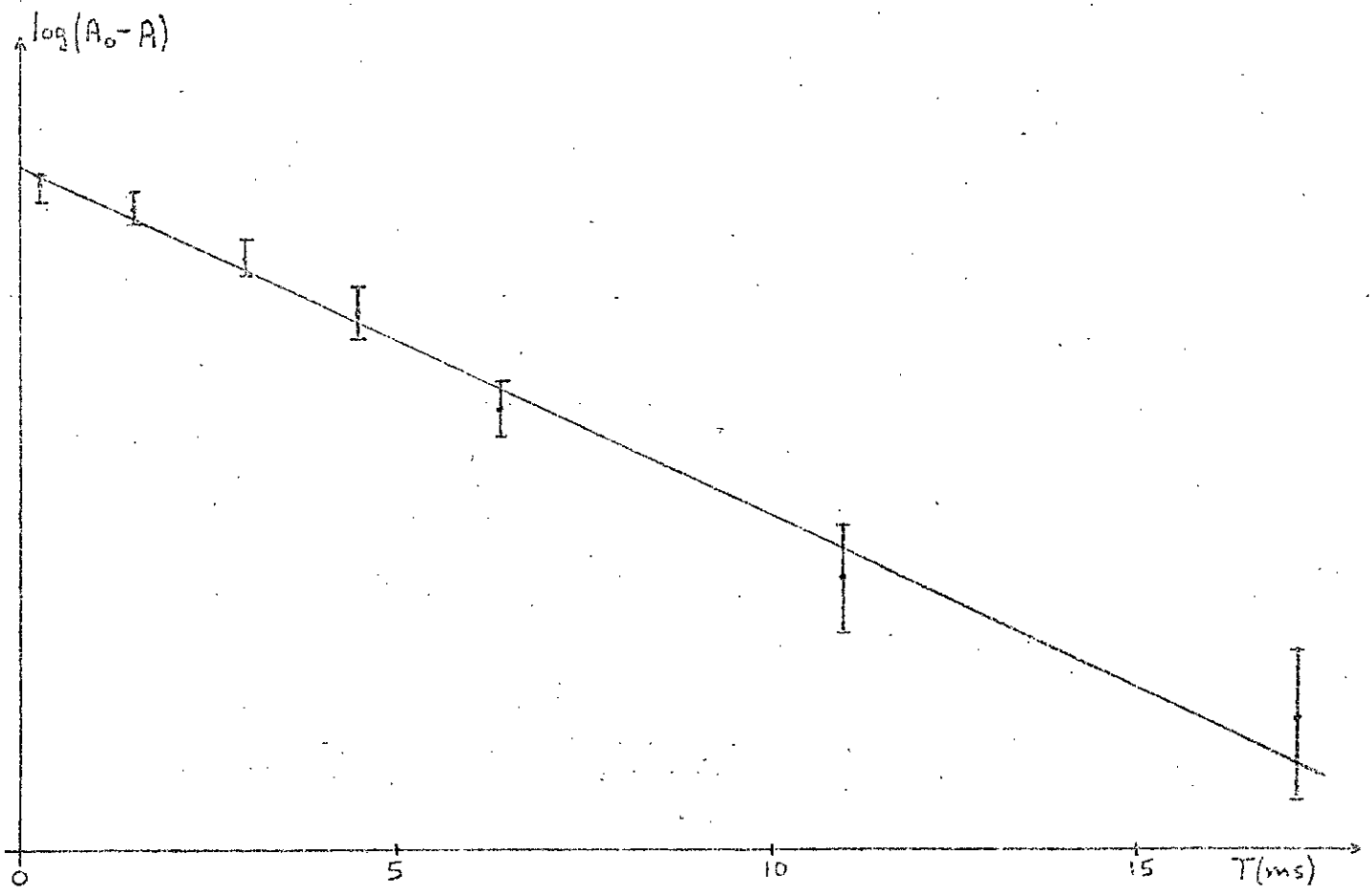

Fig. 4.1(b): Logarithmic plot of results given in Fig. 4.1(a).

where P_A is the atomic beam polarisation in the interaction region, and λ_p and λ_R are the contributions to the rate constant λ due to potassium and residual gas atoms respectively. In Section 3.1.4 the polarisation of the atomic beam in a strongly decoupling magnetic field was estimated to be 0.95; in a field of 6×10^{-3}T, this would be reduced to 0.45.

According to Equation 4.2,

$$\frac{\lambda_R}{\lambda_P} = \frac{P_A}{p(\infty)} - 1 .$$

The difference between the equilibrium electron polarisation ($p(\infty) = 0.40$) and atomic beam polarisation ($P_A = 0.45$) might therefore be ascribed to spin relaxation effects, with

$$\frac{\lambda_R}{\lambda_P} \simeq 0.1 .$$

However, there are two other possible sources of this discrepancy. The calculation of atomic beam polarisation involved idealising assumptions about the symmetry of the six-pole field, and the accuracy of alignment of the atomic beam system; the quoted figure could be reduced by imperfections in these aspects, although the direct measurements (Sect. 3.1.4) suggested that the polarisation in the interaction region was unlikely to be much below 0.40. Another possibility is that the value adopted for the effective Sherman function is an overestimate. If the

experimentally derived value of the Sherman function at zero foil thickness (0.29) given by Mikaelyan et al. is used instead of the theoretical value (0.34) derived by Holzwarth and Meister, correction for foil thickness yields a value for the effective Sherman function of 0.18, instead of 0.21; the equilibrium electron polarisation (corresponding to $A_o = 8.5 \times 10^{-2}$) then becomes

$$p(\infty) = 0.47.$$

Because of these uncertainties, the most that can be said about relaxation effects is that the corresponding rate constant λ_R appears to be at least an order of magnitude smaller than the rate constant characterising the polarising effect of the atomic beam. This is understandable, since the spin-flip cross-section for most residual gases is likely to be very much smaller than the potassium spin-exchange cross-section (see Section 3.2.4).

If relaxation effects are discounted, the experimental results suggest that

$$\lambda_P = \lambda = 87\,s^{-1}.$$

A reliable theoretical estimate of this quantity under the present experimental circumstances was difficult to obtain. According to Section 3.2.4, when losses from the trap may be neglected

$$\lambda_P = Q_e N v;$$

in Section 3.2.7 it was pointed out that because the atomic beam did not fill the trap, v must be replaced by v', the path

length traversed in the interaction region per unit time. The value of v' will depend both on the momentum distribution in the trapped electrons and on the radial extent of the electron cloud. A further complication is introduced by the fact that the atomic beam did not have a uniform density within its defined radius of 3mm; a plot of the radial intensity distribution, taken with the Langmuir-Taylor hot wire detector described in Section 3.1.4, showed (Fig. 4.2, curve A) that the density was highest on the axis, falling off sharply towards the perimeter. Thus both the width of the interaction region traversed by a given electron, and the average atomic density in the neighbourhood of its path, would depend on the radial and azimuthal co-ordinates of the guiding centre of the electron's cyclotron orbits.

These considerations were made quantitative by assuming that the radial density distribution in the atomic beam was described by

$$\rho = \rho_0 \left(\frac{3 - r}{2}\right) \quad \text{for} \quad r \geq 1$$

$$\rho = \rho_0 \quad \text{for} \quad r \leq 1$$

where r is the radial distance from the atomic beam axis (in mm).

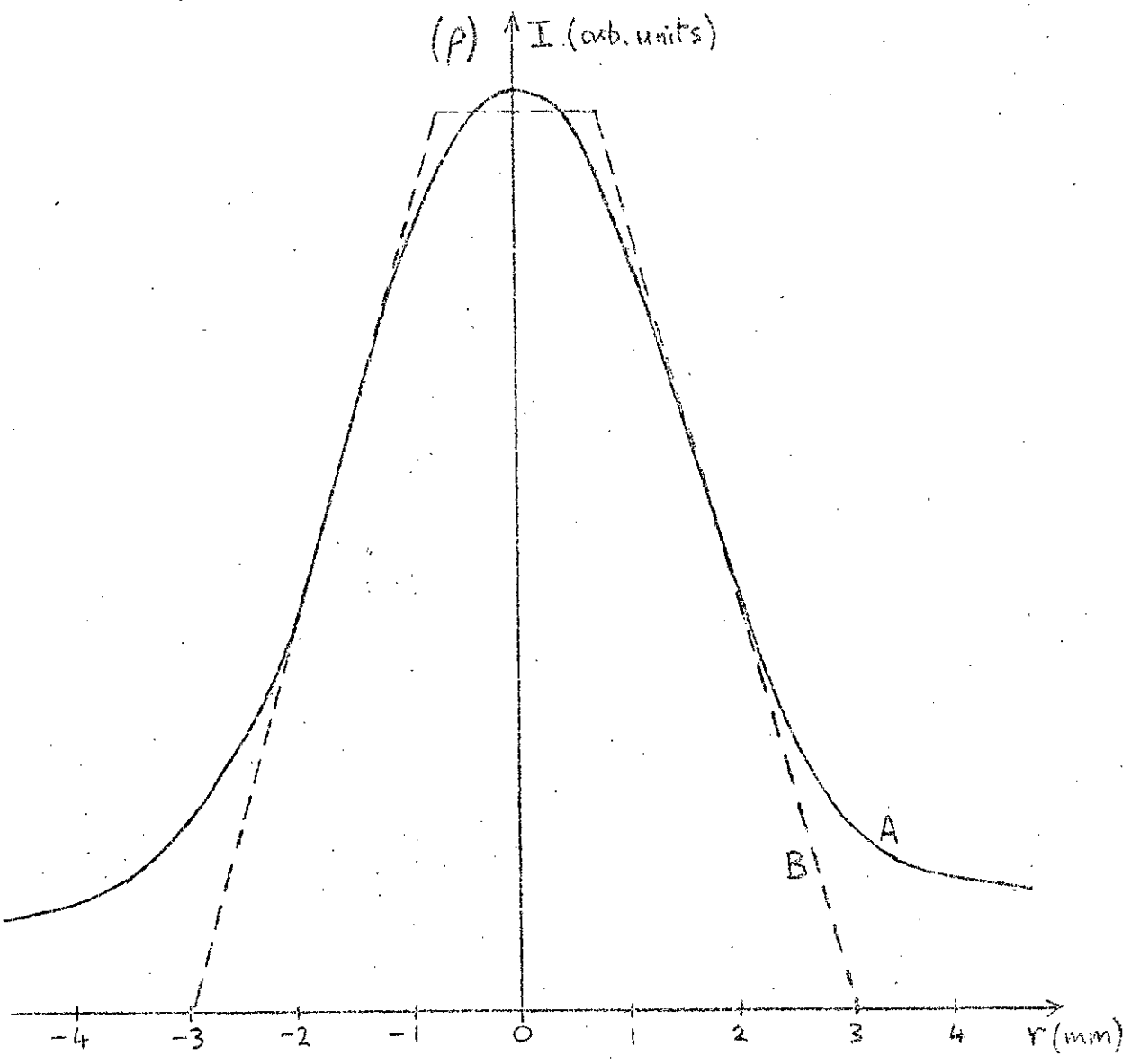

Fig. 4.2: A - Radial atomic beam intensity distribution I (r)
B - Simplified radial density distribution (r)

This curve, and its relationship to the measured intensity distribution, is shown in Fig. 4.2. An electron travelling on the z axis would pass through the centre of this distribution; the width of the interaction region traversed by such an electron would be $2r_A = 6$ mm., and the average atomic density over the electron's path would be (see Appendix 5)

$$\langle \rho \rangle = 0.67\, \rho_o .$$

The value $N = 3.1 \times 10^{14}$ m^{-3} quoted in Section 3.1.3 was the average number density of atoms within a cylinder of radius 3 mm. coaxial with the z axis in the trap. In terms of ρ_o,

$$N = 0.48\, \rho_o ;$$

thus

$$\rho_o = 6.5 \times 10^{14}\ \text{m}^{-3} ; \qquad \langle \rho \rangle = 4.4 \times 10^{14}\ \text{m}^{-3} .$$

Assuming that the orientation of momentum vectors in the trapped electron ensemble is rapidly randomised by collisions, the average value of v' is (see Section 3.2.7)

$$\langle v' \rangle = \frac{2\sqrt{3}\,\omega_z r_A}{\pi} = 3.3 \times 10^5\ \text{m s}^{-1}.$$

Thus the expected value of λ_p corresponding to the foregoing assumptions is

$$\lambda_p := Q_e \langle \rho \rangle \langle v' \rangle$$
$$= 1.5 \times 10^{+20}\, Q_e\ \text{s}^{-1}.$$

The above case, in which the electron oscillates through the centre of the atomic beam, provides an upper limit to λ_p, since both $\langle \rho \rangle$ and $\langle v' \rangle$ have maximum values. A lower limit may be derived by considering an electron which moves on a trajectory such that the guiding centre of the cyclotron orbits precesses round the z axis at a radius $r_A = 3$ mm.

(see Fig. 4.3). If the precession radius exceeds this value, some of the axial oscillations will not intersect the atomic beam at all; however, such an electron would be lost from the trapped ensemble (Section 2.4.1). It was pointed out in Section 3.2.7 that the width of the interaction region and the average atomic density experienced by a precessing electron would vary periodically with the precession angle. In Appendix 5, the magnitudes of these effects were estimated for an electron with precession radius r_A; Fig. 4.4 shows the variation with precession angle θ of the average atomic density $\langle\rho\rangle$, and of the function

$$F(\theta) = \langle\rho\rangle \sin\theta .$$

The average value of λ_p characterising an ensemble of electrons precessing at a radius r_A is obtained by averaging over the precession angle:

$$\langle\lambda_p\rangle = \frac{2}{\pi}\int_0^{\pi/2} Q_e \langle\rho\rangle\langle v'\rangle \, d\theta$$

$$= \frac{2\sqrt{3}}{\pi} Q_e r_A \omega_z . \frac{2}{\pi}\int_0^{\pi/2} F(\theta)\, d\theta .$$

Carrying out a numerical integration of $F(\theta)$:

$$\langle\lambda_p\rangle = 0.6 \times 10^{20}\, Q_e \;\; s^{-1} .$$

It may thus be stated that the measured polarisation rate constant should be between the limits $0.6 \times 10^{20}\, Q_e\; s^{-1}$ and $1.5 \times 10^{20}\, Q_e\; s^{-1}$. The actual value will depend on the radial distribution of the electrons. The lower limit is unlikely to be approached, since it would correspond to a situation in which the electron cloud was much more dense on the periphery than on the axis. The effect of diffusion will be to produce

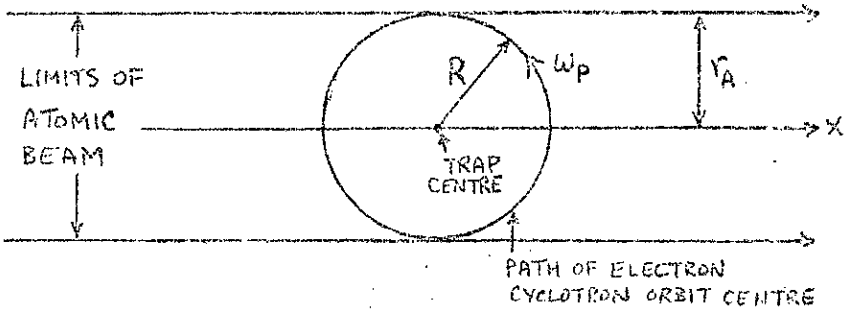

Fig. 4.3: Limiting precession radius for trapped electron.

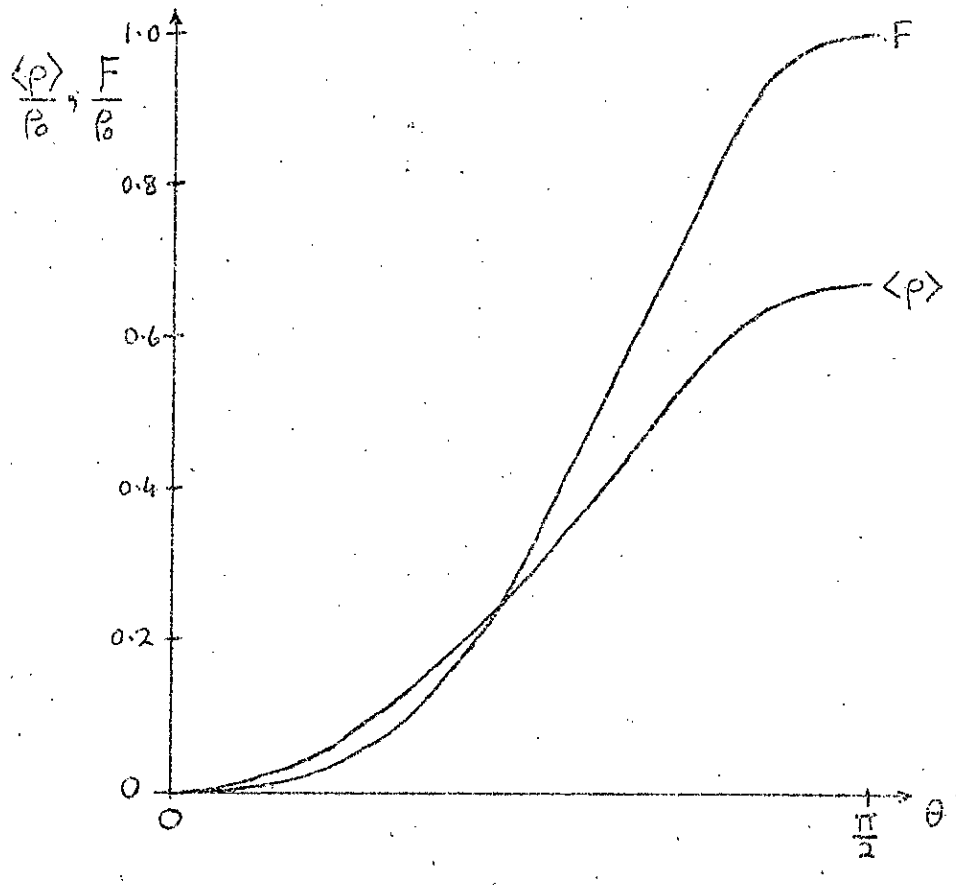

Fig. 4.4: $\langle\rho\rangle$ and F versus precession angle θ.

a uniform distribution; the corresponding value of λ_p, which will be about $1.0 \times 10^{20}\ Q_e\ s^{-1}$, is probably a more realistic lower bound.

In the experimental circumstances to which the measurements quoted above pertain (trap depth 1.5 volts, magnetic field 6×10^{-3} T), losses from the trap were usually small but significant. From this it could be deduced that, at least for the greater part of the trapping period, the trapped electron cloud had a radial extent comparable to $r_A = 3$ mm. Assuming, therefore, that

$$\lambda_p = 1.0 \times 10^{20}\ Q_e\ s^{-1},$$

the measured value of $87\ s^{-1}$ for λ_p implied that

$$Q_e = 0.87 \times 10^{-18}\ m^2 .$$

Comparison with the results of Farago and Siegmann, and of Rubin et al., which were discussed in Section 1.2.2, shows a reasonably satisfactory general agreement; more detailed discussion, including an estimate of the uncertainty in the present value of Q_e, is deferred until Section 4.1.4.

4.1.3. Effect of Increase in Atomic Beam Density

A further series of electron polarisation measurements was carried out, in which the experimental conditions were identical to those of the measurements described in Section 4.1.2., except that the atomic beam density was doubled. There were two purposes behind this. One was to confirm that the rate constant λ_p was linearly dependent on the atomic beam density; the other was to establish whether it would be possible to use the higher density in further measurements. The advantage of using a more dense beam would be that a given electron polarisation could be achieved in a shorter trapping time. However, at the normal temperature of 583K, the oven was already operating outwith the conditions for which molecular flow might be expected in the channel, as pointed out in Section 3.1.3. Consequently, the oven temperature had to be increased to 613K, corresponding to a pressure increase of ~ 3 times, in order to double the beam intensity; it was feared that the resultant increase in the size of the vapour cloud in front of the oven hole, together with the increase in background pressure in the oven chamber, might reduce the polarisation of the atomic beam emerging from the sixpole magnet.

The results of the measurements, shown in Table 4.3 and Fig. 4.5, confirmed this suspicion. As before, a least mean squares fit of the curve

$$A = A_0 \left(1 - e^{-\lambda t}\right)$$

Trapping time T (ms)	Asymmetry A (10^{-2})	Uncertainty ΔA (10^{-2})
0.3	0.6	$\pm$0.3
1.5	2.2	$\pm$ 0.4
3.0	3.1	$\pm$ 0.3
4.5	4.0	$\pm$ 0.4
6.4	4.7	$\pm$ 0.3
17.2	7.1	$\pm$ 0.5

Table 4.3: Electron scattering asymmetry versus trapping time (well depth 1.8V, atomic beam intensity doubled).

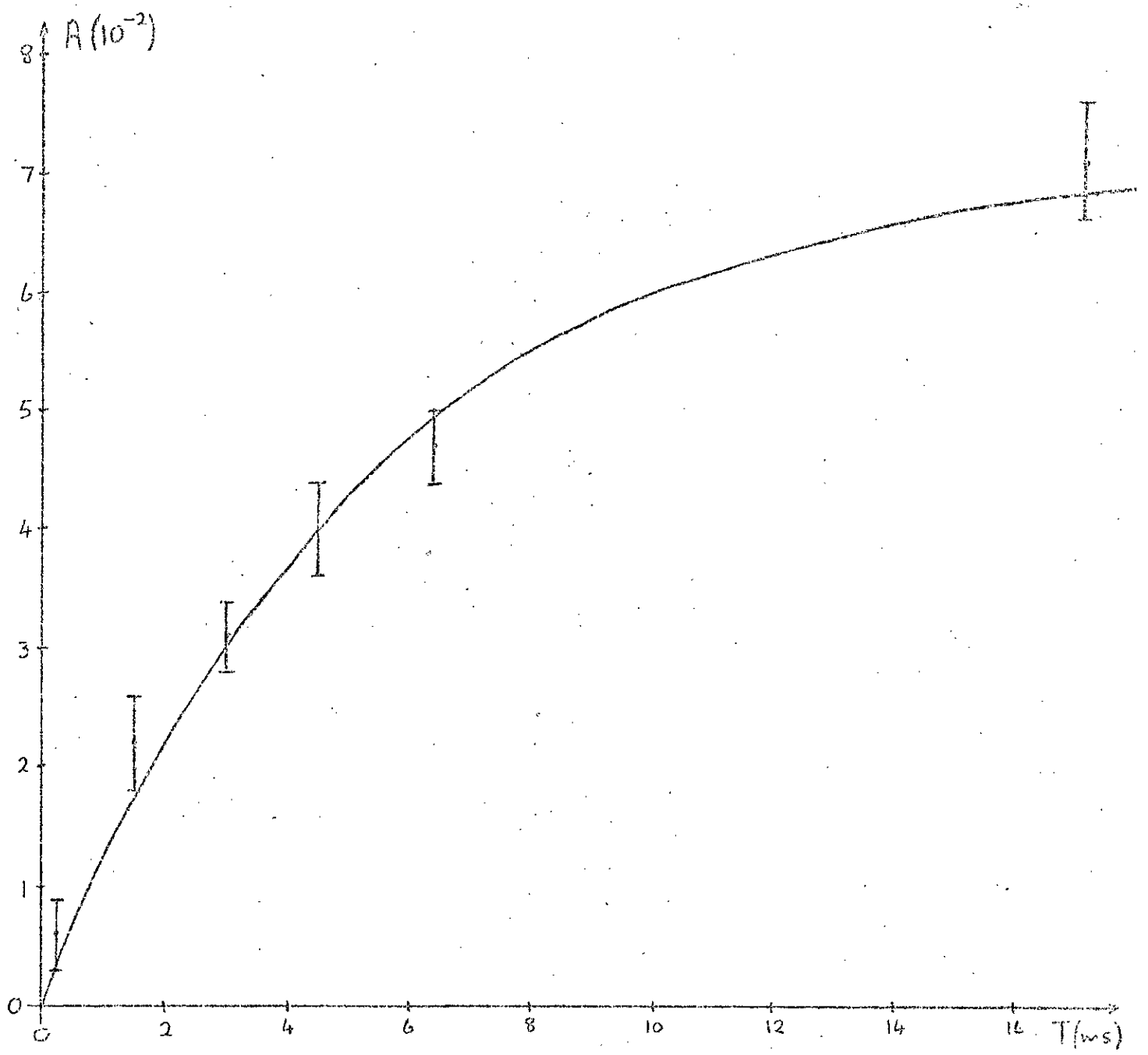

Fig. 4.5: Electron asymmetry versus trapping time (D = 1.8 volts; atomic beam density doubled).

to the measured points was performed; the resulting parameters were

$$A_o = 7.2 \times 10^{-2}$$

$$\lambda = 184\ s^{-1}.$$

The rate constant was increased by a factor 2.1, in satisfactory agreement with the prediction. However, the equilibrium polarisation was reduced by a factor 0.84. Because of this apparent depolarisation, the later measurements were done at the reduced beam density.

4.1.4. Effect of Increase in Trap Magnetic Field

The previous measurements were performed with an axial magnetic field of 6×10^{-3}T in the trap. At higher magnetic fields, the effective atomic beam polarisation in the trap will be increased; the equilibrium electron polarisation should therefore also be increased, unless the depolarising effects mentioned in section 2.2.1 become significant.

A series of measurements was therefore carried out with a magnetic field of 10^{-2}T, in order to establish whether or not the equilibrium electron polarisation was still consistent with the predicted atomic beam polarisation. Since the trap output current diminished rapidly with increasing magnetic field, this was the highest field for which polarisation measurements could be conveniently made. The results are shown in Table 4.4 and Fig. 4.6; the best least mean squares fit used the parameters

Trapping time T (ms)	Asymmetry $A(10^{-2})$	Uncertainty $\Delta A\ (10^{-2})$
1.5	2.6	$\pm$ 0.4
3.2	4.1	$\pm$ 0.4
4.8	5.1	$\pm$ 0.4
5.8	6.9	$\pm$ 0.4
11.0	8.6	$\pm$ 0.4
17.0	9.0	$\pm$ 0.4

Table 4.4: Electron scattering asymmetry versus trapping time (well depth 1.8V, trapping field increased).

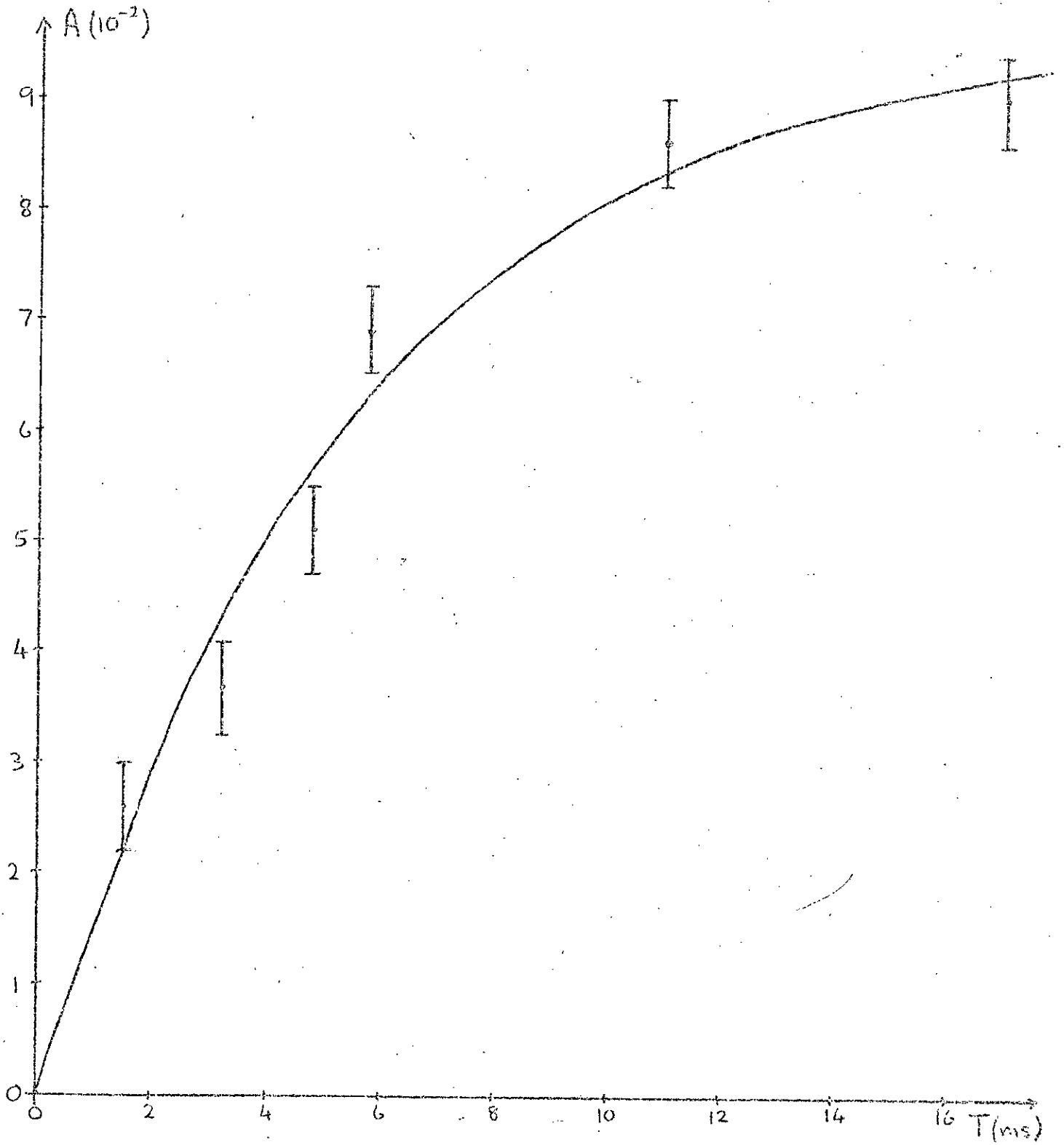

Fig. 4.6: Electron asymmetry versus trapping time (D = 1.8V; increased magnetic field in trap).

$$A_o = 9.6 \times 10^{-2} ; \qquad \lambda = 188\ s^{-1}.$$

From Fig. 3.12, it may be deduced that when the trap magnetic field was increased from 0.6×10^{-3}T to 1.0×10^{-2}T, the effective atomic beam polarisation should have increased by a factor 1.26. Comparing the above figures with those quoted in Section 2.2.1., it appears that the equilibrium electron polarisation, proportional to A_o, increased only by a factor 1.13. However, these figures also suggest that the polarisation rate constant increased by a factor 2.2. Some increase in λ_p was anticipated, since it was expected that at the higher magnetic field the trapped electron cloud would be initially more closely confined to the trap axis; the rate of radial diffusion would also be reduced, since the diffusion constant is proportional to B^{-2} (Section 2.4.1). The considerations of Section 4.1.2 suggested that an increase in λ_p by a factor of up to 1.5 could be explained in this way, but it did not seem possible that a change in radial distribution could more than double the rate constant.

The apparent conflict between these two sets of results is largely resolved when it is noted that a considerable range of pairs of values for A_o and λ_p may be found to give a reasonably good fit to a particular set of data. The quality of the fit may be described quantitatively by calculating the value of

$$K = \frac{\chi^2}{n} = \frac{1}{n} \sum_{i=1}^{n} \left(\frac{\Delta_i^2}{\sigma_i^2} \right),$$

where Δ_i is the difference between the measured value of A at the trapping time T and the corresponding value predicted by the fitted curve, σ is the standard error in the experimental value, and n is the total number of results in the set. In the present case, the criterion was adopted that if $\kappa < 1$, the fit was good.

The best fit to the results given in Table 4.2 was obtained with $A_o = 8.5 \times 10^{-2}$, and $\lambda = 87\ s^{-1}$, as previously stated; in this case, K = 0.50. The corresponding values for the results given in Table 4.4 with higher magnetic field, were $A_o = 9.6 \times 10^{-2}$, $\lambda = 188\ s^{-1}$, and K = 0.88. Thus both of these fits are good, by the above criterion.

In order to establish whether the rate constants derived for two sets of results are significantly different, it is necessary to obtain an estimate of the uncertainty in the predicted values. If the optimum fit to a given set of results has parameters A_o', λ', consider the effect of altering the rate constant λ' by an amount $\Delta\lambda$. If A_o is then adjusted to minimise χ^2, a new fit will be obtained with parameters $A_o' + \Delta A_o$, $\lambda' + \Delta\lambda$; the value of χ^2, characterising the quality of the fit, will of course be greater than that for the parameters A_o', λ'. We define the uncertainty in λ as that value of $\Delta\lambda$ for which the value of χ^2 is increased by unity. The uncertainty in A_o is similarly defined.

These uncertainties were calculated for the two sets of results under discussion. For the results of Table 4.2 ($B = 6 \times 10^{-3}$T), the fitting parameters, with uncertainties, were

$$A_o = (8.5 \pm 1.0) \times 10^{-2}$$

$$\lambda = 87 \pm 20 \ s^{-1};$$

for the results of Table 4.4 ($B = 10^{-2}$T):

$$A_o = (9.6 \pm 0.5) \times 10^{-2}$$

$$\lambda = 188 \pm 19 \ s^{-1}.$$

It is important to note that these deviations are not independent; a choice of the lower limit in A_o, for example, implies a simultaneous choice of the upper limit of λ. This may be emphasised by writing the limits in the following way:

$$\left.\begin{array}{lllll} 7.5 & < A_o < & 9.5 & (\times 10^{-2}) \\ 107 & > \lambda > & 67 & (s^{-1}) \end{array}\right\} \text{for } B = 6 \times 10^{-3} \text{T};$$

$$\left.\begin{array}{lllll} 9.1 & < A_o < & 10.1 & (\times 10^{-2}) \\ 207 & > \lambda > & 169 & (s^{-1}) \end{array}\right\} \text{for } B = 10^{-2} \text{T}.$$

When the results are expressed in this way, it is clear that they do not conflict with the prediction that the value of A_o should have increased by a factor 1.25 due to the increase in magnetic

field. Taking the values

$$\left.\begin{aligned} A_0 &= 7.8 \times 10^{-2} \\ \lambda &= 100 \ s^{-1} \end{aligned}\right\} \quad \text{for } B = 6 \times 10^{-3} \text{ T},$$

and

$$\left.\begin{aligned} A_0 &= 10.0 \times 10^{-2} \\ \lambda &= 172 \ s^{-1} \end{aligned}\right\} \quad \text{for } B = 10^{-2} \text{ T},$$

which are consistent with the above limits, both the increase in the equilibrium polarisation (a factor 1.28) and the increase in the rate constant (a factor 1.7) are in satisfactory agreement with the predictions made on theoretical grounds. Conversely, if these predictions are accepted as valid, they may be invoked to reduce the uncertainties in the results, since only a restricted range of the possible values of the parameters will combine in the predicted ratios. Thus the harmonisation of the two sets of results with theoretical considerations leads to the conclusion that

$$\left.\begin{aligned} A_0 &= (7.8 \pm 0.3) \times 10^{-2} \\ \lambda &= (100 \pm 6) \ s^{-1} \end{aligned}\right\} \quad \text{for } B = 6 \times 10^{-3} \text{ T}$$

$$\left.\begin{aligned} A_0 &= (9.8 \pm 0.3) \times 10^{-2} \\ \lambda &= (179 \pm 10) \ s^{-1} \end{aligned}\right\} \quad \text{for } B = 10^{-2} \text{ T}.$$

In the light of these considerations, the estimate of the spin-exchange cross-section given in Section 4.1.2 must be

modified. It was there calculated that

$$\lambda_p = 1.0 \times 10^{20} Q_e \ s^{-1} ;$$

the presently adopted experimental value of 100 s^{-1} for λ_p therefore implies a cross-section value

$$Q_e = 1.0 \times 10^{-18} \ m^2.$$

There is, of course, a considerable uncertainty in this estimate. Since

$$\lambda_p = Q_e \langle \rho \rangle \langle v' \rangle , \qquad \text{(Section 4.1.2)}$$

uncertainties in the values adopted for $\langle \rho \rangle$ and $\langle v' \rangle$ will combine with the uncertainty ($\sim$ 6%) in λ_p. The magnitude of $\langle \rho \rangle$ depended on the estimate of N, the average number density of the atomic beam in the trap (Section 3.1.3); this was a rather indirect measurement, and it was considered that it could be in error by $\pm$20%. The uncertainty in $\langle v' \rangle$ arose principally from the lack of knowledge of the radial distribution of the electrons; bearing in mind the discussion of the effect of changes in radial distribution in Section 4.1.2., and the measurements quoted in Section 4.1.4., it seemed unlikely that the error was greater than 10%.

Thus the obvious uncertainties in the experimental parameters upon which Q_e depends, suggest (a fairly pessimistic) uncertainty of 50% limits

on the derived value for Q_e :

$$0.7 \times 10^{-18} m^2 < Q_e < 1.5 \times 10^{-18} m^2.$$

Systematic errors could also arise from the failure of one or more of the assumptions on which the foregoing derivation was based. For example, it was assumed in the evaluation of $\langle v' \rangle$ that the momenta of the electrons in the interaction region were randomly distributed in direction; if instead the electrons had purely axial momentum, the value of $\langle v' \rangle$ would be reduced by a factor $3^{-\frac{1}{2}}$, and the estimate of Q_e given above would be correspondingly too low. However, the various assumptions must be judged on their merits, and the quoted uncertainty does not include an assessment of their plausibility. In fact, the overall consistency of the results, and the general agreement with the measurements of other workers, provide some ground for optimism in this regard.

4.2. POLARISATION MEASUREMENTS WITH DIFFERENT TRAP DEPTHS.

4.2.1. Measurements.

The measurements quoted and discussed in Section 4.1. were all made with a trapping potential well of nominal depth 1.5 volts. In the present section, measurements of the polarisation of electrons trapped in potential wells of depth 3.0 volts and 4.5 volts are reported. These measurements were part of a programme to find empirically the optimum conditions for operation of the apparatus as a source of polarised electrons;

it was also hoped that the results could be interpreted in such a way as to yield information about the energy dependence of the spin-exchange cross-section.

It was found that the maximum average trapped output current at very short trapping times ($< \tau_{ms}$) was achieved with a trap depth of 3 volts. As the well depth was further increased, the current dropped slowly. When the well depth was reduced below 1 volt, the current decreased rapidly, and at 0.5 volts was too low to be measurable. It was expected that the capacity of the trap would increase with increasing well depth (see Section 2.2.2); the decrease in output current at depths above 3 volts may have been due to the increase in the diffusion constant (Section 2.4).

Measurements of electron polarisation as a function of trapping time with a well depth of 3.0 volts are shown in Table 4.5 and Fig. 4.7; The corresponding results for a well depth of 4.5 volts are given in Table 4.6 and Fig. 4.8. Comparison of these data with the results given in Table 4.2 and Fig. 4.1 for a well depth of 1.8 volts, reveals a systematic decrease, with increasing well depth, of the polarisation achieved in a given trapping time. The effective atomic beam polarisation in the trap region was expected to depend only on the magnetic field, which was 6×10^{-3} T in all the above cases. It was therefore assumed that the asymptotic asymmetry $A_o = 7.8 \times 10^{-2}$, derived in Section 4.1.4 for the 1.8 volt deep well, would also

Trapping time T (ms)	Asymmetry A (10^{-2})	Uncertainty $\Delta A(10^{-2})$
1.5	1.3	$\pm$ 0.5
3.2	1.0	$\pm$ 0.5
4.8	2.0	$\pm$ 0.5
5.8	2.0	$\pm$ 0.5
11.0	3.3	$\pm$ 0.5
17.0	4.3	$\pm$ 0.5

Table 4.5: Electron scattering asymmetry versus trapping time (well depth 3.0V).

Trapping time T (ms)	Asymmetry A (10^{-2})	Uncertainty ΔA (10^{-2})
1.5	-0.5	$\pm$ 0.4
3.2	-0.2	$\pm$ 0.4
4.8	1.2	$\pm$ 0.4
5.8	0.7	$\pm$ 0.4
11.0	1.6	$\pm$ 0.4
17.0	2.6	$\pm$ 0.5

Table 4.6: Electron scattering asymmetry versus trapping time (well depth 4.5V).

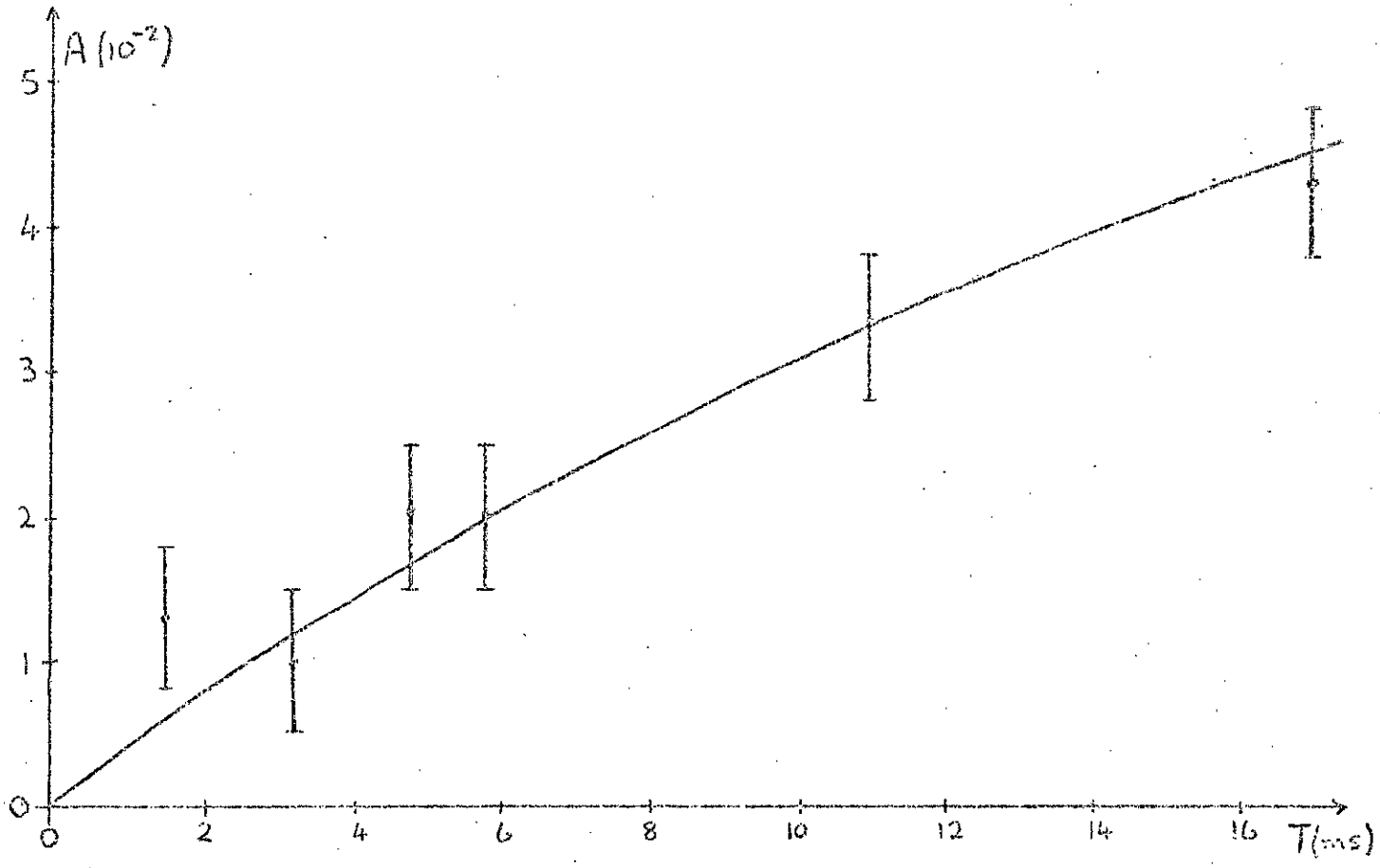

Fig. 4.7: Electron asymmetry versus trapping time (D = 3.0V).

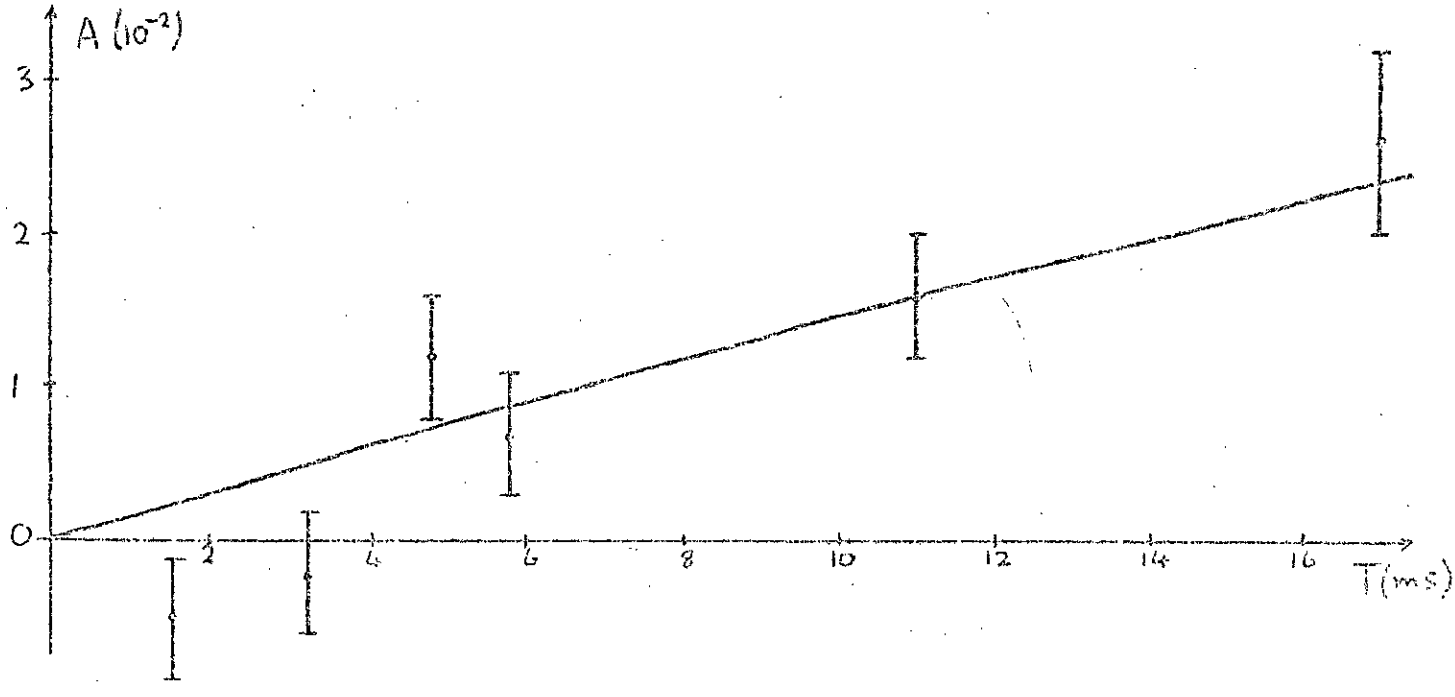

Fig. 4.8: Electron asymmetry versus trapping time (D = 4.5V).

characterise the results obtained with well depths of 3.0 volts and 4.5 volts. The least mean squares fits performed under this assumption are shown on the appropriate graphs; the corresponding values for the rate constant are

$$\lambda_p = (51 \pm 6)\ s^{-1} \qquad \text{for D = 3.0 volts}$$

$$\text{and } \lambda_p = (21 \pm 3)\ s^{-1} \qquad \text{for D = 4.5 volts.}$$

The uncertainties quoted above assume a fixed value of A_o, and are therefore smaller than those derived when A_o is also varied to minimise χ^2.

4.2.2. Interpretation

The rate constant λ_p is given by

$$\lambda_p = Q_e \langle \rho \rangle \langle v' \rangle \qquad \text{(Section 4.1.2)}$$

The measurements quoted above showed that λ_p decreased rapidly with increasing trap depth: in the well of depth 4.5 volts, had fallen to under a quarter of its value in the well of depth 1.8 volts. This effect can be interpreted in terms of the energy dependence of Q_e; first, however, the dependence of $\langle \rho \rangle$ and $\langle v' \rangle$ on D must be discussed.

In Section 4.1.2 it was shown that $\langle v' \rangle \propto \omega_z$, the frequency of axial oscillation of the trapped electrons. In turn, $\omega_z \propto D^{\frac{1}{2}}$. If this dependence were the only varying factor in λ_p, it would be expected that the rate

constant would increase with increasing well depth. Thus the observed decrease becomes even more significant when this dependence is taken into account.

The dependence of $\langle\rho\rangle\langle v'\rangle$ on the radial distribution of the electrons was discussed in Section 4.1.2, where it was pointed out that this quantity would have a higher value for a trapped electron cloud of limited radial extent than for a diffuse cloud. The diffusion constant will increase with increasing electron energy; it might therefore be expected that increased rapidity of radial diffusion in the deeper wells would lead to a reduction in the appropriate value of $\langle\rho\rangle\langle v'\rangle$. However, it was shown in Section 4.1.2 that changes in the radial electron distribution were unlikely to lead to changes in $\langle\rho\rangle\langle v'\rangle$ by a factor much greater than 1.5. In addition, the results of Section 4.1.4 implied that the distribution in a well of 1.8 volts depth, with a magnetic field of 6×10^{-3}T, must already be almost uniform.

It could therefore be deduced that

$$Q_e \propto \lambda_P D^{-\frac{1}{2}}$$

where Q_e is interpreted as the spin-exchange cross-section averaged over the distribution of electron energies present in the well of depth D.

Hence if $Q_e = 1.0 \times 10^{-18}$ m^2 for D = 1.8 volts

then $Q_e = 0.39 \times 10^{-18}$m^2 for D = 3.0 volts

and $Q_e = 0.13 \times 10^{-18}$m^2 for D = 4.5 volts

The problem of determining the electron energy distribution in a potential well of depth D volts was dealt with in Section 2.3. The curve in Fig. 2.20 implied an energy distribution with a half width not greater than 0.8 eV in the electron beam passing through the open trap; this was reflected in the analysis of the output of the trap with a nominal well depth of 1.5 volts, illustrated by Fig. 2.33. Since the methods of investigation used were sensitive only to the axial component of electron momentum, the results were useful only as a guide in estimating the average electron kinetic energy in the interaction region; this was taken as 1 eV in the well of nominal depth 1.5 volts. The well depth was increased by altering the potential on the central electrode, maintaining the gates at the same potential relative to the filament. It was therefore expected that the average kinetic energy in the interaction region would be $\sim$ 2.5 eV in the well of depth 3.0 volts, and $\sim$ 4.0 eV in the well of depth 4.5 volts. Little overlap was thus expected between the energy distribution in the different wells; this expectation was supported by the magnitude of the changes observed in λ_p when the well depth was altered.

The uncertainties in the absolute values of Q_e in wells of depth 3.0 volts and 4.5 volts will be of the same relative magnitude as that previously estimated for the 1.8 volt deep well, (Section 4.1.4.). The three values are collected in

Table 4.7, and displayed as a function of energy in Fig. 4.9. In this figure, the horizontal bars represent the spread of electron energies in the trap, which was taken to be about 1eV (see Section 2.3). The vertical bars represent the estimates previously given of the uncertainty limits on the measured values of Q_e. It should perhaps be emphasised that the magnitude of the latter reflect principally the difficulty of measuring the average number density $\langle \rho \rangle$ of the atomic beam in the trapping region, and of estimating the appropriate value of $\langle v' \rangle$ (see Section 4.1.2). Thus the upper limit is an attempt to define the maximum value of Q_e consistent with the experimental results; this would correspond to a combination of an underestimate of $\langle \rho \rangle$ by 20°/o, and a simultaneous underestimate of $\langle v' \rangle$ by 10°/o. The random error associated with the fitting of the polarisation curve to the measured points is small in comparison ($\pm$ 6°/o for D = 1.8V, $\pm$ 12°/o for D = 3.0V, $\pm$ 14°/o for D = 4.5V); it is also taken into account in assigning the uncertainty limits.

An underestimate in the value of $\langle \rho \rangle$ or $\langle v' \rangle$ would be systematic, in the sense that it would affect equally the measurements made at different trapping depths; all the measurements of Q_e would be increased by a constant fraction. Hence although the outer limits on the error bars reflect the uncertainty in the absolute values of Q_e, the form of the dependence of Q_e upon energy is determined more accurately than they suggest. Only the random errors contribute to the uncertainties in the relative values of Q_e

Average electron energy (eV)	$Q_e(10^{-18}m^2)$	Statistical uncertainty	Uncertainty limits
1.0	1.0	$\pm$ 0.06	+ 0.5
			- 0.3
2.5	0.39	$\pm$ 0.05	+ 0.22
			- 0.14
4.0	0.13	$\pm$ 0.02	$\pm$ 0.08
			- 0.05

Table 4.7: Values of Q_e calculated from results of present experiment.

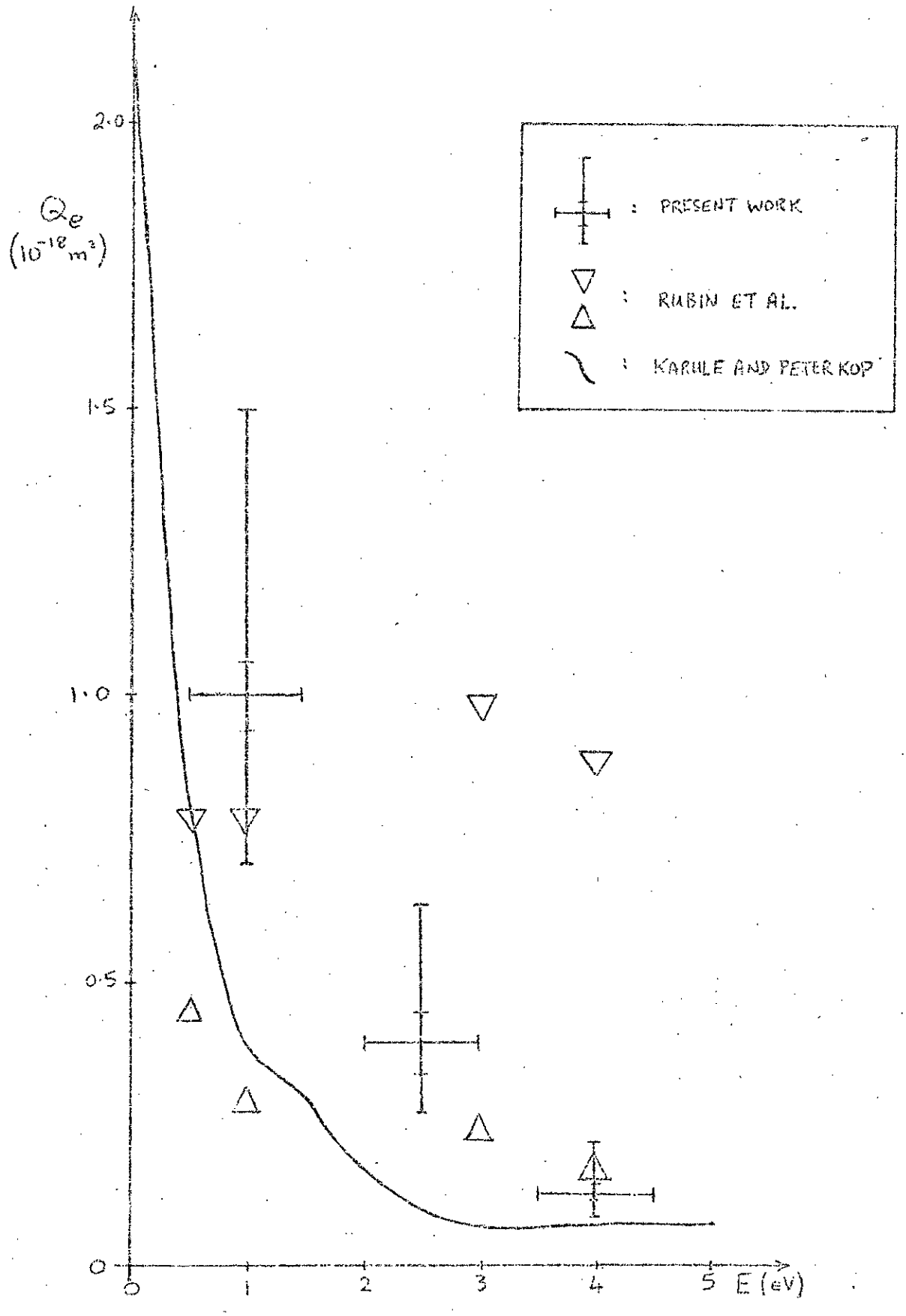

Fig. 4.9: Potassium electron spin exchange cross-section Q_e as a function of electron energy E.

at different average electron energies; they are shown separately on Fig. 4.9.

Fig. 4.9 also shows the measurements of Rubin et al., and a theoretical curve derived from the work of Karule and Peterkop (see Section 1.2.2). Before a comparison may be made with the present results, however, it must be noted that these previous estimates relate only to elastic spin exchange scattering. In the present case, inelastic processes may also have contributed to the observed rate of spin exchange in the two deepest wells, in which the average electron energy was well above the excitation threshold. Indeed, the results of Karule and Peterkop imply (Wykes, 1971) that the inelastic spin exchange cross-section is at least a factor 2 greater than the elastic spin exchange cross-section at an electron energy of 3eV. An increase in the observed rate of spin exchange could also occur as a result of the two-stage process in which an electron suffers a direct inelastic collision, followed by an elastic spin exchange collision at the lower energy. The theoretical results predict that, in a trapping time of 10 ms, this two stage process has about the same probability of occurrence as a single stage elastic spin exchange.

Thus the results given here for average electron energies of 2.5 eV and 4.0 eV must be taken as upper bounds on the total elastic cross-section; they are therefore consistent with the theoretical predictions of Karule and Peterkop. For an average electron energy of 2.5eV, our experimental value for Q_e is 3.9 times the theoretical value, while for an average

energy of 4.0eV, the experimental value is a factor 1.9 times the theoretical value. It is perhaps significant that the two stage process referred to above is expected to be less significant at the higher energy, since the predicted cross-sections for the second collisions (elastic spin exchange at the reduced energy) are 4.3×10^{-19} m^2 for an electron energy of 0.9eV (2.5eV - 1.6eV), and 1.2×10^{-19} m^2 for an electron energy of 2.4eV (4.0eV - 1.6eV).

Only elastic processes could have contributed significantly to the rate of spin exchange measured in the trap of depth 1.8 volts, since only a very small fraction of the electrons had energies above the excitation threshold. Thus the value of the spin exchange cross-section calculated from these measurements ($Q_e = 1.0 \times 10^{-18}$ m^2) may be compared directly with the limits of Rubin et al. (0.27×10^{-18} m$^2 < Q_e < 0.8 \times 10^{-18}$ m^2), and with the theoretical prediction from Karule ($Q_e = 0.39 \times 10^{-18}$ m^2). The lower limit of the present result ($Q_e = 0.7 \times 10^{-18}$ m^2) is consistent with the limits of Rubin et al.; a considerable discrepancy exists between our measurement and the theoretical prediction. It may be noted, however, that the theoretical value of Q_e is highly dependent on electron energy in the range 0-1eV; at an electron energy of 0.4eV the predicted value is 1.04×10^{-18} m^2. The measurements of electron energy distribution in the trap, discussed in Section 2.3, yielded only a crude indication of the average energy and energy spread; while they certainly suggested that the average electron energy was higher than 0.6eV, they were not reliable enough to establish beyond doubt a discrepancy

between theoretical and experimental values of Q_e in the energy range around 1eV.

Taken together, the present results provide confirmation of the general form of the energy dependence of the spin exchange cross-section. This is of practical significance from the point of view of the utilisation of the spin exchange process to provide a source of polarised electrons, since it shows that the kinetic energy of the electrons in the interaction region must be low ($< 1eV$) if high electron polarisation is to be achieved at short trapping times. In the present case, although the highest average trap output current was achieved with a well depth of 3.0 volts, the apparatus is operated as a source of polarised electrons with a trap depth of 1.5 volts, in order to obtain a sufficiently high rate of spin transfer.

4.3. CONCLUSIONS.

The method proposed by Byrne and Farago (1965) for the production of a polarised electron beam, by means of a spin exchange interaction between trapped electrons and a polarised potassium atomic beam, has been investigated. A pulsed beam of polarised electrons has been generated by this method, with 10^5 electrons per pulse, a pulse length of the order of one microsecond, and a polarisation of 0.5 at a repetition rate of 55 Hz. The repetition rate could be increased at the expense of the polarisation; at a repetition rate of 120 Hz the polarisation was reduced to 0.4 . The polarisation and average intensity of the electron beam was limited principally by the properties of the trap in which the electrons were confined during the interaction; as a result of various suggested improvements, it should be possible to increase the polarisation to 0.8, and the average intensity by several orders of magnitude.

From a study of the behaviour of this polarised electron source, it has been possible to derive estimates of the cross-section for spin exchange collisions between potassium atoms and electrons, at three different average kinetic energies in the range 0-4eV. These values of the spin exchange cross-section are in reasonable agreement with previous experimental results, and confirm the theoretical prediction of a rapid decrease in cross-section with increasing energy over this energy range.

APPENDIX I. CLOSING OF TRAP INPUT GATE (Section 2.3.3.).

Adopting the notation and assumptions of Section 2.3.3, we consider an electron trapped in the unsymmetrical well shown in Fig. A1.1. The potential distribution for $z > 0$ is static, while that for $z < 0$ is changing in such a way that it retains a parabolic form. It is assumed that this change is adiabatic, so that the potential distribution may be taken as approximately static over one period of oscillation of an electron in the well.

We consider such a period, at a stage in the closure of the gate when the energy level of the electron is $\mathcal{E}'$. In that fraction of the period which the electron spends in the region $z < 0$, its motion is approximately simple harmonic, with equation of motion

$$z = A \sin \omega t,$$

where

$$\omega = \frac{1}{z_0} \left(\frac{2eV_I}{m} \right)^{\frac{1}{2}},$$

and

$$A = \left(\frac{z_0^2 \mathcal{E}'}{V_I} \right)^{\frac{1}{2}}.$$

The potential at z is given by

$$V(z) = V_I \left(\frac{z^2}{z_0^2} \right);$$

since $\frac{\partial V_I}{\partial t}$ is so small that ω may be assumed constant over one period, the explicit dependence of $V(z)$ on time may be written

$$\frac{\partial V(z)}{\partial t} = \frac{\partial V_I}{\partial t}\left(\frac{A^2 \sin^2 \omega t}{z_o^2}\right). \qquad \text{A1.1.}$$

The electron will travel from $z = 0$ to $z = -z_o$ and back to $z = 0$ in time $\tau_{/1} = \pi/\omega$. If the change in V_I in this time is ΔV_I, the corresponding change in the total energy of the electron may be obtained by integrating Equation A1.1 over the time interval π/ω , assuming $\frac{\partial V_I}{\partial t}$ constant; this gives

$$\Delta \mathcal{E} = \frac{\partial V_I}{\partial t}\left(\frac{A^2}{2 z_o^2}\right)\cdot\frac{\pi}{\omega} = \frac{\partial V_I}{\partial t}\left(\frac{\mathcal{E}'}{2V_I}\right)\cdot\frac{\pi}{\omega}.$$

In the remaining fraction of the total period, which the electron spends in the region $z > 0$, its motion is again simple harmonic, but now with angular frequency

$$\omega_o = \frac{1}{z_o}\left(\frac{2eV_o}{m}\right)^{\frac{1}{2}}.$$

It will therefore travel from $z = 0$ to $z = z_o$ and back to $z = 0$ in time $\tau_{o/2} = \pi/\omega_o$; in this time there will be no change in the total electron energy, since the potential in this region is not explicitly time-dependent. Meanwhile, V_1 will change by an amount

$$\frac{\partial V_I}{\partial t}\cdot\frac{\pi}{\omega_o}.$$

Thus the total period of oscillation is

$$T = \pi\left(\frac{1}{\omega} + \frac{1}{\omega_0}\right);$$

in this time, V_I changes by an amount

$$\Delta V_I = \frac{\partial V_I}{\partial t} \cdot \pi\left(\frac{1}{\omega} + \frac{1}{\omega_0}\right),$$

and the energy level of the electron changes by an amount

$$\Delta \mathcal{E}' = \frac{\partial V_I}{\partial t}\left(\frac{\mathcal{E}'}{2V_I}\right)\cdot\frac{\pi}{\omega}.$$

The relationship between V_I and $\mathcal{E}'$ is therefore given by the solution of the differential equation

$$\frac{d\mathcal{E}'}{dV_I} = \frac{\mathcal{E}'}{2V_I}\left[1 + \frac{\omega}{\omega_0}\right]^{-1} = \frac{\mathcal{E}'}{2V_I}\left[1 + \left(\frac{V_I}{V_0}\right)^{\frac{1}{2}}\right]^{-1}:$$

$$\mathcal{E}' = C V_I^{\frac{1}{2}}\left[1 + \left(\frac{V_I}{V_0}\right)^{\frac{1}{2}}\right]^{-1} \qquad \text{A1.2.}$$

The arbitrary constant C is determined by the condition that the original energy level is $\mathcal{E}$, so that the electron becomes trapped when $V_I = \mathcal{E}$; this implies that

$$C = \mathcal{E}^{\frac{1}{2}}\left[1 + \left(\frac{\mathcal{E}}{V_0}\right)^{\frac{1}{2}}\right] \qquad \text{A1.3.}$$

When the gate is completely closed, $V_I = V_0$. In this case, we obtain from Equations A1.2 and A1.3 the final electron energy

level in the closed trap:

$$\varepsilon' = \tfrac{1}{2}\varepsilon\left[1 + \left(\frac{V_0}{\varepsilon}\right)^{\frac{1}{2}}\right] \qquad \text{A1.4.}$$

In terms of the parameters $\alpha = \frac{\varepsilon}{V_0}$, $\alpha' = \frac{\varepsilon'}{V_0}$, Equation A1.4 becomes

$$\alpha' = \tfrac{1}{2}\left(\alpha + \alpha^{\frac{1}{2}}\right).$$

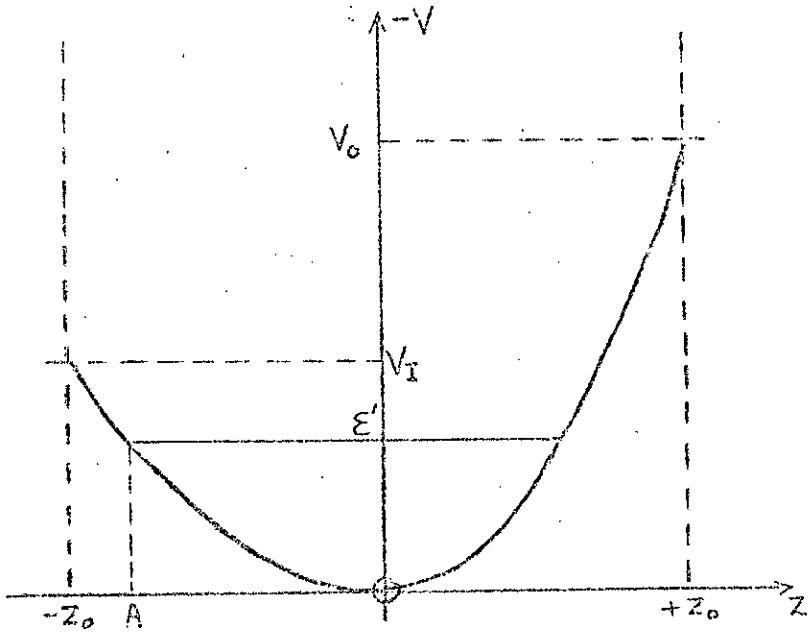

Fig. A1.1: Trapping in unsymmetrical well.

APPENDIX 2. SELECTIVE EJECTION OF TRAPPED ELECTRONS (Section 2.3.4.)

We consider first the effect on the energy level of a trapped electron of an adiabatic change in the trapping well depth. It is assumed that the potential at $\pm z_0$ remains constant; for convenience, this is defined as zero potential, (see Fig. A2.1). The potential at the centre of the trap is then $+ D'$, where D' is the changing trap depth, and the potential at z is

$$V = D'\left(1 - \frac{z^2}{z_0^2}\right).$$

The energy level of the electron $\mathcal{E}'$ is defined, as usual, in such a way that the kinetic energy at the centre of the well ($z = 0$) is $e\mathcal{E}'$ electron volts; since the electronic charge e is negative, $\mathcal{E}'$ is also a negative quantity. The total electron energy E is given in this case by

$$E = |e|\left(D' - |\mathcal{E}'|\right). \qquad \text{A2.1.}$$

Assuming again that the potential distribution changes adiabatically, the motion of the electron may be described by

$$z = A \sin \omega t,$$

where

$$A = \left(\frac{z_0^2\,|\mathcal{E}'|}{D'}\right)^{\frac{1}{2}}.$$

An argument similar to that employed in Appendix I shows that the change ΔE in the total electron energy during one period of the oscillation of the electron is

$$\Delta E = |e|\,\Delta D'\left(1 - \frac{A^2}{2z_o^2}\right) = |e|\,\Delta D'\left(1 - \frac{|\mathcal{E}'|}{2D'}\right),$$

where $\Delta D'$ is the corresponding change in well depth. From Equation A2.1, the change in energy level $\mathcal{E}'$ is then

$$\Delta|\mathcal{E}'| = \Delta D' - |e|^{-1}\Delta E = \Delta D'\left(\frac{|\mathcal{E}'|}{2D'}\right).$$

This yields the differential equation

$$\frac{d|\mathcal{E}'|}{dD'} = \frac{|\mathcal{E}'|}{2D'},$$

the solution to which is

$$\mathcal{E}' = C(D')^{\frac{1}{2}}.$$

If the original energy level was $\mathcal{E}$, in a well of depth D, the arbitrary constant C is defined as

$$C = \mathcal{E}D^{-\frac{1}{2}};$$

thus

$$\mathcal{E}' = \mathcal{E}\left(\frac{D'}{D}\right)^{\frac{1}{2}} = \mu^{\frac{1}{2}}\mathcal{E},$$

where μ is the ratio of final to initial trap depth.

In terms of $\beta = \frac{|\varepsilon|}{D}$, and $\beta' = \frac{|\varepsilon'|}{D'} = \mu^{-1}\frac{|\varepsilon'|}{D}$:

$$\beta' = \mu^{-\frac{1}{2}}\beta \qquad \text{A2.2.}$$

After the well depth has been reduced from D to D' by a pulse on the central electrode, the output gate is lowered by an amount δD; this will cause a further change in energy level, from ε' to ε''. If this corresponds to a change in output gate potential from V_o to V_o', measured relative to the bottom of the new well (Fig. A2.2.), the treatment is similar to that used in Appendix I, and the relationship between the final energy level ε'' of an electron and the final output gate potential V_o' may be obtained directly from Equation A1.2 by the substitution $V_I \rightarrow V_o'$:

$$\varepsilon'' = C(V_o')^{\frac{1}{2}}\left[1 + \left(\frac{V_o'}{V_o}\right)^{\frac{1}{2}}\right]^{-1}.$$

In this case the initial condition is that $\varepsilon'' = \varepsilon'$ when $V_o' = V_o$; thus

$$C = 2\varepsilon' V_o^{-\frac{1}{2}},$$

and

$$\varepsilon'' = 2\varepsilon'\left(\frac{V_o'}{V_o}\right)^{\frac{1}{2}}\left[1 + \left(\frac{V_o'}{V_o}\right)^{\frac{1}{2}}\right]^{-1}. \qquad \text{A2.3.}$$

An electron will be ejected by this process if $\frac{\varepsilon''}{V_o'} \geqslant 1$; it may be shown immediately from Equation A2.3 that then the

limiting case, with $\varepsilon'' = V_o'$, corresponds to an energy level before alteration of the output gate potential, such that

$$\frac{\varepsilon'}{V_o} = \frac{1}{2}\left(\frac{V_o'}{V_o}\right)^{\frac{1}{2}}\left[1+\left(\frac{V_o'}{V_o}\right)^{\frac{1}{2}}\right] \qquad \text{A2.4.}$$

In terms of the parameters

$$\beta' = \frac{|\varepsilon'|}{D'} = \frac{\varepsilon'}{V_o}$$

$$\mu = \frac{D'}{D}$$

and $$\delta = \frac{V_o - V_o'}{D} = \mu\left(1-\frac{V_o'}{V}\right),$$

Equation A2.4 can be written

$$\beta' = \frac{1}{2}\left[\left(1-\frac{\delta}{\mu}\right) + \left(1-\frac{\delta}{\mu}\right)^{\frac{1}{2}}\right]. \qquad \text{A2.5.}$$

Considering now the complete process, illustrated in Fig.A2.3, we wish to find the lowest energy level in the original well, of depth D, such that an electron in that level will be released after the application of the two pulses to the central and output gate electrodes. From Equations A2.5 and A2.2, this level is characterised by

$$\beta = \frac{|\varepsilon|}{D} = \mu^{\frac{1}{2}}\beta' = \frac{1}{2}\left[\left(\frac{\mu-\delta}{\mu^{\frac{1}{2}}}\right) + (\mu-\delta)^{\frac{1}{2}}\right].$$

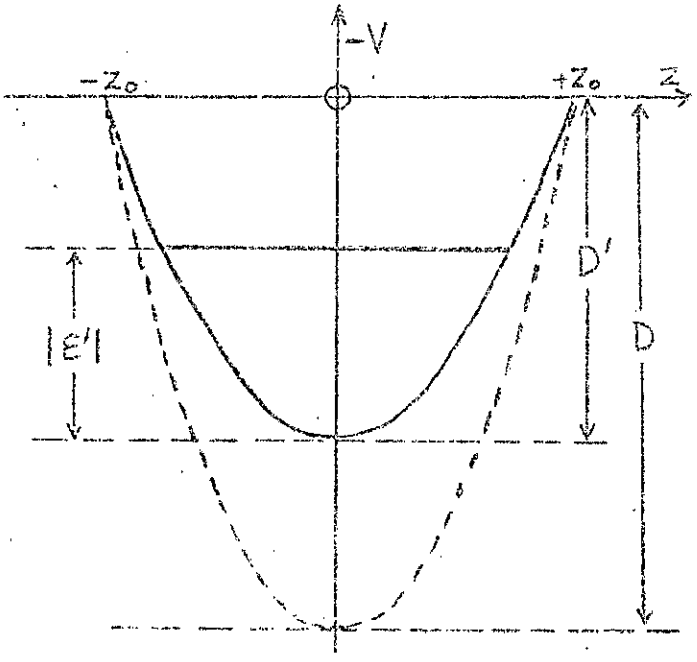

Fig. A2,1: Raising of trap bottom.

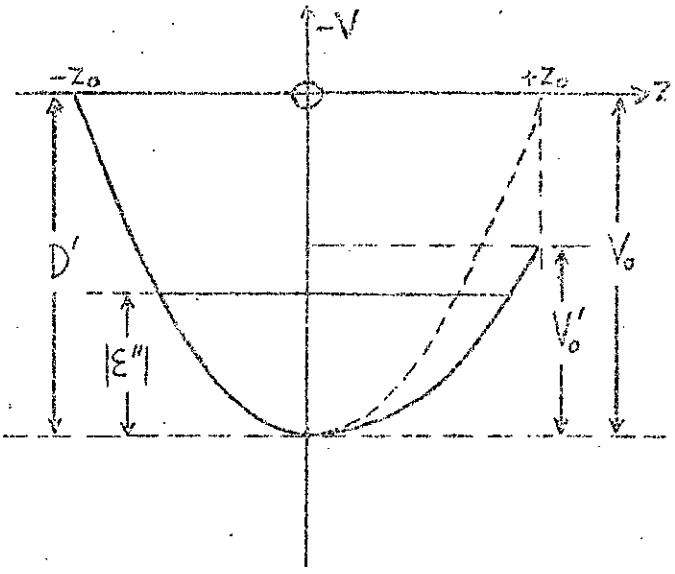

Fig. A2.2: Lowering of output gate.

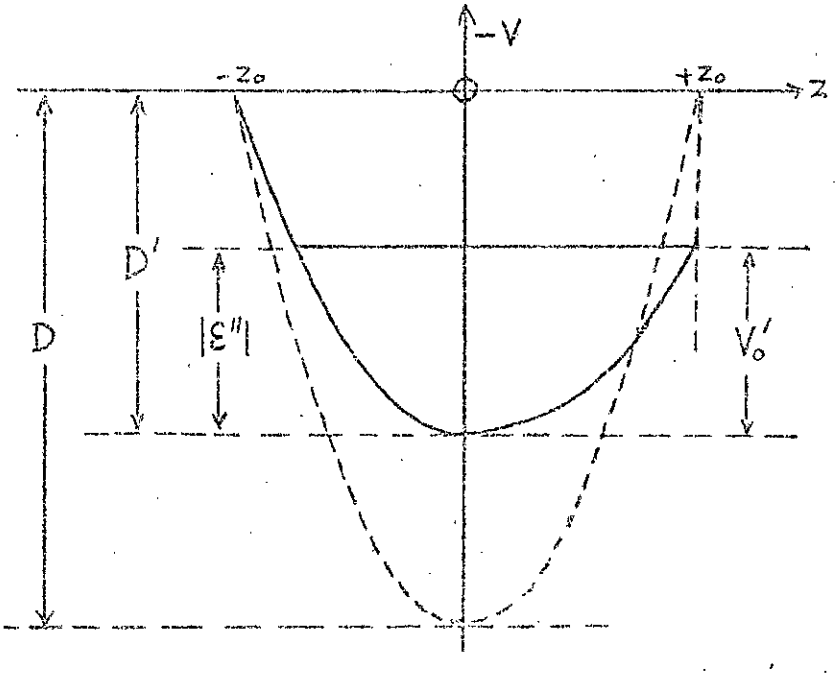

Fig. A2.3.: Combined process leading to ejection.

APPENDIX 3. RADIAL DIFFUSION IN THE TRAP (Section 2.4.1)

The simplified case is considered in which any given electron orbit centre performs random walk in the (R,θ) plane, with steps of constant length $\langle r^2 \rangle^{\frac{1}{2}}$. It may easily be verified that

$$n(R,t) = \frac{N_o}{4\pi D t} e^{-\frac{R^2}{4Dt}} \qquad \text{A3.1}$$

is a solution of the two dimensional diffusion equation

$$\frac{\partial n}{\partial t} = D \nabla^2 n , \qquad \text{A3.2}$$

using the notation of Section 2.4.1. (Sommerfeld, 1949, p.59). This solution is independent of θ, and has the radial form of a Gaussian function with half width proportional to $t^{\frac{1}{2}}$. It is therefore appropriate to a situation in which N_o electrons are concentrated on unit length of the z axis at time $t = 0$.

The value of the diffusion constant D may be deduced by considering the net flux of electrons across a small area perpendicular to an arbitrary direction X in the R,O plane. If $\underline{i}$ is the unit vector in the X direction, the flux per unit area per unit time is

$$F = -\frac{\nu_c}{2} \langle x^2 \rangle \left(\underline{i} . \nabla n \right) \qquad \text{A3.3}$$

where ν_c is the collision frequency and $\langle x^2 \rangle$ the mean square displacement in the X direction per collision (Kennard, 1938, p.286).

It may also be deduced from the general diffusion equation A3.2 (Chandrasekhar, 1943) that

$$F = -D(\underline{i}.\nabla n) \; ; \qquad \text{A3.4}$$

comparing the two expressions for F, we find that

$$D = \tfrac{1}{2} \nu_c \langle x^2 \rangle .$$

Since in the two dimensional case, $\langle x^2 \rangle = \frac{1}{2}\langle r^2 \rangle$,

$$D = \tfrac{1}{4} \nu_c \langle r^2 \rangle .$$

By applying Equation A3.4 to the distribution given in Equation A3.1, choosing the unit vector $\underline{i}$ in the radial direction, we find that the flux of electrons across unit area at a radial distance R from the axis at time t is

$$F = \frac{N_0 R}{8\pi D t^2} e^{-\frac{R^2}{4Dt}} .$$

Thus if N is the number of electrons remaining inside a cylinder of unit axial length and radius R_0 at time t,

$$\frac{dN}{dt} = -2\pi R_0 F$$

$$= -\frac{N_0 R_0^2}{4Dt^2} e^{-\frac{R_0^2}{4Dt}} . \qquad \text{A3.5}$$

The fraction of the original number of electrons in the cylinder

remaining after a time t is

$$f(t) = 1 - \frac{N}{N_0} = 1 - \int_0^t \frac{R_0^2}{4Dt^2} e^{-\frac{R_0^2}{4Dt}}$$

$$= 1 - e^{-\frac{1}{\lambda t}}$$

A3.6

with $$\lambda = \frac{4D}{R_0^2} = \nu_c \frac{\langle r^2 \rangle}{R_0^2} .$$

The time taken for the trap population to decrease to half of its original number is

$$T_{1/2} = (\lambda \ln 2)^{-1}$$

$$= \frac{1 \cdot 44 \, R_0^2}{\nu_c \langle r^2 \rangle}$$ A3.7

In Section 3.2.1, it was assumed that the rate of loss of electrons was given by

$$\frac{dN}{dt} = - \alpha \nu_c N ;$$

this implied that $N = N_0 e^{-\alpha \nu_c t}$, so that the fraction remaining after a time t would be

$$f'(t) = 1 - e^{-\alpha \nu_c t} ,$$

A3.8

and half the population would be lost in time

$$T'_{1/2} = \frac{\ln 2}{\alpha \nu_c} = \frac{0 \cdot 69}{\alpha \nu_c} .$$

A3.9

It is in fact possible to find a solution to the diffusion equation (Eqn.A3.2) which has such a time dependence; the radial distribution is then a Bessel function (Hasted (1964), p. 20). In the experimental situation, the time dependence of the losses would be more complicated than that of either Equation A3.6 or Equation A3.8, since the initial radial distribution would not be a simple function. A rough estimate of the value of α appropriate to the present circumstances may nevertheless be obtained by comparing Equations A3.7 and A3.9; this comparison shows that the function f(t) in Equation A3.7 may be approximated by the function $\mathfrak{f}'(t)$ of Equation A3.9 by setting

$$\alpha = \frac{2 \cdot 1 \langle r^2 \rangle}{R_o^2} .$$

The nature of this approximation is illustrated in Fig A3.1.

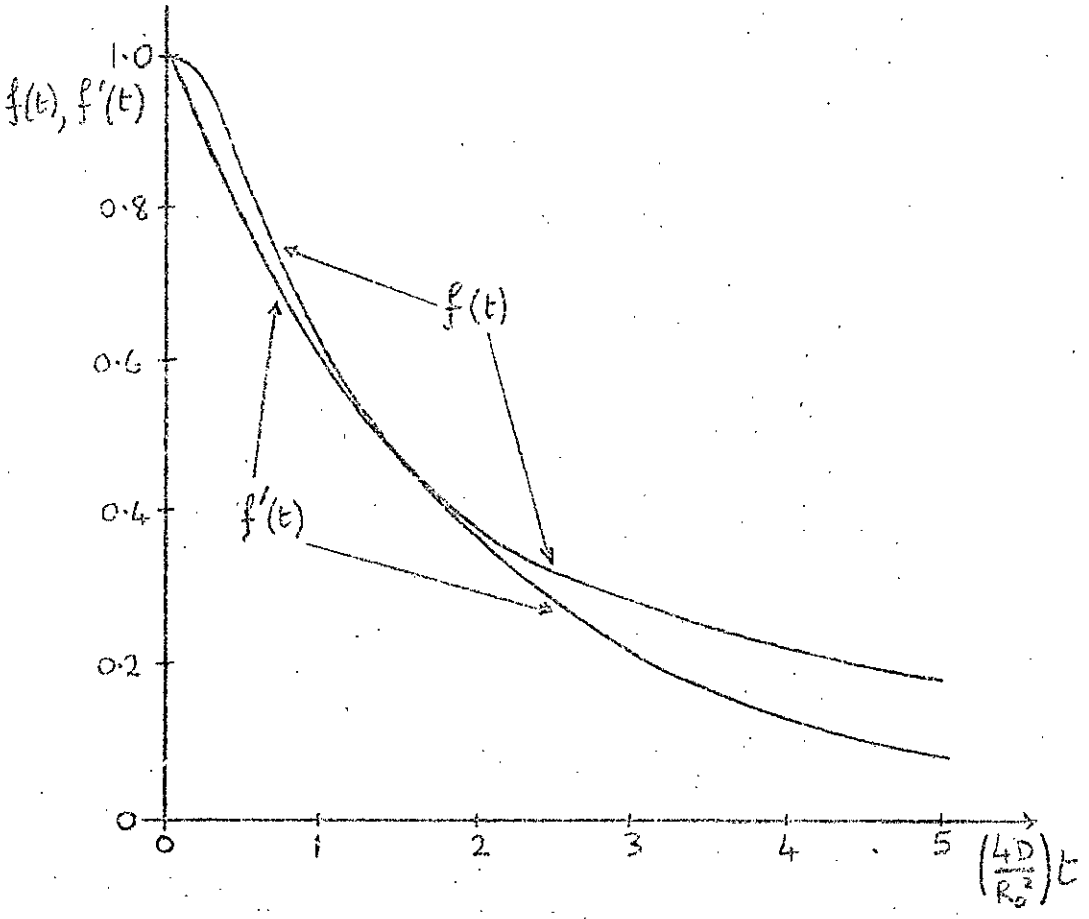

Fig. A3.1: Comparison of f(t) and f(t).

APPENDIX 4:

FORM OF EQUATION 3.2 WHEN $a \ll 1$ (SECTION 4.1.2.)

From Section 3.2.2, the rate of change of electron polarisation with time is

$$p = \frac{\mu(1 - e^{-\lambda t})}{1 - \nu e^{-\lambda t}}, \qquad 3.2.$$

where $$\lambda = \left[(a_{11} - a_{22})^2 + 4a_{12}a_{21}\right]^{\frac{1}{2}}$$

$$\mu = \frac{1}{2a_{12}}\left[\lambda - (a_{11} - a_{22})\right]$$

and $$\nu = \frac{(a_{11} - a_{22}) - \lambda}{(a_{11} - a_{22}) + \lambda};$$

the coefficients a_{ij} are defined in Section 3.2.1.

In terms of $\delta = a_{11} - a_{22}$

and $$\chi = \frac{4a_{12}a_{21}}{(a_{11} - a_{22})^2},$$

$$\lambda = \delta\left[1 + \chi\right]^{\frac{1}{2}},$$

$$\nu = \frac{1 - \left[1 + \chi\right]^{\frac{1}{2}}}{1 + \left[1 + \chi\right]^{\frac{1}{2}}}.$$

If $\chi \ll 1$,

$$\nu \simeq -\tfrac{1}{4}\chi \ll 1.$$

Now $$\chi = \frac{4a_{12}a_{21}}{(a_{11} - a_{22})^2}$$

$$= \frac{4P^2}{(1 + \lambda_R/\lambda_P)^2}\left[\left(\frac{\alpha}{1-\alpha}\right)^2\left(\frac{S}{Q_e}\right)^2 + \left(\frac{\alpha}{1-\alpha}\right)\left(\frac{S}{Q_e}\right)\right]$$

in terms of the symbols defined in Section 3.2. $P^2\left(1 + \frac{\lambda_R}{\lambda_P}\right)^{-2} \leqslant 1,$

the equality pertaining to the case of the complete polarisation of the atomic beam, and absence of relaxation effects. The theoretical results of Karule and Peterkop (1965) imply that at an electron energy of IeV,

$$\frac{S}{Q_e} \simeq -0{\cdot}3.$$

Hence, if $\alpha \ll 1$,

$$\nu = -\tfrac{1}{4}\lambda = -\frac{p^2}{\left(1+\frac{\lambda_R}{\lambda_P}\right)^2}\cdot\alpha\left(\frac{S}{Q_e}\right) \ll 1.$$

Equation 3.2. then takes the approximate form

$$p \simeq \mu\left(1-e^{-\lambda t}\right).$$

APPENDIX 5:

EFFECT OF NON-UNIFORM ATOMIC DENSITY IN TRAP (SECTION 4.1.2.)

We consider an atomic beam flowing in the x direction, with a density cylindrically symmetric about the x axis; if r is the perpendicular distance from the x axis, the density is given by

$$\rho = \rho_0 \qquad \text{for} \quad r \leq r_1 \qquad \text{A5.1.}$$

$$\rho = \rho_0 \left[1 - \frac{r - r_1}{R - r_1} \right] \qquad \text{for} \quad r \geq r_1 \qquad \text{A5.2.}$$

An electron travelling with uniform velocity in the z direction, through the centre of the atomic beam, would experience an average atomic density

$$\langle \rho(0) \rangle = \frac{1}{R} \int_0^R \rho \, dz = \frac{1}{R} \int_0^{r_1} \rho_0 \, dz + \frac{1}{R} \int_{r_1}^R \rho_0 \left[1 - \frac{z - r_1}{R - r_1} \right] dz$$

$$= \rho_0 \left(\frac{R + r_1}{2R} \right).$$

In the present case, $R = 3$ mm., $r_1 = 1$ mm;

$$\therefore \quad \langle \rho(0) \rangle = 0.67 \, \rho_0 .$$

Consider now an electron precessing slowly around the origin in the x,y plane at a radius R, while oscillating rapidly across the beam in the z direction (See Fig. A5.1). Once again, we assume uniform electron velocity magnitude in the region of interaction with the atomic beam. At a time when the angle of precession is Θ, the width of the atomic beam traversed by the electron is $2R\sin\Theta$ (see Fig. A5.2). We now calculate the

average atomic density $\langle \rho(\theta) \rangle$ over this path.

Two cases must be considered:

(i) $\theta < \theta_c$: (where $\cos\theta_c = r_1/R$)

In this case, the electron moves always in a region where the atomic density is given by A5.2; the average density is therefore

$$\langle \rho(\theta) \rangle = \frac{1}{R\sin\theta} \int_0^{R\sin\theta} \rho_0 \left[1 - \frac{r - r_1}{R - r_1} \right] dz$$

$$= \frac{\rho_0}{R\sin\theta} \int_0^{R\sin\theta} \left[1 - \frac{(R^2\cos^2\theta + z^2)^{\frac{1}{2}} - r_1}{R - r_1} \right] dz$$

$$= \rho_0 \left[1 + \frac{r_1}{R - r_1} - \frac{R}{2(R-r_1)} \left\{ 1 + \frac{\cos^2\theta}{2\sin\theta} \ln\left(\frac{1+\sin\theta}{1-\sin\theta} \right) \right\} \right]$$

(ii) $\theta > \theta_c$:

In this case, the electron moves in a region of uniform density (Equation A5.1) for $|z| < |z_1|$, where

$$z_1^2 = r_1^2 - R^2\cos^2\theta ;$$

the integration must therefore be performed in two parts.

$$\langle \rho(\theta) \rangle = \frac{1}{R\sin\theta} \left\{ \int_0^{z_1} \rho_0 \, dz + \int_{z_1}^{R\sin\theta} \rho_0 \left[1 - \frac{(R^2\cos^2\theta + z^2)^{\frac{1}{2}} - r_1}{R - r_1} \right] dz \right.$$

$$= \rho_0 \left[1 + \frac{r_1}{R - r_1} \left(1 - \frac{z_1}{R\sin\theta} \right) - \frac{R}{2(R-r_1)} \left\{ 1 - \frac{z_1 r_1}{R^2\sin^2\theta} \right\} - \frac{R}{4(R-r_1)} \frac{\cos^2\theta}{\sin\theta} \left\{ \ln\left(\frac{1+\sin\theta}{1-\sin\theta} \right) - \ln\left(\frac{r_1 + z_1}{r_1 - z_1} \right) \right\} \right]$$

The function $\langle \rho(\theta) \rangle$, with r_1 = 1 mm., R = 3 mm., is shown in Fig. 4.4.

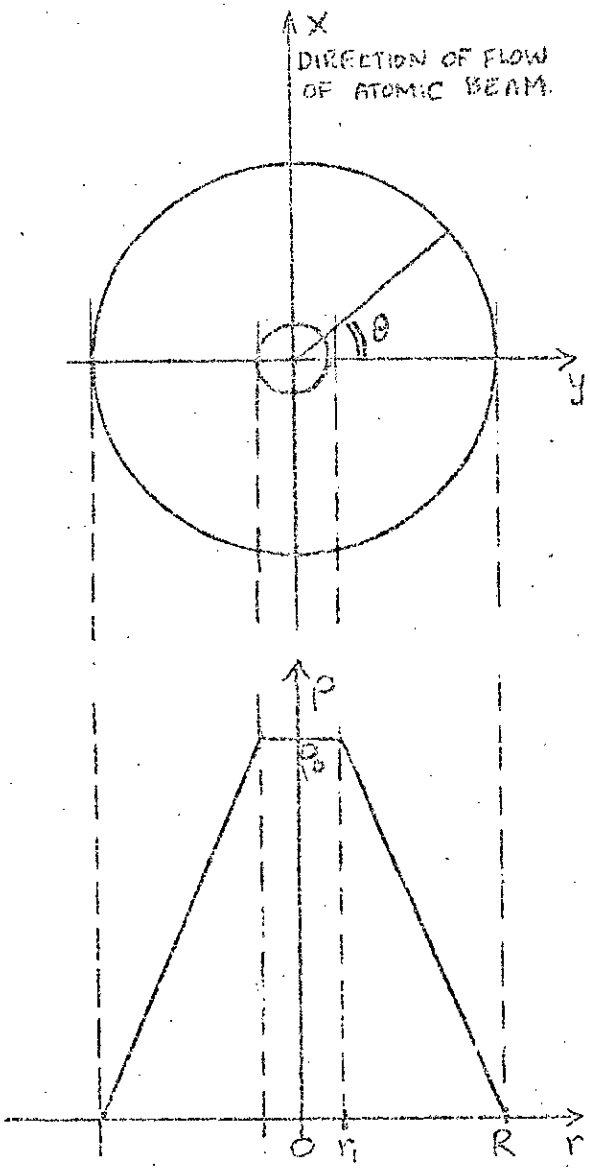

Fig. A5.1: Atomic beam density distribution.

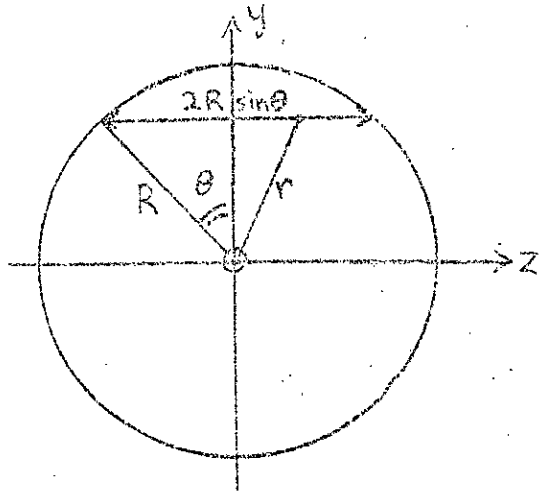

Fig. A5.2: Variation of width of interaction region with θ.

REFERENCES

Bernheim (1965): Bernheim, R.A.,"Optical Pumping" (Benjamin,1965)

Brash (1969): Brash, H.M., Ph.D. Thesis, University of Edinburgh, (unpublished).

Brash et al: Brash, H.M., Campbell, D.M., Farago, P.S., Rae,AG.A. Siegmann,H.Chr.,and Wykes,J.S., Proc. Roy. Soc. Edin. 68A (1969) 158.

Brode (1929): Brode,R.B., Phys.Rev. 34 (1929)673.

Burke and Schey (1962): Burke,P.G. and Schey,H.M., Phys. Rev. 126 (1962) 163.

Byrne (1969): Byrne,J., private communication.

Byrne and Farago (1965): Byrne,J. and Farago,P.S., Proc. Phys. Soc. 86 (1965) 801.

Cavanagh (1957): Cavanagh,P.E., Turner, J.F., Coleman,C.F., Gard, G.A., and Ridley,B.W., Phil. mag. 21(1957) 1105.

Chandrasekhar (1943): Chandrasekhar,S., Rev. Mod. Phys. 15(1943)1.

Collins et al. (1968): Collins,R.E., Bederson,B., Goldstein,M. and Rubin,K., Minutes of 21st annual Gaseous Electronics Conference, Boulder, Colorado (1968).

Dehmelt (1958): Dehmelt,H., Phys.Rev. 109 (1958) 381.

Farago 1965): Farago,P.S., Advances in Electronics and Electron Physics, 21 (1965) 1.

Farago and Siegmann (1966): Farago,P.S. and Siegmann,H,Chr., Phys. Lett. 20 (1966) 279.

Franck and Hertz (1914): Franck,J. and Hertz,G., Verh.der Phys. Ges. 16 (1914) 457.

Franken et al. (1958): Franken,P., Sands,R. and Hobart,J., Phys. Rev.Lett. 1 (1958) 22.

Gerlach (1924): Gerlach,W. and Stern,O., Ann.Phys. 74 (1924) 673.

Graff et al. (1968): Graff,G., Major,F.G., Roeder,R.W.H. and Werth,G., Phys.Rev.Lett. 21 (1968) 340.

Hasted,(1964): Hasted,J.B.,"Physics of Atomic Collisions" (Butterworth, 1964).

Holzwarth and Meister (1964): Holzwarth,G. and Meister,H.J., Nucl.Phys 59 (1964) 56.

Karule and Peterkop (1965): Karule,E.M. and Peterkop,R.K.,"Atomic Collisions III" (Latrian Academy of Sciences, Riga, (1965).

Karule (1965): Karule,E.M.,"Atomic Collisions, III" Latrian Academy of Sciences, Riga, 1965.)

Kennard (1938): Kennard,E.H.,"Kinetic theory of Gases" McGraw Hill, 1938).

Kessler (1969): Kessler,J., Rev.Mod.Phys. 41 (1969) 3.

Krisciokaitis and Tsai (1969): Krisciokaitis,R.J. and Tsai, W.Y., C.E.A.L. Report No. 1050 (1969).

Lee and Yang (1957): Lee.T.D. and Yang,C.N., Phys.Rev. 105 (1957) 1671.

Mikaelyan et al. (1963): Mikaelyan,L.A., Borovoi,A.A. and Lenisov,E.I., Sov.Phys.JEPT 17 (1963) 785.

Mott (1929): Mott,N.F., Proc.Roy.Soc. A124 (1929) 425.

Mott and Massey (1965): Mott,N.F. and Massey,H.S.W.,"Theory of Atomic Collisions" 3rd Ed. (Clarendon Press, Oxford, 1965).

Pierce (1954): Pierce,J.R.,"Theory and Design of Electron Beams" 2nd Ed (Van Nostrand, 1954)

Rubin et al. (1960): Rubin,K., Perel,J. and Bederson,B., Phys.Rev. 117 (1960) 151.

Schroen (1963): Schroen,W., Z.Phys. 176 (1963) 237.

Sherman (1956): Sherman,N., Phys.Rev. 103 (1956) 1601.

Shull et al. (1942): Shull,C.G., Chase, C.T. and Myers,F.E., Phys.Rev. 63 (1942) 29.

Sommerfeld (1949): Sommerfeld,A., "Partial Differential Equations" (Academic Press, 1949).

Stern (1921): Stern,O., Z.Phys. 7 (1921) 249.

Tolhoek and DeGroot (1951): Tolhoek,H.A. and DeGroot,S.R., Physica 17 (1951) 1.

Uhlenbeck and Goudsmit (1925): Uhlenbeck,G.E. and Goudsmit,S., Natururiss 13 (1925) 953.

Vass (1971): Vass,D.B., Private communication.

Wegener (1958): Wegener,H., Z.Phys. 151 (1958) 252.

Wykes (1971). Wykes,J.S., Private communication.

ACKNOWLEDGEMENTS.

I wish to offer my thanks to Professor N.Feather, F.R.S., for giving me the opportunity of carrying out this research. The advice and supervision of Professor P.S.Farago has been invaluable throughout the experiment, as was the collaboration of Dr. H.M.Brash and Dr. H.Chr.Siegmann in the early stages. Many other members of the Physics Department of the University of Edinburgh have contributed useful advice and assistance, and to all I offer my thanks. Finally I must thank my wife for her constant support and encouragement, and particularly for her help in the preparation of this thesis.